Characterizing the advantages of diverse effector secretion in *Pseudomonas aeruginosa*

Kaitlyn Denne LaCourse

A dissertation submitted in partial fulfillment of the
requirements for the degree of

Doctorate of Philosophy

University of Washington

2019

Reading Committee:
Joseph Mougous, Chair
Matthew Parsek
Joshua Woodward

Program Authorized to Offer Degree:

Microbiology

Kaitlyn Denne LaCourse

University of Washington

Abstract

Characterizing the advantages of diverse effector secretion in *Pseudomonas aeruginosa*

Kaitlyn Denne LaCourse

Chair of the Supervisory Committee:
Professor, Joseph D. Mougous
Department of Microbiology

In the environment, bacteria exist in complex communities with other bacterial species, where they compete for resources. Cells are frequently in close proximity to one another, and therefore, many bacteria have evolved pathways to intoxicate their neighbors directly. One such pathway is the type VI secretion system (T6SS) which is broadly distributed in Gram-negative bacterial species. The T6SS antagonizes nearby cells by directly injecting them with toxic antimicrobial proteins, termed effectors. Effectors target conserved, essential structures in the cell, and ultimately lead to cell death. The known biochemical activities of effectors are diverse, and T6SSs often encode multiple effectors. A single effector is enough to incapacitate a targeted cell, and therefore there is likely a benefit to the cell in deploying multiple toxins, however, this question has never been scientifically addressed. In this work, I investigate the advantages of multiple effector secretion and describe the toxic mechanism of an effector of unknown activity that synergizes with other T6SS effectors. I developed a technique to assess effector activity in parallel under a variety of environmental conditions and applied this technique to effectors of the *Pseudomonas aeruginosa* H1-T6SS. This approach revealed that T6SS effector potency is dependent on the external environment and on the activity of simultaneously

secreted effectors. Furthermore, I discovered intoxication by T6SS effectors could be species-specific–highlighting the value of secreting more than one toxin against a broad phylogenetic range of bacterial species. Finally, I contributed to a deeper understanding of how these effectors are secreted by defining critical T6SS structural protein-protein interactions. In total, these data uncovered the significance of multiple effector secretion in overcoming the unpredictability of environmental conditions during bacterial competition.

TABLE CONTENTS

LIST OF FIGURES AND TABLES

Chapter 1

Chapter 2

Chapter 3

Chapter 4

ACKNOWLEDGEMENTS

There should be no thank you greater than that to my parents, Faye and Louis LaCourse. Their support of my intellectual pursuits has been boundless, while still reminding me of the important things in life often put aside during graduate school. Their understanding and love throughout this process have been invaluable. Thank you both for always believing I could do this, even when I had lost that faith myself. I would also like to thank my fiancé, Phil Burke, who has shared in all of my accomplishments and disappointments throughout the entirety of graduate school. I will forever be thankful that he moved here from thousands of miles away to share this section of my life with me.

An exceptional chemistry teacher, Bill “Doc” McGrew, awoke my passion for science during high school. I was extremely fortunate early on during college at the University of New Hampshire to be employed during my freshman year as a media maker for the Microbiology Department. This opened up an opportunity for me to work as an undergraduate research assistant in the laboratory of Dr. Louis Tisa, where I worked for two years investigating bacterial-nematode interactions. During this time, I was directly mentored by a phenomenal graduate student, Sheldon Hurst IV, and his encouragement, support, and scientific training laid the groundwork for my graduate work and he continues to be an inspiring role model.

The Mougous Lab has been a fun, supportive, and nurturing environment, in large part due to my fantastic colleagues, many of whom have become good friends. I want to thank Hannah Ledvina, Snow Brook Peterson, Matthew Radey, Aria Eshraghi, Benjamin Ross, Marcos de Moraes, See-Yeun Ting, Katie Kelly, Daniel McLeod, Brittany Harding, Jungyun (Rachel) Kim, John Whitney, and Seemay Chou. I especially valued the mentorship, support, and friendship of Brook Peterson, Benjamin Ross, John Whitney, and Hannah Ledvina. I am also grateful to Savannah Bertolli, an undergraduate who worked with me for two years, for her hard work and dedication.

I immensely valued the comradery of many graduate students and post-docs in the Microbiology department. A special thanks to the “Kbac” group who created a welcoming community to discuss both research and the struggle of the scientific process. Graduate school would not have been the same without my close friend and classmate, Mayumi Holly, who went through many of the ups and downs of graduate school with me.

I would like to thank my committee members, Matt Parsek, Nina Salama, Josh Woodward, and David Veesler for their advice, scientific input, and support. I would especially like to thank the members of my reading committee, Josh Woodard and Matt Parsek.

Finally, thanks to my graduate advisor Joseph Mougous. Joseph’s mentorship has taken many forms over the last six years. Some of these are obvious, such as volunteering his time to train me on equipment and new techniques and helping me design and execute successful experiments. Some however, are subtler, such as how to think creatively, to follow-through tough projects with determination, and nourishing my identity a scientist. There is no end to the thanks he deserves– I owe him for my confidence moving forward in my career. Through his infectious enthusiasm, he has caused me to fall even more deeply in love with microbiology and the scientific process. I have enjoyed watching his lab grow and be successful throughout the years, and I am excited to see what they discover next.

Dedication

To my parents, Faye and Louis LaCourse

And to my bright star, Phillip Burke

Chapter 1: Introduction

I. Bacterial antagonism and the history of the type VI secretion system

Bacteria in nature live predominantly in complex microbial communities in close proximity to one another[1]. In these environments, bacteria constantly compete with other microbes for space and nutrients. As a result, they have evolved many antagonistic pathways to fight their neighbors, and these behaviors are a key driver of microbial community composition[2]. Antibacterial aggression can be either contact-independent or -dependent. Contact-independent strategies utilize the deployment of antimicrobial compounds or proteins into the extracellular milieu where they can diffuse from the producer to a target cell. Most toxins must translocate the peripheral membrane of a target cell to cause toxicity, and while small molecules can readily diffuse across, larger molecules require more sophisticated methods[3,4]. The colicin toxins of *Escherichia coli* employ one well-studied example of target cell entry[5]. Colicins are large soluble proteins composed of three domains responsible for receptor binding, translocation, and killing. The receptor-binding domain interacts with a specific receptor on the outer membrane of a target cell, and the translocation domain enables trafficking of the colicin across the membrane and through the periplasm. Once inside the cell, the toxin domain kills the cell via pore-formation or enzymatic degradation of important cellular components[5,6]. Since colicins and similar toxins depend on the presence of specific outer membrane proteins, they are limited in the phylogenetic range of cells they can target. To bypass this constraint, bacterial cells can utilize contact-dependent mechanisms to deliver toxins directly into recipient cells[7–10]. One such pathway is the bacterial type VI secretion system (T6SS), which is discussed in detail below[11].

Overview of the type VI secretion system and early history

The T6SS is a molecular machine that transfers proteins, termed effectors, directly into the periplasm of targeted cells through a syringe-like mechanism[12]. This complex spans both the inner and outer membrane of Gram-negative bacteria and resembles an inverted phage-like contractile needle that is oriented toward the outside of the cell. The structural components of

T6SSs are encoded on the bacterial chromosome in large clusters. Genes encoding effectors delivered by the secretion system can be located within the T6SS clusters but can also be scattered across the chromosome. Effector genes exist in operons with genes encoding their cognate immunity proteins to prevent self-intoxication by kin cells. These operons can also encode accessory proteins necessary for efficient delivery of their respective effector[13,14]. Is it currently believed that the primary, ancestral function of the T6SS is antimicrobial activity against other bacteria[11]. However, in some cases, the system has evolved to target eukaryotic cells. For example, members of the bacterial genus *Francisella* are intracellular parasites that utilize a divergent T6SS to survive within host cells[15,16]. The effectors of the *Francisella* T6SS target pathways that are exclusively found in eukaryotes[17]. In addition, there is emerging evidence that some T6SSs assist in ion scavenging in nutrient-poor environments–highlighting the versatility of these systems as a protein secretion platform[18–20].

The gene clusters now known to encode T6SSs were first identified in 2003 as a potential secretion pathway in *Rhizobium leguminosarum*[21]. At the time, it was noted that these gene clusters are conserved across a broad phylogenetic range of bacteria and that multiple genes in the cluster have homology to previously characterized secretion system components[21]. In 2004, a mass-spectrometric screen was implemented to measure secreted virulence factors of *Edwardsiella tarda*[22]. This approach revealed two proteins contributing to *E. tarda* virulence that are encoded on a large conserved gene cluster, now recognized to be a T6SS[22]. Through mutational analysis, the authors determined that the secretion of these two proteins is dependent on other genes in the cluster. These data led to the conclusion that this gene cluster likely contains a novel protein secretion system. Since these early observations, hundreds of T6SS clusters have been identified within the genomes of Proteobacteria[23].

These gene clusters were designated as a new, distinct type of bacterial secretion system in 2006 by the Mekalanos laboratory at Harvard Medical School. Bioinformatic analyses

suggested that these large collections of genes represent a unique secretion pathway with proteins that lack N-terminal signal sequences[24]. Many pathogenic Gram-negative bacterial species encode T6SSs, and early studies supported the role of this pathway in extracellular export of virulence factors into eukaryotic cells[25–29]. In 2010, the Mougous laboratory identified three substrates of a *Pseudomonas aeruginosa* T6SS and found that one of the secreted toxins, Tse2, is toxic to bacteria[30]. Subsequent studies demonstrated T6SSs mediate fitness against bacteria in contact-dependent conditions and that T6 effectors target essential structures in bacterial cells[25,31]. In the nine years since these initial observations, many more studies have emerged characterizing antibacterial T6SSs across diverse bacterial species, encompassing both free-living and eukaryotic-associated species (ex. pathogens, plant and animal symbionts)[11].

II. T6 effector and system diversity

A remarkable feature of T6SSs is the wealth of system and effector diversity that can be found within a single strain of bacteria and between bacterial species[11,32]. A given bacterial species can encode one to seven different T6SSs, which often vary among individual strains[23]. T6SSs can target both bacteria and eukaryotes through the secretion of transkingdom effectors[33–37]. There are also documented cases of bacteria containing multiple systems that exclusively intoxicate bacteria or eukaryotes[38,39]. In addition to the overall genetic diversity of T6SSs, a single T6SS cluster can utilize an extensive effector arsenal[32,40]. Antimicrobial T6 toxins exclusively target highly conserved and essential structures within bacterial cells[12]. Characterization of these targets, and the mechanisms that toxins utilize to subvert them can shed light on potential pathways for developing new antimicrobial therapeutics.

Methods for T6 effector identification

A method to identify putative T6SS effectors is bioinformatic analysis, which employs conserved catalytic motifs, domains, and genomic context to analyze the genomes of T6-

competent bacteria[41]. The Mougous laboratory published the earliest example of utilizing bioinformatics for effector identification in 2013[42]. This study used a bioinformatic approach to identify the shared properties of known effector-immunity pairs and then used these criteria to screen the genes of T6SS+ bacterial species. A diverse superfamily of T6SS-associated peptidoglycan-degrading effectors was uncovered using this approach. Since this initial research, leveraging standard features of previously characterized T6SS effectors has enabled the discovery of a plethora of T6SS substrates[13,43–49]. While successful, utilizing bioinformatics for effector discovery is limited by the need for prior knowledge or a hypothesis about the proteins being identified, making it difficult to uncover new biochemical activities or proteins with unique domain organizations.

Genetic analysis of T6SS-associated gene is one bioinformatic method for finding effectors lacking known T6-associated domains or toxin motifs to identify T6SS-associated genes. Hcp and VgrG are structural components of the T6-needle that also act as chaperones for specific effectors[13,45]. The genes encoding Hcp and VgrG can be organized into operons with their cognate effectors, and mutational analysis of the co-transcribed genes can identify effector–immunity pairs. This method was applied successfully to the genome of *Pseudomonas aeruginosa* to identify genes near various *vgrG* genes, ultimately facilitating the discovery of *tse5* and *tse6*. This technique has also revealed effectors of *Agrobacterium tumefaciens*, *Serratia marcescens*, *Pantoea*, and *Erwinia* species[13,40,45,50,51]. While a single T6SS can utilize multiple VgrG proteins, which each have a cognate effector, they only encode a single Hcp protein. Hcp can associate with multiple effectors which are not necessarily encoded nearby the *hcp* gene and can be found throughout the genome.

Proteomic experiments offer a discovery-based approach that can reveal effectors without known features or genomic locations. There are two documented experimental designs for effector identification using proteomics that leverage either substrate secretion or intracellular stability. Substrates secreted by a T6SS can be identified by comparing the proteins in the

supernatant of the wild-type versus a T6-defective strain by semi-quantitative mass-spectrometry[15,30,42]. This method was first used in *P. aeruginosa* and facilitated the detection of Tse1, Tse2, and Tse3[30]. Since this initial study, comparative secretome analyses have been employed to identify effectors in *Vibrio cholerae*, *Aeromonas hydrophilia*, *Burkholderia* species, *Serratia marcescens*, *Flavobacterium johnsoniae* and enterohemorrhagic *E. coli* (EHEC)[15,28,52–56]. A second proteomics approach exploits the knowledge that the T6 chaperone Hcp stabilizes its cognate effectors intracellularly[57]. This technique utilizes comparative mass-spectrometry to measure the intracellular proteome of a wild-type strain and a Δ*hcp* strain to reveal proteins with lower abundance in the Δ*hcp* background. Determining which proteins have lower intracellular stability in the absence of Hcp facilitated the identification of Tse4 in *Pseudomonas aeruginosa*, a lower abundance protein not previously detected by secretome analysis[13]. This same principle could be applied to any known T6SS adapter or chaperone necessary for effector stability. The limitations of proteomics for T6 effector discovery lie in the fact that the *in vitro* conditions required for T6 secretion are not known for many organisms, and that proteins of interest must be present in sufficient abundance for detection by mass-spectrometry.

Biochemical activities of antimicrobial effectors by molecular target

Cell wall: Peptidoglycan (PG) is the major structural component of the bacterial cell wall, and therefore is a common target for many antimicrobial molecules[58,59]. PG provides structural strength to the cell wall and counteracts changes in osmotic pressure experienced by the cell[60]. PG is a polymer consisting of sugars and amino acids that form a mesh-like layer within the periplasm of Gram-negative cells. The sugar component forms the backbone of the polymer and consists of alternating molecules of N-acetylglucosamine (NAG) and N-acetylmuramic acid (NAM). Two polymers of the sugar backbone are interconnected by short peptide bridges attached to NAM that cross-link together. Antibacterial T6 toxins disrupt PG structure by targeting either the glycan backbone or the peptide crosslinks. There are four divergent families of

glycoside hydrolase effectors, Tge1-3 and VgrG3, that cleave between the NAG–NAM bonds in the glycan backbone[12].

Additionally, there are six families of PG amidase effectors, Tae 1-5 and TaeX, that cleave specific bonds within the peptide crosslinks[12,61]. PG-associated effectors are toxic in the periplasmic compartment of the cell. Loss of PG stability due to toxin activity leaves cells susceptible to lysis in low osmolarity conditions where the increasing internal turgor pressure causes cells to swell[62].

Plasma Membrane: The inner membrane is another conserved and essential component of the bacterial cell. This membrane is composed of a phospholipid bilayer and acts as a permeability barrier for most molecules, including ions. It also is the location for transport of molecules into the cell. and plays a role in energy production by maintaining the ion gradients in cells. These gradients provide the energy for the proton motive force in cells which is responsible for the production of ATP[63]. T6 effectors interrupt membrane integrity through phospholipase and pore-forming activity[12]. There are five families of phospholipases that directly target the membrane by hydrolyzing its component lipids: Tle1-4 have phospholipase A_1 or A_2 activity and Tle5 has phospholipase D activity[64]. The bacterial membrane is also susceptible to disruption by pore-forming toxins, which create large pores or small ion-channels that dissipate essential chemiosmotic gradients. There are three known T6 pore-forming toxins, VasX, Tse4, and Ssp6[65–67]. VasX has a C-terminal domain with homology to a bacteriocin called colicin Ia, a pore-forming toxin that forms voltage-gated ion-conducting channels across the plasma membrane[65]. Tse4 has no homology to any characterized proteins but was recently shown to form ion-specific pores within the membrane of *P. aeruginosa* and cause membrane depolarization[66]. Ssp6 is similar in activity to Tse4 and creates small cation-selective pores that damage both the inner and outer membrane of cells[67]. Both phospholipase and pore-forming effectors are exclusively active against their membrane substrate when they are in a periplasmic environment. Phospholipase

activity on the membrane contributes to cell lysis, while pore-forming toxins induce bacteriostasis through disrupting the ion gradients necessary for ATP generation.

DNA/RNA: All T6SS nucleic acid-targeting effectors characterized thus far are DNA endonucleases belonging to several evolutionarily distinct families[40,46,50,68–70]. There are many uncharacterized T6 effectors predicted to possess DNase, RNase, and deaminase activity by bioinformatic analyses[47]. While is it simple to envision how a DNase or RNase toxin inhibits cellular activity, the toxicity of deaminase toxins is less clear. Instead of physically cleaving DNA/RNA, deaminases would modify a nucleotide by the removal of an amino group. For example, cytosine would become uracil, which would be removed from the DNA and replaced with thymine by base excision repair[71]. Too much deamination could ultimately lead to the degradation of functional DNA. In contrast, low levels of deamination, over time, could result in single nucleotide polymorphisms that alter the coding sequence of the DNA and potentially have fitness consequences over time. Deaminases have never been described as antibacterial proteins, and it is intriguing to see that many predicted bacterially-produced antimicrobial toxins contain deaminase-like domains.

Metabolites and proteins: Two metabolites are known to be targeted by T6 effectors, the co-factors B-nicotinamide adenine dinucleotide (NAD^+) and NAD^+ phosphate ($NADP^+$). These molecules are essential for anabolic and catabolic processes required for homeostasis and growth. T6 effectors Tse6/Tne1 and Tne2 intoxicate cells by hydrolysis and removal of the nicotinamide moiety from NAD^+ and $NADP^+$[72,73]. Depletion of these essential co-factors causes cellular growth arrest.

In a bacterial cell, FtsZ is an essential protein responsible for orchestrating cell wall synthesis between dividing cells[74,75]. FtsZ is the only known proteinaceous target of a T6-effector[76]. An ADP-riboslytransferase toxin, Tre1, modifies FtsZ by adding an ADP-ribose moiety to an amino acid that is critical for filament formation[76]. Lack of filament formation leads to cell elongation, rapid growth arrest, and loss of cell viability.

III. What factors drive bacterial T6 effector diversity?

Antimicrobial T6SS effectors degrade conserved, essential structures within the cell, and accordingly, single effectors are sufficient to kill a cell or to terminate growth[12,32]. Despite this, there are multiple experimentally-characterized T6SSs that deliver a diverse cocktail of effectors that target multiple structures in the cell[32,77]. Before my thesis, there has been no published research investigating the advantages of secreting multiple effectors, or how their biochemical activities could impact each other's downstream effects on the target cell. I present four hypotheses of biological functions for collective effector secretion, which may not be mutually exclusive (Figure 1).

Antimicrobial resistance

The T6SS is a complex macromolecular machine that provides a fitness advantage dependent on the intoxication of nearby bacteria. If a T6SS+ cell only utilized one or two effectors against a target, and the targeted population developed resistance to these effectors, the T6SS would become functionally useless and would drain resources from the cell. Therefore, by delivering multiple effectors that act on different molecules, the probability of the intoxicated species developing resistance is decreased (Figure 1.1a). This idea is supported by the success of using multiple antibiotics to minimize the risk of evolving resistance[78]. However, given the essentiality and structural conservation of T6SS effector targets, it is unlikely that preventing the rise of antimicrobial resistance is the sole or major selective pressure driving effector expansion.

Species-specific toxins

T6SSs have the potential to mediate antagonistic interactions with a wide phylogenetic range of bacterial species. While the molecules targeted by T6-effectors are essential, they can be modified or have unique structural features. One hypothesis for multiple effector secretion is

to overcome intrinsic resistance and to maximize host range in the target species (Figure 1.1b). There are several documented cases of unique bonds and strain-specific arrangement of peptides in peptidoglycan in *Mycobacteria*, *Bordetella pertussis, Caulobacter crescentus*, and *Streptococcus pneumoniae*, which in some cases are associated with antibiotic resistance[79–83]. Lipid membranes are composed of a variety of glycerophospholipds and phosphorus-free lipids. There are dramatic changes in the relative abundance of these lipid species across Proteobacteria[84]. Bacterial resistance or vulnerability to phospholipases could be mediated by the abundance of an effectors preferred phospholipid in the membrane. For example, many bacteria have low amounts of phosphotidylserine (PS), but it is a major constituent in membranes from *Bdellovibrio bacteriovorus* and Flavobacterium species[85,86]. Accordingly, these species would likely accrue more damage from a phospholipase with high affinity to PS than other species might.

Environmental influence on effector efficacy

An alternative hypothesis is that effectors differentially contribute to recipient cell intoxication dependent on the external environment (Figure 1.1c). The integrity of many cellular structures is integral to surviving changes to external environmental conditions. Peptidoglycan protects the cell and maintains cell shape during changes in extracellular osmolarity, which directly affects the internal turgor pressure of the cell. Without a functional cell wall, cells will lyse in low salt environments[87]. Two T6SS effectors that target peptidoglycan, Tse1 and Tse3, are toxic in low osmolarity conditions[31]. This phenotype is abrogated in growth media containing higher concentrations of NaCl; an environment where Tse1 and Tse3 are less efficacious[31]. The Gram-negative inner membrane is another structure crucial for proper cellular growth. Damage to the inner membrane results in increased sensitivity to extracellular ions that the membrane occludes from the cytoplasm[88]. The activity of antimicrobial pore-forming toxins could result in ion-sensitivity of the cell, causing growth arrest in high salinity environments. Therefore, it is plausible

that multiple effector secretion is a bet-hedging strategy of T6SS-competent bacteria to maximize their chances of success in many environmental contexts.

Synergy between effector activities

Simultaneous deployment of diverse effectors could allow for synergistic downstream interactions (Figure 1.1d). Synergy, in this case, would be defined as instances in which the activity of two or more effectors on recipient cells is greater than the sum of their respective activities. To our knowledge, there has never been a study on toxin synergy from bacteria that deploy multiple antimicrobials from any secretion pathway. However, many studies have shown synergetic activities between combinations of antimicrobials and commercial antibiotics, and it is unlikely that bacteria have not evolved to capitalize on biochemical synergy among toxins[89–92].

IV. Model T6SS organism: *Pseudomonas aeruginosa*

P. aeruginosa is a Gram-negative γ-proteobacterium found in a broad range of environments including soil, freshwater, and in association with animals. *P. aeruginosa* is also an opportunistic pathogen of immunocompromised individuals, chronic wounds, and the lungs of cystic fibrosis (CF) patients. These infections can result in acute disease and are often difficult to treat, leading to high rates of morbidity and mortality[93]. Chronic infection by *P. aeruginosa* correlates with loss of bacterial diversity within wounds and the CF lung, which typically contain polymicrobial communities[94,95]. Since *P. aeruginosa* flourishes in a wide range of environments, it must likely encounter many types of bacterial species. Therefore, it needs to encode antibacterial antagonistic pathways to promote successful integration into its niches. One such pathway, and the major focus of this dissertation, is the contact-dependent toxin delivery pathway: the type VI secretion system[96].

The *P. aeruginosa* genome encodes three non-redundant, functionally distinct T6SSs, named the Hcp secretion islands I-III (H1-H3 T6SSs)[97]. Historically, the H1-T6SS is the first

bacterial T6SS determined to have antibacterial activity, and as such, it is the most well-studied T6SS within *P. aeruginosa*[30]. The activity of the H1-T6SS provides a growth advantage to *P. aeruginosa* when in close proximity to other antagonistic bacteria in the same ecological niche. This competitive advantage is accomplished through the direct secretion of seven biochemically distinct antimicrobial effectors into targeted cells, named type VI exported 1-7 (Tse1-7). Within the periplasm, Tse1 and Tse3 degrade PG, while Tse4 and Tse5 are predicted to disrupt the inner membrane. In the cytoplasm, Tse6 targets NAD(P)+, Tse7 cleaves DNA, and Tse2 induces bacteriostasis through an unknown activity. Two global system regulate the H1-T6SS in *P. aeruginosa*. It is negatively regulated by LasR and MvfR-mediated quorum sensing (QS) and post-transcriptionally activated by the Gac/Rsm system by removing RsmA repression in response to an unknown signal in kin cell lysate[98,99]. Additionally, the H1-T6SS is post-translationally activated by a T6-exclusive threonine phosphorylation pathway[97,100]. The sheer number of pathways involved in regulating the H1-T6SS highlights how fine-tuned the activity of this system needs to be for efficient employment.

The H2-T6SS and H3-T6SS act on both prokaryotes and eukaryotes through the secretion of phospholipase effectors[101]. Both H2 and H3-T6SSs are positively regulated through LasR and MvfR QS and repressed by RsmA[98,102]. The H2-T6SS is repressed by iron presumably due to the presence of two putative Fur boxes in its promoter region[103]. The H3-T6SS is most active in stationary phase and is positively regulated by RpoN[104]. On the surface, it appears that each T6SS in *P. aeruginosa* is most functional at different stages of cell population growth. It is plausible that each T6SS could be used against the same bacterial competitor throughout their conflict together, if not concurrently [102].

V. Thesis objectives

Over the eight years since the activity of a T6SS antibacterial effector was first documented, various studies have elucidated the diverse biochemical activities found within T6SS

effectors. However, prior studies have failed to evaluate the biological significance of multiple effector secretion. The goal of my thesis research has been to:

1) Identify the biochemical activity of a potent H1-T6SS effector, Tse4

2) Investigate the advantages of multiple antimicrobial toxin secretion

3) Determine if encoding multiple antibacterial T6SSs increases the phylogenetic range of targetable species

The H1-T6SS of *P. aeruginosa* was the model system for these studies, as it is genetically tractable, and its effectors and regulation are well-characterized. The findings generated from this work have contributed to the deeper understand behind T6 effector organization and function.

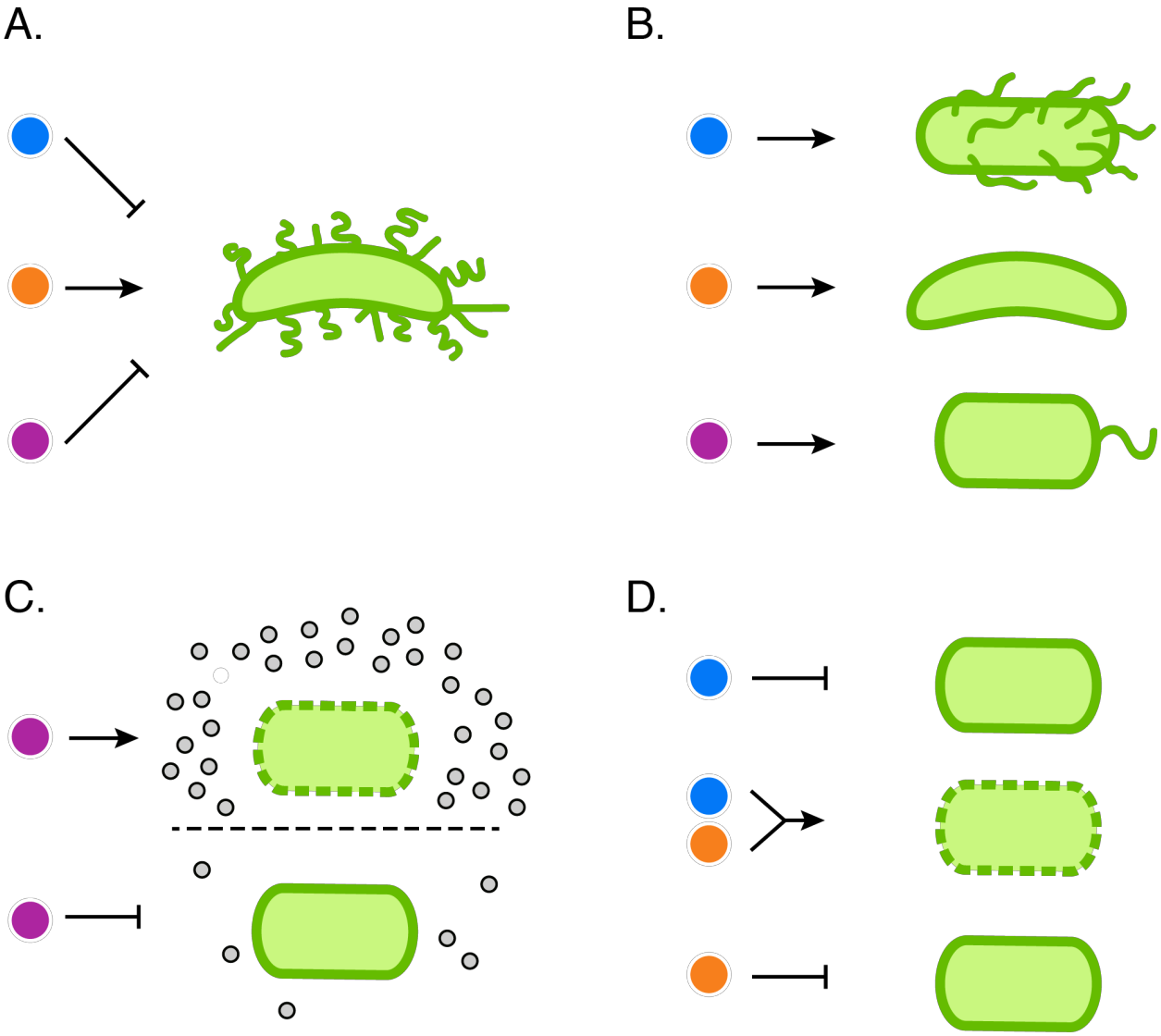

Figure 1.1: Factors hypothesized to drive T6SS effector repertoire diversity
(**A**) Circumnavigating resistance occurring in the target during bacterial competition. (**B**) Species-specific toxin development. (**C**) Effector efficacy depends on the external environment. (**D**) Effector activities are synergistic with one another.

Chapter 2: A *Pseudomonas aeruginosa* T6SS utilizes a pore-forming antibacterial toxin: Tse4

Portions published in: **LaCourse K.,** Peterson SB., Kulasekara HD., Radey MC., Kim J., Mougous JD. Conditional toxicity and synergy drive diversity among antibacterial effectors. *Nature Microbiology* 3, 400-446. (2018).

I. Abstract

The type VI secretion system (T6SS) is a contact-dependent antimicrobial delivery pathway found widely distributed among proteobacteria. These antimicrobials, termed effectors, target conserved, and essential structures in bacterial cells. To date, seven antibacterial effectors have been identified for the Hcp Secretion Island-I-encoded-T6SS (H1-T6SS) of *Pseudomonas aeruginosa*. While the functions of four of these effectors are defined, the mechanism of intoxication by the remainder is unclear. Using co-culture competitions and live-cell quantitative microscopy, we discover that one of these proteins, Tse4, is a bacteriostatic toxin. Through analyzing the consequences of Tse4 activity in bacterial cells, we found this toxin disrupts specific ion gradients resulting in the loss of membrane potential. Tse4 is a membrane protein with an extended C-terminal glycine zipper necessary for function. While Tse4 resembles no characterized proteins, homologs can be found within the *Pseudomonas* and *Burkholderia* genera. These results suggest that Tse4 is the founding member of a new family of pore-forming toxins, and characterization of this protein will provide insight into the function of these effectors.

II. Introduction

Polymicrobial communities are fundamentally important in virtually all ecosystems, and bacterial typically live through their entire lifecycle in close proximity to other bacterial cells. Accordingly, a large portion of bacterial growth and physiology is influenced by their interactions with neighboring cells. It is now appreciated that a driving force of community development is antagonistic interactions between strains and species within their niche, and a plethora of pathways are therefore dedicated to antibacterial toxin secretion[2,10]. One antimicrobial mechanism widely used by Gram-negative bacteria is the type VI secretion system (T6SS). The T6SS is a contact-dependent macromolecular machine that delivers toxic antimicrobial proteins, termed effectors, directly into neighboring cells[12]. While T6SSs can target both eukaryotic and

prokaryotic cells, overwhelming literature suggests the role of this pathway is to mediate antimicrobial competition between bacteria[11].

Myriad antimicrobial T6SS effectors have been identified across a broad phylogenetic range of bacterial species. Biochemical characterization of these effectors demonstrates that T6 toxins are an extensive reservoir of biochemical and structural diversity. These include distinct families of peptidoglycan hydrolases, phospholipases, nucleases, and NAD(P)+ glycohydrolases[11,12]. Additionally, there are particular examples of a T6 ADP-ribosylating toxin that targets the essential cell-division factor FtsZ, and a probable pore-forming toxin VasX[65,105]. Secretion of effectors into recipient cells can result in cell lysis or growth arrest. Since these toxins are incredibly potent, T6+ bacteria encode cognate immunity proteins genes to their specific effector to prevent self-intoxication[30]. These immunity proteins are intracellularly localized to the compartment their respective toxins target is found. The biochemical functions of only a small portion of identified T6SS substrates are known, highlighting the potential for new antimicrobial toxin discovery through characterization of undefined effector activities[11].

The opportunistic pathogen, *Pseudomonas aeruginosa*, has an antibacterial T6SS, the H1-T6SS, that secretes seven unique effector proteins into target bacterial cells[13,45]. Several of these effectors are not related to any previously characterized proteins and have mechanisms that cannot be easily predicted, suggesting they likely represent novel antibacterial toxins. Here, we report the detailed characterization of the effector Tse4. Tse4 (PA2774) is a small effector identified in a study using a mass-spectrometry approach. Its mode of action is unknown and is not readily predictable from sequence-based or structural prediction methods[13]. Tse4 is toxic in the periplasm of cells, and its immunity protein, Tsi4, is predicted to localize to the inner membrane. We reveal Tse4 is a membrane protein that disrupts specific ion gradients *in vivo* and ultimately depolarizes the cytoplasmic membrane resulting in bacteriostasis. Tse4 contains a conserved glycine zipper motif necessary for function suggesting the protein oligomerizes to form channels in the inner membrane. Homologs of Tse4 can be found throughout the *Pseudomonas*

and *Burkholderia* genera implying that Tse4 potentially defines a new family T6SS-delivered, ion-selective pore-forming toxins.

III. Results

Tse4 in an antibacterial toxin and induces bacteriostasis within target cells

As a first step towards characterizing Tse4, we utilized the iterative-search tool Jackhmmer to identify distantly related homologs by amino acid identity and found 236 homologs in 164 species[106]. These homologs were encoded in a bicistron with a predicted cognate immunity protein and were primarily restricted to the *Pseudomonas* and *Burkholderia* genera (Figure 2.1a). To access the toxicity of Tse4 we performed co-culture competitions of a PAO1 strain lacking the immunity protein Tsi4 against different donor strains under contact-inducing growth conditions. These intraspecies competitions utilized *P. aeruginosa* in the Δ*retS* background to facilitate constitutive activation of the H1-T6SS. This allows for robust intraspecific competition phenotypes independent of physiological stimulators[99]. We found that donor strains possessing Tse4 and a functional T6SS display a roughly 3 log-fold advantage against a Δ*tse4* Δ*tsi4* recipient (Figure 2.1b).

To access the capacity of Tse4 to mediate interspecies antagonism, we co-cultured wild-type PAO1 and *E. coli* containing the IncP-type RP4 conjugative plasmid known to stimulate the PAO1 H1-T6SS through lysis of a subset of the *Pseudomonas* population[99,107]. We found PAO1 targets *E. coli* RP4 through its H1-T6SS, and that the activity of Tse4 was responsible for approximately half of the intoxication mediated by T6S and the fitness defect in the *E. coli* strain could be partially restored by plasmid-borne expression of *tsi4* (Figure 2.1c).

To determine the cellular consequences of Tse4-intoxication, we examined the effect of Tse4 delivery to a sensitive strain on cell viability using co-culture assays. Intoxication by Tse4 promoted growth inhibition without an apparent diminishment of viability, indicative of a bacteriostatic mechanism (Figure 2.1d). Additionally, we monitored the division time of a self-

intoxicating Δ*tsi4* strain compared to a parental strain (Δ*retS*) by time-lapse microscopy and the image analysis software SuperSegger[108]. By analyzing frame-by-frame PAO1 doubling events, it was apparent that Δ*tsi4* cells have longer division times than an unintoxicated strain (Figure 2.1e). Taken together, these data indicate that Tse4 is a potent antimicrobial toxin whose activity results in target cell growth arrest.

Tse4 is a membrane protein with a conserved glycine zipper motif essential for its function

As observed for all T6SS effector–immunity pairs characterized to date, we found that Tse4 and its cognate immunity determinant, Tsi4, directly interact (Figure 2.2a)[30,109]. Both possess predicted transmembrane domains predicted by TMHMM and cellular fractionation determined that Tse4 resides in the membrane (Figure 2.2b)[110]. Additionally, a prior mass spectrometry-based study demonstrated both proteins localize to the inner membrane of *P. aeruginosa* (Figure 2.2d)[111]. Tse4 is also characterized by a high content of glycine residues, many of which are in configurations reminiscent of glycine zipper motifs (Figure 2.2d). These sequences can promote multimerization of transmembrane segments and frequently occur in proteins that induce pores, including bacterial toxins[112]. To test the importance of these residues for Tse4 function, we generated a panel of mutants in which glycine residues predicted to form a transmembrane glycine zipper were substituted for valine. All of these mutants exhibited decreased Tse4-mediated intercellular intoxication (Figure 2.2e) Substitutions at G176 and G184 also impacted Tse4 secretion and stability, thereby complicating interpretation of the intoxication defects of these alleles (Figure 2.2F). However, proteins containing G180V or G186V substitutions were produced and secreted at wild-type levels, indicating specific disruption of toxin activity. Alleles encoding substitutions in adjacent non-glycine residues (A187V and A188V) had no impact on Tse4 function despite diminished secretion. These observations led us to hypothesize that the effector has the potential to form channels in the inner membrane and compromise membrane integrity.

Intoxication by Tse4 results in cellular ion sensitivity

The localization of Tsi4 suggests that Tse4 targets the bacterial membrane. The inner membrane functions as a barrier to maintain ion gradients inside and outside the cell and disruption to the membrane can result in extracellular ion sensitivity. To measure salt-sensitivity, we compared the growth of a Tse4 self-intoxicating strain, Δt*si4*, on media containing various salts under contact promoting conditions. This strain displayed a profound, T6S-dependent growth defect on media containing sodium chloride (150 mM) or lithium chloride (20 mM) at concentrations sub-inhibitory to the wild-type (Figure 2.3a).

In contrast, significant growth inhibition was not observed in media containing potassium chloride or sucrose at levels equiosmolar to that of sodium chloride. This increased sensitivity to Na^+ or Li^+ ions was not due to increased expression of Tse4 under those growth conditions (Figure 2.3b). These data suggest that Tse4 activity promotes sensitivity to monovalent cations.

If ion sensitivity in Tse4-intoxicated strains is due to increased intracellular cations, we reasoned increased expulsion of Na^+ could rescue growth. NhaA plays a crucial role in Na^+ homeostasis in *E. coli*, and deletion results in increased Na^+ sensitivity[113,114,115]. We performed an intraspecies co-culture competition with a Tse4-donor (ΔretS) in excess against a Tse4-sensitive strain expressing NhaA. We found NhaA expression increases recovery of the Tse4-sensitive recipient, and a catalytic point mutation in *nhaA* abrogated this benefit (Figure 2.3c)[113]. Both NhaA and $NhaA D^{163N}$ were expressed in similar quantities in these experimental conditions (Figure 2.3d). To ensure the positive effect of NhaA expression is specific to Tse4-intoxicated cells, and not to overall cell growth, we tested the recovery of cells targeted by Tse2, another T6-delivered effector known to induce bacteriostasis, and saw no phenotype (Figure 2.3c). This result provided additional evidence that Tse4-intoxicated cells have difficulty maintaining normal intracellular sodium homeostasis.

Next, we sought to determine whether external sodium concentrations during interbacterial competition affect the potency of Tse4 and its contribution to T6SS-mediated fitness. To test this, we co-cultured PAO1 and *E. coli* on 3% LB agar plates without NaCl and those supplemented with 150 mM NaCl (for reference, traditional LB contains 171 mM NaCl, or 5g/L). The addition of NaCl to the external environment increased the contribution of Tse4 to overall fitness by 100 fold (Figure 2.3e,f). This finding shows the salinity of the external environment influences the toxicity of Tse4. It is tempting to suggest that Tse4 would be a desirable effector for T6SS+ organisms in habitats with higher salinity (salt-water and soil near irrigation sites)[116,117]. These observations, taken together with the glycine zipper motif we found in Tse4, led us to hypothesize that the effector forms pores in the inner membrane of intoxicated cells.

Tse4 intoxication mirrors that of other antimicrobial pore-forming toxins

Perhaps the most well-studied antimicrobial pore-forming toxins are colicins and small-antimicrobial peptides. The characteristic features of these toxins are depolarization of recipient cell membrane, followed by a rapid release of intracellular K^+ leading to bacteriostasis and cell death[5,118,119]. Tse4 induction leads to growth arrest and ion permeability of the inner membrane, and it disrupts the proton motive force (PMF). The proton motive force is essential for ATP-generation in bacterial cells and is composed of the $\Delta\Psi$ (membrane potential), and the ΔpH (change in pH across the inner membrane)[120]. To measure the $\Delta\Psi$ component of the PMF, we used the membrane potential-sensitive fluorescent dye $DiOC_2(3)$[121]. Tse4 intoxication results in a dramatic decrease in $\Delta\Psi$, nearly to the level of an ionophore-treated control (Figure 2.4a). Therefore, Tse4 activity almost completely dissipates the membrane potential of the inner membrane.

Bacteria concentrate potassium ions in their cytoplasm, and thus their release to the milieu is a convenient measure of membrane pore formation. Therefore, we monitored

potassium release from Tse4-intoxicated cells using inductively-coupled plasma optical emission spectroscopy (ICP-OES). One hour after Tse4 induction, the level of extracellular potassium detected from a strain lacking Tsi4 approached that of mechanically lysed cells (Figure 2.4b). Immunity to Tse4 inhibited the accumulation of extracellular potassium and allowed cells to concentrate potassium intracellularly during this period. We next asked whether the action of Tse4 allows the translocation of larger, organic molecules. Neither propidium iodide (668 Da) nor *o*-nitrophenyl-β-galactopyranoside (301 Da) accessed the cytoplasm of Tse4-intoxicated cells (Figure 2.4c). However, control cells treated with pyocin S5, a bacterial toxin previously shown to form large, non-selective pores, were permeable to both molecules. This data implies that Tse4 induces membrane pores that accommodate ions but exclude larger organic molecules.

In trying to understand both potential ion selectivity and if Tse4 disrupts the remaining portion of the PMF, we measured pH homeostasis in intoxicated cells. By employing the pH-sensitive green fluorescent protein pHluorin2, we found that Tse4-intoxicated cells maintain the ΔpH indicating an intact proton gradient (Figure 2.4d)[122]. In total, our data indicate that Tse4 promotes highly selective membrane permeability and allows Na^+ and K^+ across the inner membrane but excludes protons.

Tse4 forms pores in lipid bilayers in vitro

The data from this study support that Tse4 forms ion-selective channels in the inner membrane and could represent a unique family of antimicrobial pore-forming toxins. To both access the direct activity of Tse4 on the lipid membrane *in vitro* and to pursue the structure of the effector, we purified Tse4 both alone and in complex with its immunity protein Tsi4 (Figure 2.5a). In order to determine the structure of Tse4, we attempted to crystallize both Tse4 and the Tse4–Tsi4 complex. The Tse4–Tsi4 complex crystallized in several conditions and the

highest resolution of x-ray diffraction obtained is 11Å, which is not able to resolve secondary structure (Figure 2.5a).

Before we began *in vitro* assays with Tse4, we confirmed Tse4 was folded properly using circular dichroism (CD). CD analysis determined that purified Tse4 retains secondary structure, and the spectra suggest the protein contains primarily α-helices, a hallmark of most pore-forming toxin domains (Figure 2.5b)[123,124]. To test the ability of Tse4 to form pores, purified Tse4 was added to a chamber with an artificial membrane, under a voltage-clamp set up in non-symmetrical conditions. Incorporation of Tse4 generates a current that fluctuates between an open and closed state, revealing that Tse4 can form ion-conducting channels (Figure 2.5c). Although we cannot definitively rule out alternative mechanisms by which Tse4 may act, the most parsimonious explanation for our findings is that Tse4 acts by facilitating the formation of ion-selective membrane pores (Figure 2.6).

IV. Discussion

In this study, we demonstrated that Tse4 is a pore-forming toxin that generates cation-specific channels, resulting in depolarization of the cell and ultimately leading to bacteriostasis and cell death. Tse4 is the founding member of a new family of T6SS-delivered pore-forming toxins and is distinct from previously characterized proteins proposed to form membrane pores.

Tse4 homologs are found primarily in the *Pseudomonas* and *Burkholderia* genera and contributes to interspecies competition. Tse4 activity results in growth inhibition, as demonstrated by co-culture competition and analytical time-lapse microscopy. Since Tse4 is toxic in the periplasm and *in silico* prediction identified hydrophobic patches resembling transmembrane domains, we investigated whether Tse4 was a membrane-associated toxin. Tse4 partitioned with the membrane component of fractionated cells and its purification required detergents to remain in solution, indicating the effector is a membrane protein. These findings are the first example of

a T6SS-toxin that is membrane-associated has been shown to halt cell growth, suggesting it caused membrane leakiness rather than lysis indicative of significant membrane disruption.

The membrane of bacterial cells is essential for the establishment of many ion gradients. The electron transport chain generates an electrochemical gradient of protons, called the proton motive force (PMF), by the export of protons outside the cell-membrane[120]. The total PMF is composed of both the proton gradient (ΔpH) and the transmembrane electrical potential ($\Delta\Psi$). The PMF transports solutes against their electrochemical gradients, allowing for accumulation of K^+ within the cell and expulsion of Na^+ outside the cell. The disruption of either the ΔpH or the $\Delta\Psi$ results in less energy for import and export of molecules into the cell as well as decrease intracellular ATP levels. We found that intoxication by Tse4 results in almost total loss of intracellular K^+, and sensitizes cells to Na^+ and Li^+, both monovalent cations are typically excluded from cells. Since the majority of our experiments were performed on LB media containing 171 mM NaCl, and only residual K^+, the influx of Na^+ depolarizes the cell membrane resulting in a loss of $\Delta\Psi$. Interestingly, Tse4 does not affect the ΔpH suggesting the pores are impermeant to H^+. This finding suggests Tse4 pores are structured to selectively allow only specific ions through the channel, the most likely of which given our data are monovalent cations.

At the molecular level, it would be interesting to uncover how Tse4 and homologous pore-forming toxins mediate ion selectivity within the channel, and if these proteins differ in structure from other characterized pore-forming toxins. Cation-selective channels often have a set of conserved acidic residues that interface with the cation to promote selectivity, and intriguingly, Tse4 has two conserved aspartate residues within its first transmembrane domain[125,126]. Therefore, it is tempting to hypothesize these amino acids could help coordinate ion selectivity. Structurally, many pore-forming toxins domains consist of several α-helical bundles that are configured to be amphipathic on the peripheral surface in order to protect a buried hydrophobic

α-helical hairpin[124]. Circular dichroism analysis of purified Tse4 suggests the protein is composed of entirely α-helices which is consistent to previous reports of toxins with similar activity.

Lastly, we found Tse4 potency relies on the concentration of the extracellular salinity, raising a couple of attractive ideas. One is that there are likely other effectors with conditional efficacy depending on the external environment. Previous studies noted that peptidoglycan-targeting T6-effectors are toxic in media with low osmolarity and adding NaCl to the media rescued intoxicated cells viability[31]. This implies that Tse4 activity and peptidoglycan hydrolase activity are reciprocally efficacious depending on salinity. One potential idea is that each secreted effector will not be maximally effective in a given environment. Secreting multiple toxins could be a bet-hedging strategy where a T6SS+ organism increases their chances of competitive success in any condition.

V. Materials and Methods

Bacterial strains, plasmids and growth conditions

All *P. aeruginosa* strains were derived from the sequenced strain PAO1[127] and were grown on Luria–Bertaini (LB) medium at 37 °C supplemented as appropriate with 30 μg ml^{-1} gentamicin, 25 μg ml^{-1} irgasan, 75 μg ml^{-1} tetracycline, 5% (*w/v*) sucrose, 0.2 mM IPTG (isopropyl β-D-1-thiogalactopyranoside), 0.02% (w/v) arabinose and 40 μg ml^{-1} X-gal (5-bromo-4-chloro-3-indolyl β-D-galactopyranoside). *Escherichia coli* was grown in LB medium supplemented as appropriate with 15 μg ml^{-1} gentamicin, and 0.2 mM IPTG. *E. coli* strains DH5α, BL21(DE3) and SM10 (Novagen) were used for plasmid maintenance, gene expression and conjugative transfer, respectively. Plasmids pPSV39-CV was used for inducible expression in *P. aeruginosa* and *E. coli*. Site-specific chromosomal insertions in *P. aeruginosa* were generated using pUC18-Tn7t-pBAD-*araE* (*glmS*) or pMiniCtx-1 (*attB*) as previously described[128,129].

Growth competition assays

For *P. aeruginosa* competitions, the recipient strain contained *lacZ* (tetracycline resistant) inserted at the neutral phage attachment site (*attB*) to enable its differentiation or selection from the unlabeled donor strain when plated on LB containing X-gal (40 μg ml^{-1}) or tetracycline (75 μg ml^{-1}). Overnight cultures of donor and recipient strains were washed, A_{600} standardized, and mixed at the ratios indicated. Competition mixtures (5 μl) were then spotted in triplicate on a 0.2 μm nitrocellulose membrane overlaid on a 3% (w/v) agar plate of the indicated media and incubated face up at 37 °C for 8 h unless denoted otherwise. Competitions were harvested from the nitrocellulose membrane and resuspended into LB medium. Initial and final populations of donor and recipient cells were enumerated following serial dilution on appropriate selective or differentiation media. The competitive index (CI)is defined as:

$$\mathrm{CI} = \frac{\mathrm{Final}\left(\frac{\text{donor c. f. u.}}{\text{recipient c. f. u.}}\right)}{\mathrm{Initial}\left(\frac{\text{donor c. f. u.}}{\text{recipient c. f. u.}}\right)}$$

P. aeruginosa toxicity assays

For toxicity assays, overnight cultures of *P. aeruginosa* expressing mCherry from a neutral site chromosomal gene insertion (attTn7::*mCherry*) were normalized to an OD_{600} of 1, diluted in 10-fold increments, and each dilution was spotted onto LBNS 3% (*w/v*) agar plates supplemented with the indicated solutes. Plates were incubated 16 hours at 37°C, then fluorescence was imaged using a FluorChem Q imaging system (Protein Simple).

Potassium release assays

P. aeruginosa strains were grown overnight in a low K^+ media (10 mM bis-tris propane pH 7.0, 5 mM succinate, 2 mM $MgCl_2$, 5 mM $(NH_4)_2SO_4$, 1 mM Na_2HPO_4, 10 μM $Fe(NH_4)SO_4$, 0.1% (*w/v*) tryptone, 0.005% (*w/v*) yeast extract). Overnight cultures were back diluted 1:100 in low K^+ media,

grown to mid-log phase, pelleted by centrifugation at room temperature, and the OD_{600} set to 2 in a 5 mL volume of low K^+ medium. Cultures were then induced with 0.02% (*w/v*) arabinose for the indicated times, cells were pelleted by centrifugation, and the supernatant collected and sterilized through a 0.2 μm cellulose acetate membrane filter (VWR, Radnor, PA). As a positive control for maximal potassium release, cells were lysed by sonication and subsequent boiling. Potassium measurements were performed by inductively coupled plasma-optical emission spectrometry (ICP-OES Optima 8300, Perkin Elmer, Waltham, MA) operating both 766.4 and 404.7 nm emission lines. Data were calibrated with a potassium standard (Sigma-Aldrich).

Cytoplasmic membrane permeability assays

Propidium iodide (668.4 Daltons): Overnight cultures of *P. aeruginosa* strains were diluted 1:100 in LB medium, grown to mid-log phase, and induced for one hour with 0.02% (*w/v*) arabinose or incubated with the pore-forming protein control (5 μg/mL pyocin S5). Cells were collected by centrifugation and washed twice with 1 mL phosphate buffer saline (PBS, pH 7.1). Bacterial cells equivalent to 1 mL at OD_{600}=1 were incubated with 5 μg/mL propidium iodide in the dark for 10 min, then fluorescence was measured (ex. 353 nm/ em. 353 nm).

ONPG (301.3 Daltons): Overnight cultures of bacterial strains encoding *lacZ* inserted at attB were diluted 1:100 in LB, grown to mid-log phase, and induced for one hour with 0.02% (*w/v*) arabinose or incubated with the pore-forming protein control (5 μM pyocin S5). Bacterial cells equivalent to 1 mL at OD_{600}=0.5 were collected by centrifugation and washed twice with 1 mL PBS. Cells were resuspended in 1 mL PBS, diluted 1:10 into PBS containing 2 mM *o*-nitrophenyl-β-glactoside (ONPG, Research Products International, Mount Prospect, IL), and shaken at 37°C for 1.5 hours. Absorbance at 420 nm was then measured to quantify ONPG turnover by intracellular β-galactosidase.

Membrane potential studies

Overnight cultures of bacterial strains were diluted 1:100 in LB medium, grown to mid-log phase, and induced with 0.02% (*w/v*) arabinose for one hour. Cells were pelleted by centrifugation and the OD_{600} set to 1. Cells (10 μl) were added to a staining mixture containing 30 μM $DiOC_2(3)$. (Thermo Fisher) and 5 mM EDTA ± 5 μM carbonyl cyanide *m*-chlorophenyl hydrazine (CCCP, Sigma-Aldrich) and incubated at room temperature for 10 minutes in the dark. Samples were analyzed on a BD LRSII flow cytometer with excitation at 488 nm and reading emission using GFP 530/30 (505 LP) and BV605 610/20 (585 LP). We recorded 10,000 events and gated out forward scatter and side scatter outliers before data analysis (between 300-700 events were removed). The red/green (BV605/GFP) fluorescence intensity values for each population were determined.

Intracellular pH assays

The pH-sensitive protein pHluorin2 (a GFP derivative) was used to monitor intracellular pH levels. This protein was expressed in *P. aeruginosa* via IPTG induction from the plasmid pPSV39-CV::*pHluorin2*. Overnight cultures of strains carrying this plasmid were diluted 1:100 in LB medium with 0.2 mM IPTG, grown to mid-log phase, then treated with 0.02% (*w/v*) arabinose for one hour to induce Tse4 production. Cells were pelleted by centrifugation and duplicate samples were resuspended to OD_{600}=2.5 in 200 mM potassium phosphate buffer at each of the following pHs: 5.7, 6.3, 7, and 8. 40 mM sodium benzoate was added to one sample at each pH (positive control for proton motive force disruption), while the second sample was untreated. After 20 min, we then measured the ratio of absorbance at 392 and 470 nm; low intracellular pH is indicated by a decrease in the 392/470 nm absorbance ratio for pHluorin2.

Preparation of proteins for Western blotting

To co-purify Tse4 and Tsi4, an overnight culture of *E. coli* harboring pETDuet-1 (mcs1:: *tsi4-his*$_6$, mcs2:: *vsv-g*-tse4) was diluted 1:200 in fresh media and incubated at 37°C until mid-log phase. Cultures were then induced with 0.5 mM ITPG, harvested 4 hours post-induction by centrifugation at 4,000 x g for 10 minutes, and pellets resuspended in 2 mL Wash Buffer (50 mM Tris-HCl pH 7.5, 500 mM NaCl, 2% glycerol) with 1 mg/mL lysozyme, 0.5 mg/mL DNase, and 1% Triton X-100. The resuspension was manually lysed through sonication, centrifuged at 4°C for 30 minutes at 16,000 x g, and lysates applied to 250 μL of Ni-NTA beads (Qiagen). Beads were incubated with rotation for 1 hour at 4°C, washed 3 times in 10 mL of Wash Buffer with 0.1% Triton X-100, and protein was eluted with 300 μL of Wash Buffer containing 500 mM imidazole pH 7.4 and 0.1% Triton X-100. For secretion assays, samples were prepared as previously described[100]. All proteins samples were analyzed by SDS-PAGE and Western blotting as previously described using rabbit α-VSV-G (1:5000, Sigma) and mouse α-RNAP (1:5000, BioLegend) and then detected with α-rabbit and α-mouse horseradish peroxidase-conjugated antibodies (1:5000, Sigma)[130]. Western blots were developed using chemiluminescent substrate (SuperSignal West Pico Substrate, Thermo Scientific) and imaged with a FluorChemQ (ProteinSimple, San Jose, California).

Circular dichroism (CD)

(CD) spectra were collected on a JASCO J-815 CD spectropolarimeter. Tse4 was diluted to 20 μM into CD buffer (25 mM HEPES pH 7.5, 100 mM NaCl, and 0.1% DDM). CD spectra were acquired over a wavelength range of 250-180 nm with a data pitch of 0.5 nm and with a scanning speed of 10 nm/min. To overcome the high absorbance of the buffer the bandwidth was set to 15 nm. (This work was done with the help of the Klevit laboratory at the University of Washington)

Microscopy

Overnight cultures were diluted 1:50 or 1:100 in LB and incubated with aeration at 37°C until an OD_{600} of 0.5–0.7 was reached. 1–2 µl of the bacterial suspension was spotted onto a 2% *wt/vol* agarose growth pads (prepared using Vogel Bonner minimal media containing 0.2% wt/vol potassium nitrate and 0.01% wt/vol casamino acids) and sealed to prevent evaporation. Microscopy data were acquired using NIS Elements (Nikon) acquisition software on a Nikon Ti-E inverted microscope with a 100x oil objective, automated focusing (Perfect Focus System, Nikon), and a CCD camera (Andor). Growth rate were measured from TLFM sequences acquired at 25-min intervals.

Purification and Crystallization

Protein expression constructs (pETDuet-1 mcs1:: *tsi4-his*$_6$, mcs2:: *vsv-g*-tse4 and pET15b::*tse4*) were transformed into E. Coli BL21 (DE3) cells. Cells were grown at 37°C in 2XYT with shaking to A_{600} 0.5 prior to induction with 0.5 mM IPTG. Post-induction, cells were grown for 16 hours at 18°C before being pelleted by centrifugation and flash-frozen. Cell pellets were resuspended in 40 mL of 40 mM Tris-HCl pH 8.0, 500 mM NaCl, 2% glycerol with additional 10 µl of 10 mg/mL DNase , 10 µl 100 mg/mL lysozyme, and 40 µl of 100mM PMSF. This resuspension was passed through a homogenizer 3x to lyse the cells. Homogenized cells were spun at 42K RPM for 1 hour in an ultracentrifuge using a Ti45 rotor. Supernatant containing the periplasmic and cytoplasmic fractions was discarded, and the membrane pellet was resuspended with a dounce homogenizer in the original lysis buffer and then incubated with 1.5% DDM for 3 hours at 4°C, while rocking. Insoluble matter was spun down in an ultracentrifuge at 42K for 1 hours in a Ti70 rotor. Supernatant was saved as the soluble membrane protein fraction. This was passed over a 1mL resin bed volume of Ni-NTA super flow beads using gravity filtration, and the flow-through was re-applied over the column once. This was washed with 50x the bed volume of wash buffer: 40 mM Tris-Hcl pH 8.0, 500 mM NaCl , 2% glycerol, 15 mM imidazole, 0.04% DDM. The sample was

batch eluted twice with 1 mL wash buffer + 300 mM imidazole. The resulting protein from Ni-NTA chromatography was concentrated using a 50K MWCO concentrator using a Thermo Scientific Sorvall ST110R. 500ul of this sample was applied to a Superdex s200 increase 10/300 GL gel filtration column equilibrated with 20 mM Tris-HCl pH 8.0, 100 mM NaCl, 0.017% DDM). The resulting protein elution was used for *in vitro* experiments and for crystallography.

Proteins were concentrated to 15 mg/mL and screened for crystallization conditions using the hanging drop vapor diffusion technique and commercially available crystallization suites (MCSG1-4, Anatrace and MemGold 1-2, Molecular Dimensions). After 1 week, polycrystalline clusters of the Tse4–Tsi4 complex were obtained in 24% PEG400 and 0.05% ADA pH 6.5. Crystals were-flash frozen in 30% PEG400 and diffraction data collected on the BL502 beamline at the ALS, Lawrence Berkeley National Laboratory). (This work was performed by Kaitlyn L. in both the Mougous laboratory at the University of Washington and the Gonen Laboratory at Janelia Research Campus in Virginia as a visiting scientist.)

Planar Lipid Bilayer Electrophysiology

Planar lipid bilayer currents were recorded using an Axopatch 200B. Membraned were painted on a 50-μM aperture of a 1 mL white Delrin cup with 3% (wt/vol) 1,2-diphytanoyl-*sn*-glycerol-3-phosphocholine (DphPC from Avanti) in undecane. Measurements were recorded at 40 mV, and the membrane was bathed in a bilayer chloride buffer (5 mM succinate, 5 mM phosphate, 1 mM EDTA, 100 mM sodium chloride). 5μl of 0.1 mg/mL purified Tse4 was added to the cis chamber for analysis. (This work was done with the help of Dr. Bryan Krantz's laboratory at the University of Maryland)

VI. Figures

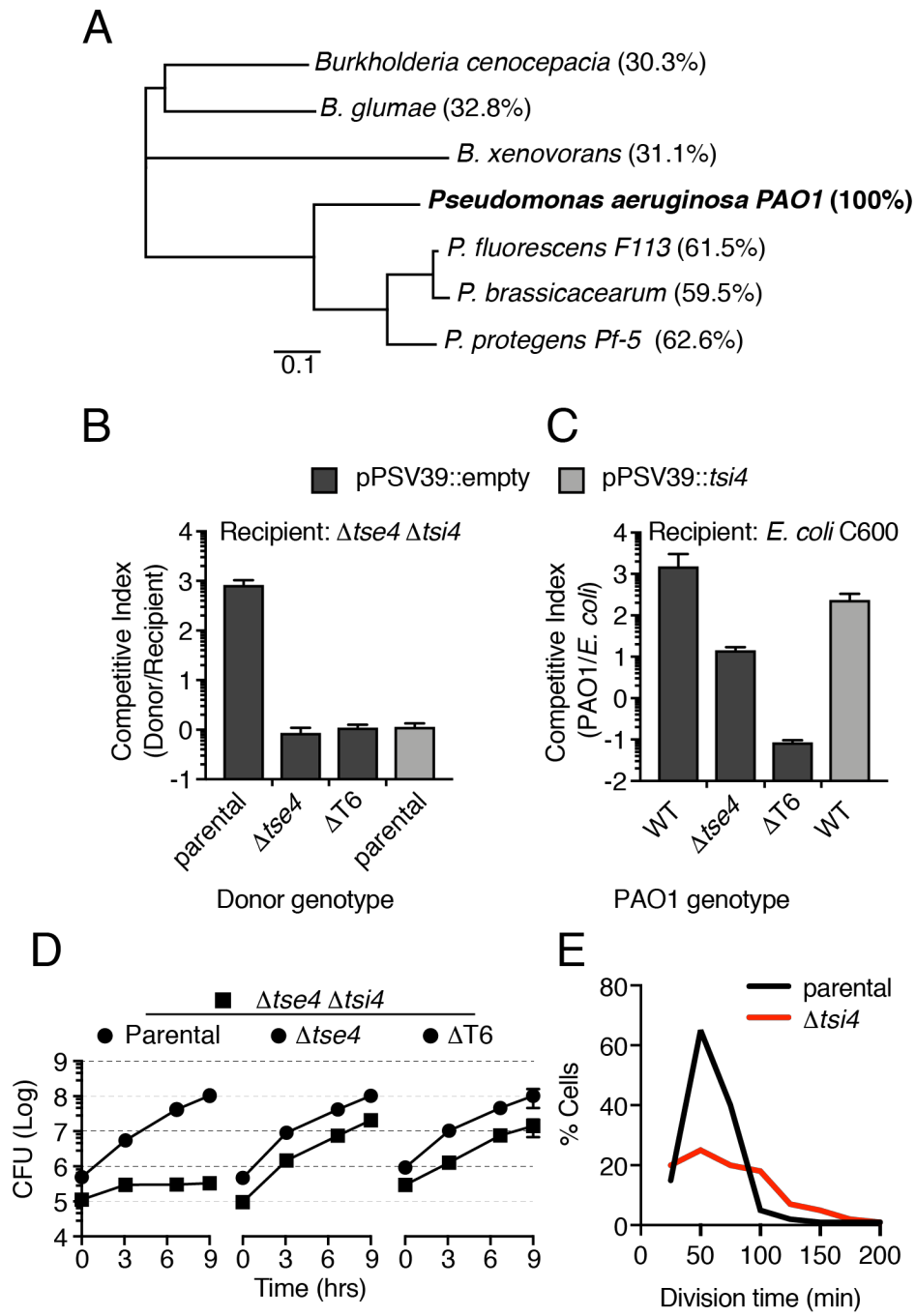

Figure 2.1: Tse4 is a toxic protein that induces bacteriostasis in targeted cells
(**A**) Tree of *P. aeruginosa* Tse4 homologs by % amino acid ID. (**B**) Intraspecies co-culture competition of *P. aeruginosa* with constitutive T6+ activity (Δ*retS*) with a Tse4-sensitive recipient (Δ*tse4* Δ*tsi4*). (**C**) Interspecies co-culture competition of *P. aeruginosa* and *E. coli* C600. (**D**) Growth of a Tse4-suseptible strain (Δ*tse4* Δ*tsi4*) and the indicated co-cultured strains on a solid medium. CFU, colony-forming units. (**E**) The division time of cell populations determined through microscopy using the SupperSegger software.

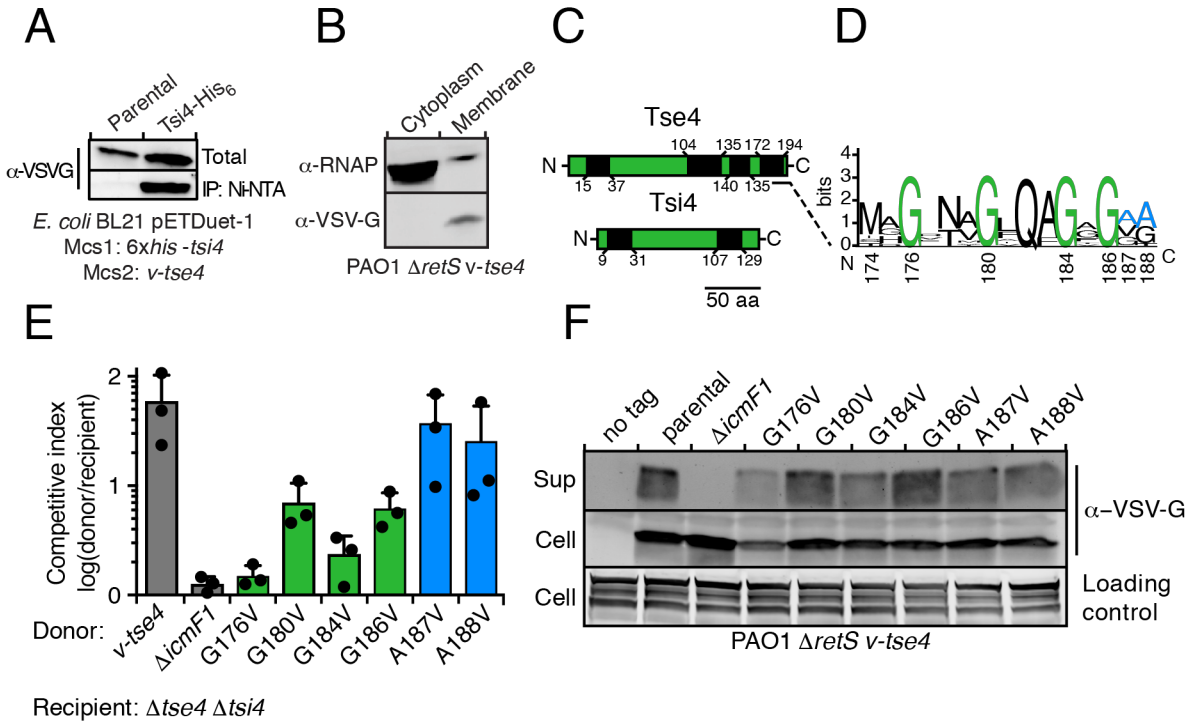

Figure 2.2: A functional transmembrane glycine zipper is important for Tse4 activity(**A**) Immunoblot detecting total and bead-associated fractions of a nickel-NTA precipitation assay from E. coli expressing N-terminally VSV-G epitope-tagged Tse4 (V–Tse4) and C-terminally hexahistidine-tagged (Tsi4-His6). This experiment was repeated two times independently with similar results. (**B**) Western blot probing for Tse4 and RNAP in the cytoplasmic and membrane fractions of *P. aeruginosa*. (**C**) Predicted transmembrane regions (black) in Tse4 and Tsi4 as determined by TMHMM. (**D**) Sequence logo depicting C-terminal region of conserved glycine residues generated from alignment of 12 Tse4 homologs representing its sequence diversity in the non-redundant database. Conserved glycines are colored green and residues outside the proposed zipper used for control substitutions are colored blue. (**E**) Results of growth competition experiments between donor strains expressing vsvg-tse4 alleles encoding the indicated amino acid substitutions from the native chromosomal locus versus a Tse4-sensitive recipient strain (n=3 biologically independent experiments). Data presented as mean values ± standard deviation. (**F**) Western blot analysis of the intracellular and extracellular levels of Tse4 variants produced by strains in (D) Intracellular levels of RNA polymerase (RNAP) is used as a loading control.

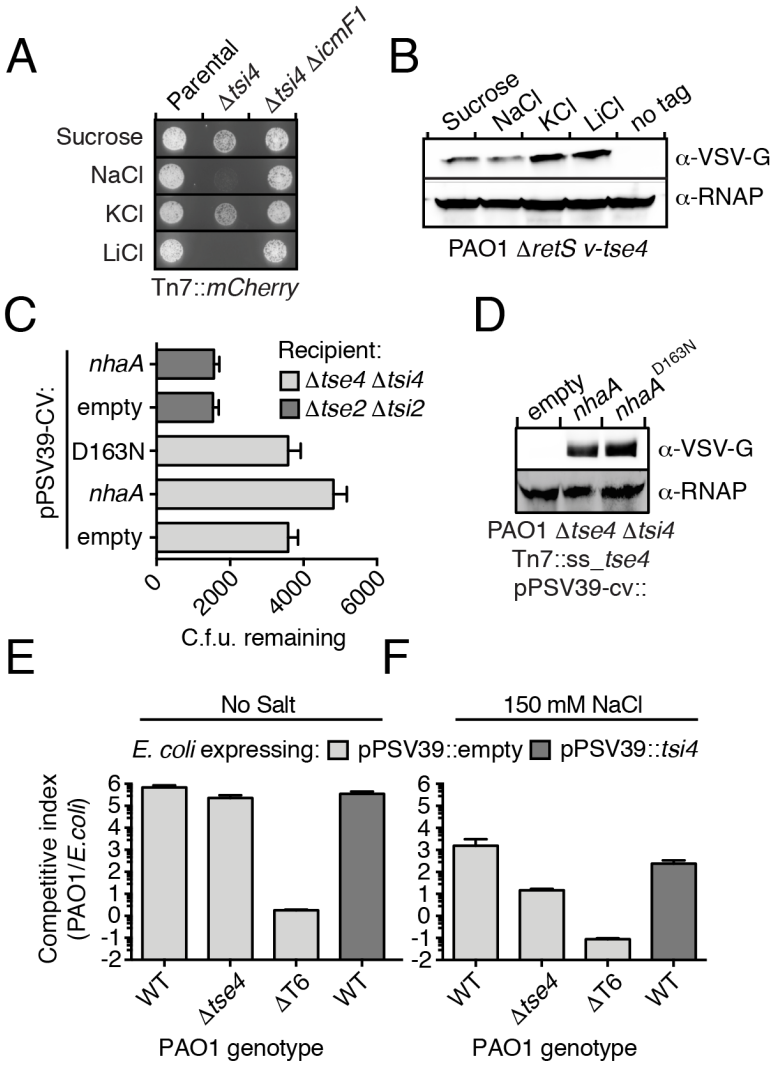

Figure 2.3: Tse4-intoxicated cells are sensitive to sodium and lithium ions
(**A**) Growth of the specified strains after a 16 h incubation on solid growth medium supplemented with the indicated solutes (sucrose, 300 mM; NaCl, 150 mM; KCl, 150 mM; LiCl, 20 mM). (**B**) Western blot of intracellular Tse5 levels from cell grown under conditions in (A). RNAP is used as a loading control. (**C**) Co-culture competition measuring the contribution of over-expressing the Na^+/H^+ antiporter form *E. coli* to the fitness of recipient cells during competition. Tse2 intoxication was used as a negative control. (**D**) Western blot of intracellular levels of NhaA under conditions used in (C). (**E+F**) Interspecies co-culture competition between PAO1 and *E. coli* performed on LB agar with and without 150 mM NaCl. *E. coli* strains harbored either an empty expression vector, or a plasmid expressing PAO1 *tsi4*.

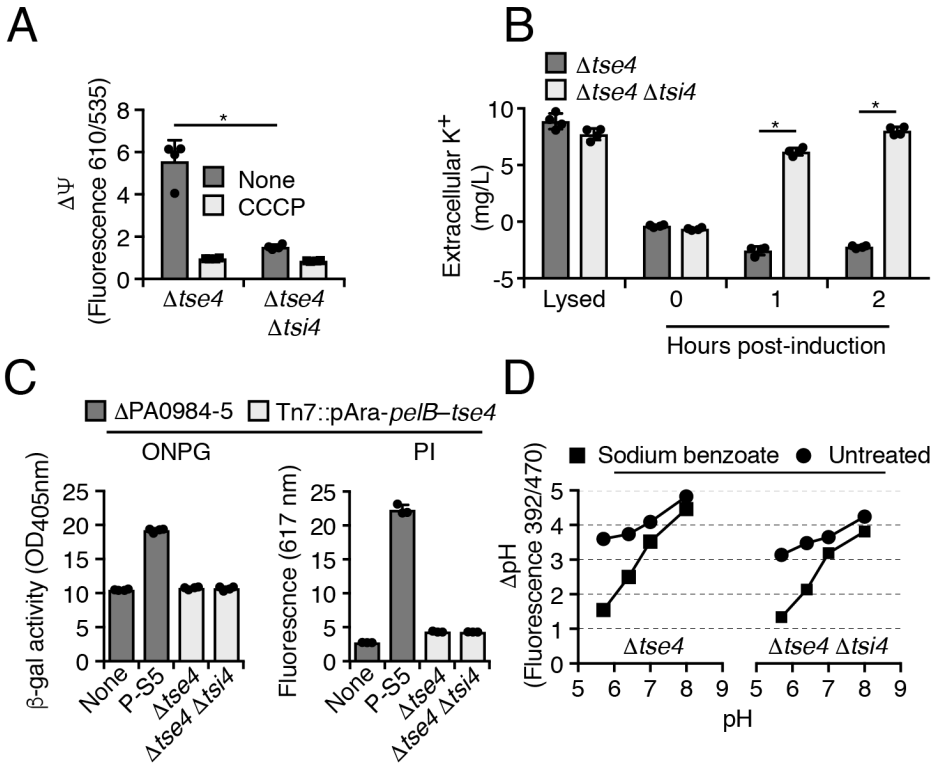

Figure 2.4: Tse4 depolarizes cell membranes via selective ion permeability
(**A**) Membrane polarization of Tse4-expressing cultures. CCCP-treated cultures (light grey) included as depolarized controls. Membrane potential is indicated by the ratio of fluorescence intensities (610/535 nm) emitted by cells treated with $DiOC_2(3)$. (**B-D**) Changes to membrane permeability assessed through ectopic, periplasmically targeted expression of Tse4 (Tn7::pAra-*pelB–tse4*) in PAO1 populations susceptible (Δ*tse4* Δ*tsi4*) or resistant (Δ*tse4*) to Tse4 intoxication. (**B**) Extracellular K^+ levels measured in the supernatants of Tse4-expressing cultures (susceptible, light grey; resistant, dark grey). Lysed cells provide the maximal concentration that can be released. (**C**) Intracellular uptake of ONPG or PI by cells rendered genetically susceptible to the non-selective pore-forming toxin pyocin S5 (dark grey bars) or by cells expressing Tse4 (light grey bars) ($n = 3$ biologically independent samples). ONPG uptake monitored through intracellular β-galactosidase-meditated release of *o*-nitrophenol ($A_{405\ nm}$); PI uptake monitored through intracellular fluorescence (617 nm). (**D**) Intracellular pH change in Tse4-expressing cells incubated in buffers of varying pH. Sodium-benzoate-treated populations included as a control for proton gradient dissipation. Intracellular pH indicated by ratio of excitation peaks (392/470 nm) exhibited by pHluorin2 expressed by each population.

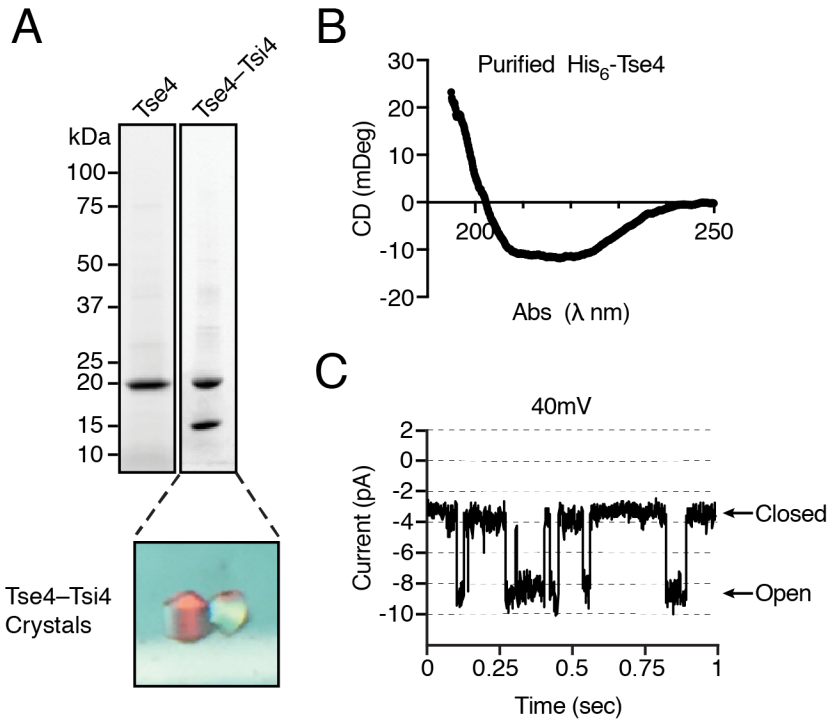

Figure 2.5: Purified Tse4 is predominately α-helical and forms pores in lipid bilayers
(**A**) Top, comassie stain of purified Tse4 and Tse4–Tsi4 complex. Bottom, crystals of the Tse4-Tsi4 complex. Bottom, crystals of the Tse4–Tsi4 complex. (**B**) Circular dichroism of 20 μM Tse4. The peak at 208 and 222 nm is indicative of a folded α-helices-containing protein. (**C**) Multiple pores formed by His_6-Tse4 were incorporated into the lipid bilayer under voltage clamp conditions. Membrane was DphPC (30 mg/mL) in undecane, and the buffer was succinate pH 5.6 with NaCl as the salt. 5 μl of 0.1 mg/mL Tse4 was added to cis-chamber.

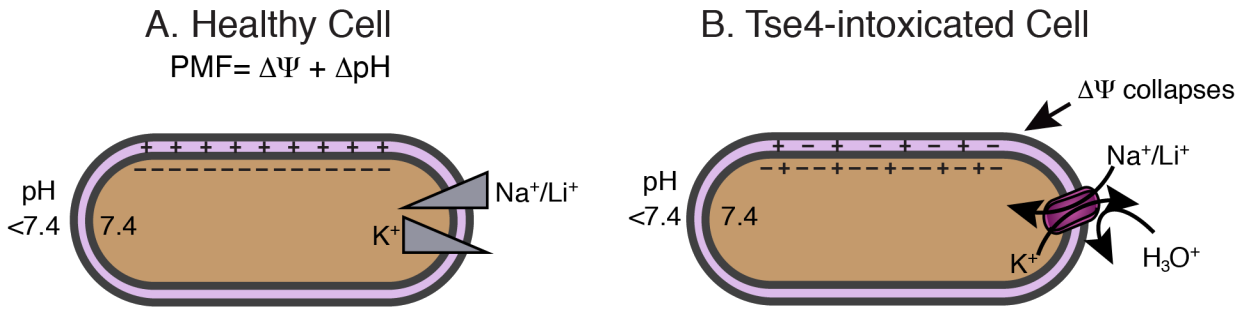

Figure 2.6: Model of Tse4 toxicity
(**A**) Schematic of a healthy bacterial cell. There is an intact membrane potential across the inner membrane. Na^+ and Li^+ ions are excluded using antiporters, while K^+ ions are accumulated using various uptake systems. These ions gradients in conjunction with the proton gradient establish the proton motive force (PMF) which cells use to generate ATP. The PMF is the sum of the membrane potential ($\Delta\Psi$) and the ΔpH. (**B**) In Tse4-intoxicated cells we hypothesize Tse4 is forming a pore in the inner membrane which allows Na^+, Li^+ and K^+ to freely traverse this barrier. This leads to the collapse of the $\Delta\Psi$ and disrupts the PMF resulting in bacteriostasis and eventual cell death.

Chapter 3: Investigating the cellular benefits of system and effector level diversity of T6SSs

Portions published in: **LaCourse K.,** Peterson SB., Kulasekara HD., Radey MC., Kim J., Mougous JD. Conditional toxicity and synergy drive diversity among antibacterial effectors. *Nature Microbiology* 3, 400-446. (2018).

I. Abstract

Bacteria in polymicrobial habitats contend with a persistent barrage of competitors, often under rapidly changing environmental conditions[1]. The direct antagonism of competitor cells is thus an important bacterial survival strategy[131]. Towards this end, many bacterial species employ an arsenal of antimicrobial effectors with multiple activities; however, the benefits conferred by the simultaneous deployment of diverse toxins are unknown. Here we show that the multiple effectors delivered to competitor bacteria by the type VI secretion system (T6SS) of *Pseudomonas aeruginosa* can act synergistically and display conditional efficacy dependent on the environment and the species targeted. Our results provide evidence that the concomitant delivery of a cocktail of effectors serves as a bet-hedging strategy to promote bacterial competitiveness in the face of unpredictable and variable environmental conditions.

II. Introduction

The T6SS is a functionally plastic pathway that is used by many bacteria to translocate toxic effector proteins into adjacent cells[18,30,132,133]. Effectors that target bacteria generally degrade conserved, essential cellular structures, and, as such, single effectors are sufficient to kill or terminate growth[12,32]. Despite the capacity of single effectors to kill target cells, the γ-proteobacterium *Pseudomonas aeruginosa* delivers a diverse cocktail of effectors that degrade, among other structures, phospholipids, peptidoglycan and nicotinamide adenine dinucleotides[31,64,72]. The T6SSs of other experimentally characterized bacteria also deliver effectors that target multiple essential molecules[32,77]. To estimate the generality of this phenomenon, we searched the genomes of 2,566 sequenced proteobacterial species for T6SS effectors with known activities. Only 42% ($n = 474$) of the species within this group that contain the T6SS also contain an effector of known activity, suggesting that many as yet undescribed effectors exist. Nevertheless, we found that 40% ($n = 196$) of these species possess a second effector with unique biochemical activity, and 25% ($n = 52$) possess three or more. Such

bacteria were identified in four of the five major classes of Proteobacteria (Figure 3.1). These data suggest that bacteria benefit from the coordinated delivery of effectors with diverse biochemical activities.

We considered the potential benefits that could select for and maintain a diversity of T6SS effectors. Utilizing multiple antibiotic mechanisms simultaneously is a well-documented strategy for minimizing the evolution of resistance[78]. This strategy might also overcome potential intrinsic resistance mechanisms present in the wide phylogenetic range of bacteria targeted by the T6SS. Preventing resistance may contribute to effector expansion, but because of the essentiality and structural conservation of T6SS effector targets, we reasoned it is unlikely to be the only selective pressure driving the extent of effector diversity observed.

Two additional benefits conferred by a diverse effector arsenal could be that the toxins act with synergy on recipient cells or that they display conditional efficacy. The former is defined by instances in which the activity of two or more effectors on recipient cells is greater than the sum of their individual activities, whereas the latter is defined by effectors that contribute to recipient cell intoxication in a manner dependent on the environmental conditions. Synergy and conditional efficacy among T6 effectors have not been explored, and we reasoned that both offered a potential explanation for the effector diversity observed. It is worth noting that these scenarios are not mutually exclusive.

III. Results

Development of Parallel Analysis of Effector Efficacy

To interrogate T6 effectors in a high-throughput fashion, we developed a sequencing-based, pooled strategy for measuring their activity during interbacterial competition (Figure 3.2). Henceforth, we refer to this method as PAEE (Parallel Analysis of Effector Efficacy). Briefly, we introduced unique barcode sequences to a library of *P. aeruginosa* strains rendered susceptible to intoxication by one or two effectors of the Hcp Secretion Island I-encoded T6SS (H1-T6SS)

through the deletion of effector–immunity gene pairs. Thus, only effectors with an experimentally defined cognate immunity determinant were included (Tse1-6). Prior studies established the antibacterial activity of these effectors, though the precise biochemical mechanisms of Tse2, Tse4 and Tse5 remain unknown (Figure 3.2a). A pool of the barcoded mutants and a barcoded toxin-resistant reference strain was then cultivated under a variety of conditions with an excess of the unmarked parental strain acting as a toxin donor. Susceptibility to intoxication was assessed by comparing the frequency of the barcode associated with a given mutant to the reference strain at the beginning and end of the experiment (Figure 3.2b,c). To uncouple the potential contribution of regulation from the inherent biochemical capacity of effectors to act synergistically or conditionally, we utilized a background of *P. aeruginosa* (Δ*retS*) in which Tse1-6 are produced constitutively[134]. Data presented herein derive from four independent repetitions of PAEE.

Prolonged cell–cell contact is critical for T6SS-mediated effector translocation[135]. Conditions that do not permit extended contact, such as cultivation on semi-solid surfaces or in liquid, thus provide a convenient means of specifically evaluating the contribution of the T6SS to fitness4. Consistent with this, we found that our barcoded effector-susceptible strains displayed fitness defects only when cultivated under T6S-conducive conditions (Figure 3.3). Moreover, we noted that the relative magnitude of individual effector activities under T6S-conductive conditions approximated those observed in earlier studies.

PAEE reveals effectors with conditional activity

With this validation of our method, we sought to examine whether T6SS effectors display conditional efficacy. We measured effector activity under growth conditions varying in parameters that are likely in flux across the environmental habitats where *P. aeruginosa* resides, including salinity, temperature, oxygen availability and pH. PAEE identified several conditions in which the relative efficacy of effectors varied compared to a reference condition, including high salinity, anaerobiosis, high temperature, and alkalinity (Figure 3.4a-d). For instance, between pH 6 and

pH 8, the relative activity of Tse5 increases seven-fold, whereas that of Tse3 decreases by 50%. Importantly, these results reproduced in pairwise interbacterial competition assays (Figure 3.5a,b). In total, we observed that the efficacy of each of the six effectors examined can be significantly altered between one or more of the conditions examined.

T6SS effector activities can be synergistic, additive, or antagonistic

Next we used PAEE to ask whether effectors can act synergistically. We found striking differences in the capacity of, and frequency by which effector pairs exhibit this behavior (Figure 3.6a-d, and Figure 3.7a-k). For example, the cumulative activity of Tse3 and Tse4 exceeds the sum of the two individual effectors in all conditions tested (Figure 3.6a). On the contrary, we did not observe an instance of synergy between Tse2 and Tse4 (Figure 3.6b). We found that effector pair synergy can also be conditional. For example, synergy between Tse1 and Tse4 was most pronounced in high salinity and synergy between Tse2 and Tse6 was detected only in anaerobiosis (Figure 3.6c and Supplementary Figure 3.7g). Though infrequent, we found that the cumulative activity of two effectors can be less than that of the most active of the two effectors alone. In these instances, intoxication by one effector apparently diminishes the potency of the other. The majority of effector pairs did not exhibit this inhibition; however, the cumulative activity of Tse4 and Tse5 was at or below that of the more active single effector under most conditions analyzed (Figure 3.6d). Pairwise co-cultivation experiments validated instances of each category of behavior observed by an effector–immunity pair in our PAEE screen (Figure 3.7l). Finally, we noted that effectors of *P. aeruginosa* do not equally participate in synergistic interactions; only Tse1, Tse4 and Tse6 were members of multiple strongly synergistic pairs (Figure 3.6e). Together, these data indicate the capacity for T6SS effectors to act both conditionally and synergistically.

The genetic background employed in PAEE enforces constitutive effector production, which minimizes the potential impact of regulatory inputs. To understand the potential for effector expression to affect conditional toxicity and synergy, we measured the expression of *tse*1-6 in

wild-type *P. aeruginosa* under conditions matching those used above. Consistent with previous data, we found that effector expression levels are positively correlated with genes encoding the T6S apparatus (p=0.03). Interestingly, we did not find that the expression of effectors is generally elevated under conditions optimal for their intrinsic activity (Figure 3.6f). These data suggest that conditional effector efficacy in *P. aeruginosa* is achieved primarily by the conditional nature of intrinsic effector mechanisms rather than by differential regulation.

The H1-system is the predominant T6SS in interspecies antagonism

We have thus far discovered that an effectors biochemical activity can be conditionally toxic as well as synergize with other T6SS-toxins functions within the same bacterial cell. We next wanted to ask whether toxin diversity could allow for more effective targeting of a wide-phylogenetic range of bacterial species that may harbor intrinsic differences within an effectors target substrate. To explore T6SS activity on interspecies antagonism, we developed a 17-member multispecies community that includes several classes of proteobacteria and more distant phyla (Figure 3.8a). All of the members in this community can grow from 22-30°C and proliferate on tryptic soy media supplemented with 0.1% cysteine. To assess the ability of *P. aeruginosa* to intoxicate these species, we utilized a 16 sequencing-based, pooled strategy to measure T6 activity during interbacterial competition. We decided to undergo a two-tier approach to address this question. The first level was to identify which *of P. aeruginosas'* three T6SSs (H1-H3), all of which contain antimicrobial toxins, are responsible for activity against targeted species. The second layer was to determine the contribution of individual effectors to T6SS toxicity.

The *P. aeruginosa* genome encodes three T6SSs, termed H1-H3, that are each capable of intoxicating other bacteria. There is no overlap in the specific activities of known effectors of these T6SSs and each system is highly regulated. The H1-T6SS is transcriptionally repressed by quorum sensing and post-transcriptionally repressed by the Gac/Rsm system[101]. This post-transcriptional repression can be relieved through the binding of an unknown ligand found in kin

cell lysate. Therefore, the H1-T6SS is active during early stages of growth when a subset of the population of nearby cells has lysed. The H2- and H3-T6SS are positively regulated by quorum sensing, and therefore would be expressed during later stages of bacterial cell growth.

Additionally, the H2-T6SS activity increases under iron-limiting conditions and at lower temperatures, while the H3-T6SS is further activated by the transcription factor RpoN, which is expressed during stationary phase[103,104]. Therefore in a natural setting, all three of these antibacterial T6SSs may not be active at the same time. However, during the timescale of a bacterial competition, we believe all three of these T6SSs may be utilized to mediate antagonism.

To identify which bacterial species are undergoing T6-mediated antagonism, we performed multispecies co-culture competitions. These assays were done in the presence of excess *P. aeruginosa* capable of using all three of its T6SSs or with a T6- mutant strain in which essential T6 structural components were deleted (*icmf1*, *icmf2*, and *icmf3*). To measure each T6SSs contribution to overall T6 activity, we made pairwise T6 inactivating mutations to yield strains with only one functional system (H1, H2, or H3). These single T6SS co-culture experiments were compared to our wild-type and T6- control strains to access their influence on recipient fitness. We found that T6-mediated antagonism was driven entirely by the activity of the H1-T6SS against the majority of species tested (Figure 3.8b,c). In rarer circumstances, each T6SS contributed to intoxication of the recipient, such as against *Xanthomonas maltophilia* (Figure 3.8d). Multiple species experienced no targeting by any *P. aeruginosa* T6SS (e.g. *E. coli*, *Listeria monocytogenes*, *Francisella novicida*; data not shown). Since a wide phylogenetic array of species is available within the community, we wondered if the H1-T6SS was targeting any particular type of bacteria. To assess this, we calculated the average change in targeted species availability in the population by class/phyla when the H1-T6SS was present versus a T6- strain. We found the H1-T6SS targeted mainly α and β-proteobacteria under our experimental conditions (Figure 3.8e). The H2-T6SS and the H3-T6SS also targeted β-proteobacteria, but to a lesser

extent (Figure 3.8f,g). Our data suggest that the *P. aeruginosa* H1-T6SS is the most commonly utilized T6SS for bacterial antagonism.

Effectors within the H1-T6SS differentially contribute to toxicity between species

To measure species-specific effector toxicity, we generated strains capable of utilizing either six of the H1-T6SS effectors (Tse1, 2, 3, 4, 6 and 7), only one of each of these effectors, or no effectors at all. Single-effector strains were produced by making combinatorial chromosomal point mutations (or in the case of *tse4*, and entire chromosomal deletion) known to inactivate the catalytic activity of the toxin[54,72,136]. Point mutations were chosen to maintain similar levels of secretion of the overall effectors, but only one protein will retain toxic activity. Tse4 is an effector delivered via the chaperone Hcp, and no known single mutation completely abrogates its function; therefore a chromosomal deletion was made for this effector. We ensured none of the other Hcp-associated effectors, Tse1-3, exhibited increased activity in a Δ*tse4* background suggesting there is not amplified secretion of these effectors (data not shown). Tse5, a VgrG-chaperone linked effector, was excluded from this study due to no apparent candidates for mutagenesis and deletion of *tse5* is known to result in increased secretion of Tse6. These strains were generated in a Δ*retS* background to facilitate constitutive activation of the H1-T6SS and to uncouple the contribution of regulation from the inherent biochemical capacity of the effectors to intoxicate a species. Additionally, the H2 and H3-T6SSs were inactivated in this background, via Δ*icmF2* and Δ*icmF3* mutations, to ensure the only T6 activity was mediated through the H1-T6SS.

We found there are multiple instances where effector contribution changes dramatically depending on the recipient organism (Figure 3.9 a-c). *P. aeruginosa* strains with only Tse4 or Tse6 phenocopy a donor strain with all effectors available when in co-culture against *Chromobacterium violaceum,* whereas against *Pseudomonas putida* they resemble a strain with no functional effectors (Figure 3.9 a,b). There were also instances where the majority of the single effector donors had similar activity to one another and an overall intermediate role to intoxication

compared to a parental and a fully inactivated strain, such as against the γ-proteobacterium *Enterobacter cloacae* (Figure 3.9c). The data generated in this initial screen shows effector toxicity changes dependent on the species of the targeted cell. This suggests that target specificity could influence effector expansion to maximize the cells competitive against a broad phylogenetic range of bacterial targets.

IV. Discussion

In this study, we developed two platforms to study T6SS effectors toxicity. The first assay, PAEE, allows for the parallel screening of the toxicity of all the T6SS effectors under different environmental conditions and in combination with each other to assess the potential for synergy. This technique applies to any T6SS with known conditions to activate intraspecies targeting. Additionally, this technique could provide insight for unknown effector functions by identifying environments that effect toxicity. For example, toxins that are potent in higher salinities most likely target the bacterial inner membrane, and those that target peptidoglycan will have increased toxicity under low osmotic conditions. The second assay is a convenient method to screen for interspecies interactions by utilizing a large multispecies community and using 16S to track changes in the population level for each species. Most T6SS interspecies competitions are performed strictly between two species in genetic backgrounds that artificially activate the donor bacterium's T6SS. We believe that our 16S sequencing assay will allow for discovery of antagonistic bacterial interactions in wildtype backgrounds, which could be more similar to the species natural targets in the environment.

One of the findings to emerge from our PAEE screening is that Tse4, an ion-specific pore-forming toxin, acts synergistically with peptidoglycan-targeting effectors Tse1 and Tse3, and the NAD^+ glycohydrolase Tse6 (Figure 3.6 a,c and Figure 3.7j). The synergy between Tse4 and cell wall-degrading effectors (Tse1, Tse3) may be achieved by activation of PMF-sensitive autolysins. Likewise, Tse4 could exacerbate the consequences of NAD^+ depletion (Tse6) by inhibiting

transporters that rely on $\Delta\psi$ to maintain cellular homeostasis particularly under anaerobic conditions where cells rely more heavily on NAD^+ for the maintenance of the PMF.

Our 16S multispecies community analysis revealed that the H1-T6SS of *P. aeruginosa* is the most active secretion system towards the species in our pool. It is important to note that the H2 and H3-T6SSs may have the potential to intoxicate these species with their effector cargo, however they are not naturally targeted in the conditions we used in our co-culture experiment. Moreover, when investigating the impact of single H1-T6SS effector secretion, we found these toxins are differentially efficacious dependent on the target organism's species. From these data, we suggest that a phylogenetic diversity in targeted species could promote effector expansion in ubiquitous T6SS+ bacteria.

Our analyses reveal the benefits to bacteria of maintaining a biochemically diverse effector repertoire. In the rapidly changing and unpredictable surroundings characteristic of life at the micron scale, the concomitant delivery of multiple effectors with a range of conditional optima may act as a bet-hedging strategy to overcome these conditions and to intoxicate a broad range of bacterial species. As a corollary, the set of effectors a bacterium possesses should provide a window into the environmental conditions in which it encounters competitors. The benefits conferred by the delivery of toxins with conditional and synergistic activities underscores the utility of combination antibiotic therapy beyond the subversion of resistance[137].

V. Materials and Methods

Strains and Media

All *P. aeruginosa* strains were derived from the sequenced strain PAO1 and were grown on Luria-Bertaini (LB) medium at 37°C supplemented as appropriate with 30 μg ml^{-1} gentamicin, 25 μg ml^{-1} irgasan, 75 μg ml^{-1} tetracycline, and 5% (*w/v*) sucrose. *Escherichia coli* was grown in LB medium supplemented as appropriate with 15 μg ml^{-1} gentamicin and strains DH5α and SM10 (Novagen,

Hornsby Westfield, Australia) were used for plasmid maintenance and conjugative transfer, respectively. Site-specific chromosomal insertions in *P. aeruginosa* were generated using pMiniCtx-1 (*attB*) as previously described.

Bioinformatic search for type VI effectors encoded by Proteobacteria

We generated custom Hidden Markov Model (HMM) profiles for experimentally validated effectors and a T6S structural gene (*tssC*) from homolog alignments using hmmscan from the HMMER 3.1b2 tool set. The effectors groups chosen for this search were: Tae1, Tae2, Tae3, Tae4, Tge1, Tge2, Tge3, Tle1, Tle2, Tle3, Tle4, Tle5, VasX and Tse4, as well as proteins containing Tox46 ($NAD(P)^+$ glycohydrolase) and Tox34 (HNH DNase) motifs. For all Proteobacterial species on the List of Prokaryotic names with Standing in Nomenclature (LPSN, http://www.bacterio.net/), a strain was selected at random and the corresponding genome downloaded from the NCBI complete genome database. Draft genomes were selected and translated if no complete genomes were available. These genomes were searched for proteins matching our custom HMM profiles. Results were binned by profile hits and filtered using E-value cut-offs. Appropriate cut-off values were selected by manually identifying the highest value for a given sequence that was found in the appropriate genomic context. For effectors, this included proximity of immunity gene candidates, *vgrG* homologs, and genes encoding accessory proteins with T6S-related domains of unknown function. Hits for *tssC* were validated by identifying adjacent genes encoding other T6S structural components.

Parallel analysis of effector efficacy screen (PAEE)

Generation of barcoded mutant strains: The pEXG2 suicide vector was used for creating in-frame chromosomal deletions in *P. aeruginosa* as previously described. Single and pairwise deletions

of the six H1-T6SS effector–immunity gene pairs in *P. aeruginosa* was used to generate 21 different strains (see Figure 3.2). The integration vector mini-CTX1 was then used to insert a unique 18 base pair barcode at the neutral phage attachment site B (*attB*) in each mutant as well as the wild-type parent strain. Finally, allelic exchange employing pEXG2 was used to introduce an in-frame deletion of *retS* in each barcoded strain.

Bacterial growth competitions*:* The 22 barcoded strains were grown for 16 hours on LB no salt (LBNS) medium agar plates, then resuspended in LBNS broth before pooling together at equal concentrations (normalized to OD_{600} 0.2) and mixed with an excess of a donor (*P. aeruginosa* PAO1 Δ*retS,* donor to recipient= 10:1). This mixture (5μl) was spotted on a 0.2 μm nitrocellulose membrane placed on 3% (*w/v*) agar plates, except as noted in Supplementary Table 3.1. Plate composition, incubation times and other varied growth conditions are described in Table 3.1. After the incubation period noted in Table 3.1, competitions were harvested into LBNS broth and washed twice with the same medium. Cells were then incubated with 10 mg/mL benzonase (Sigma-Aldrich, St. Louis, MO) for 30 min at 37°C to remove extracellular DNA and washed a final time with LBNS medium containing 5 mM EDTA to inactivate the benzonase.

Sequencing: Total DNA was extracted from washed, benzonase treated cells using the DNeasy kit (Qiagen, Hilden, Germany). The barcode region was amplified using primers containing an adaptor sequence and targeting conserved regions flanking the integrated barcodes. Amplification was monitored via SYBR Green incorporation and terminated prior to saturation. A second round of amplification was used to introduce Nexterra sequencing adapters (Illumina, San Deigo, CA) and unique indices for each library, and sequencing was performed using an Illumina MiSeq instrument (50 cycles program).

Analysis: Each read was assessed for an exact match at the barcode position using string matching, with no mismatches for any base allowed and excluding reverse complemented matches (reads that did not meet these criteria were filtered). To normalize values between

different conditions, we converted the reads for each barcoded strain into a fraction of the total reads for each individual condition. Effector activity (E_a) was calculated by a metric analogous to a competitive index using the following equation:

$$E_a = \log\left(\frac{Final\left(\frac{parent}{mutant}\right)}{Initial\left(\frac{parent}{mutant}\right)}\right)$$

Synergy was calculated as the observed activity of an effector pair compared to the expected additive value (observed/expected, o/e). The expected additive value is the sum of the individual effector activities from single effector susceptible barcoded strains minus 1. Synergy was defined as any o/e value>1, meaning the activity of the effector pair was greater than the sum of its individual effector activities. The bar for inhibition was calculated as the percent contribution of the most active effector within the pair to the expected additive value. Partially additive activity was defined by o/e values greater than the inhibitory cutoff and <1.

Effector expression analysis

Expression of T6SS effector and structural genes was measured in wild-type *P. aeruginosa* PAO1. Cultures were grown for 16 hrs in LB broth, then cells (5μL) were spotted on 0.2 μm nitrocellulose filters placed upon agar plates. Agar plate composition and incubation conditions are the same as employed in PAEE (Table 3.1). Spots were harvested from nitrocellulose and resuspended into Bacterial RNA Protect buffer (Qiagen). Cells were lysed by lysozyme treatment (1 mg/ml for 10 min) followed by sonication. RNA was purified using the RNeasy kit (Qiagen), residual DNA removed by Turbo DNAse (Invitrogen), and remaining RNA purified and concentrated using the RNA Minelute kit (Qiagen). cDNA was synthesized using the High Capacity cDNA Reverse Transcription Kit (Thermo Fisher, Watham, MA). Gene expression was measured using SYBR Green-based quantitative PCR with primers targeting each gene of interest and normalized to the housekeeping gene *rpoD*. Primer sequences are available upon

request. Two independent experiments with three technical replicates included were performed for each measurement.

Growth competition assays

For *P. aeruginosa* competitions, the recipient strain contained *lacZ* (tetracycline-resistant) inserted at the neutral phage attachment site (*attB*) to enable its differentiation or selection from the unlabeled donor strain when plated on LB containing X-gal (40 μg ml^{-1}) or tetracycline (75 μg ml^{-1}). Overnight cultures of donor and recipient strains were washed, OD_{600} standardized, and mixed at the ratios indicated. Competition mixtures (5 μl) were then spotted in triplicate on a 0.2 μm nitrocellulose membrane overlaid on a 3% (*w/v*) agar plate of the indicated media and incubated face up at 37°C for 8 hrs unless denoted otherwise. Competitions were harvested from the nitrocellulose membrane and resuspended into LB medium. Initial and final populations of donor and recipient cells were enumerated following serial dilution on appropriate selective or differentiation media. The competitive index (CI) is defined as:

$$CI = \frac{Final\left(\frac{donor\ c.f.u.}{recipient\ c.f.u.}\right)}{Initial\left(\frac{donor\ c.f.u.}{recipient\ c.f.u.}\right)}$$

16S sequencing study

Generation of single effector strains: The singe effector strains were generated by making combinatorial chromosomal point mutations previously demonstrated to inactivate each toxin. The parental background for these mutations was PAO1 Δ*retS* Δ*tse5* Δ*icmF2* Δ*icmF3*–a strain with constitutive T6S, lacking functional H2 and H3-T6SS and the effector of unknown function Tse5.

The point mutations utilized were Tse1 C30A, Tse2 S80A, Tse3 E250Q, Tse6 D396A, and Tse7 H230A[30,31,68,72]. A clean deletion of *tse4* was made to ensure there was no residual activity in our assays due to a lack of knowledge of residues important for catalytic activity.

Bacterial growth competitions: Overnight cultures were grown at 30°C on tryptic soy agar + 0.1% cysteine (TSAC). P. aeruginosa PAO1 and the multispecies community was mixed at a 10:1 ratio by OD_{600} (PAO1 OD 2 and multispecies pool OD 0.2). Within the multispecies community, all bacteria were set to an OD_{600} of 0.2 and mixed 1:1. 5 μL of these mixtures was spotted onto a nitrocellulose membrane on a 3% agar TSAC plate and incubated at 30C for 24 hours.

Sequencing: Total DNA was extracted from washed, benzonase treated cells using the DNeasy kit (Qiagen, Hilden, Germany). The V4 region of the 16S gene was amplified and sequenced using barcoded dual-index primers. These samples were normalized using the Kapa Biosystems Library qPCR Mastermix Quantification kit and sequenced on a MiSeq using a 500 cycle MiSeq V2 reagent kit. (The V4 16S amplification and sequencing was performed at the Microbial Systems Molecular Biology Laboratory at the University of Washington).

Analysis: 16S sequencing read were analyzed using the software MICCA[138], a tool for accurate taxonomic profiling of metagenomic data. MICCA quality filters reads, *de novo* clusters operational taxanomic units (OTUs) and assigns taxonomy by phylogenetic tree inference. To normalize values between different conditions, we converted the reads for each species into a fraction of the total reads for each individual condition. A value was calculated by a metric analogous to a competitive index using the following equation:

$$y = \left(\frac{Final\left(\frac{species}{total\ population}\right)}{Initial\left(\frac{species}{total\ population}\right)}\right)$$

Statistics

All statistical tests were performed in GraphPad Prism 7.0 with α=0.05; p-values less than 0.05 are indicated by asterisks (*).

VI. Figures

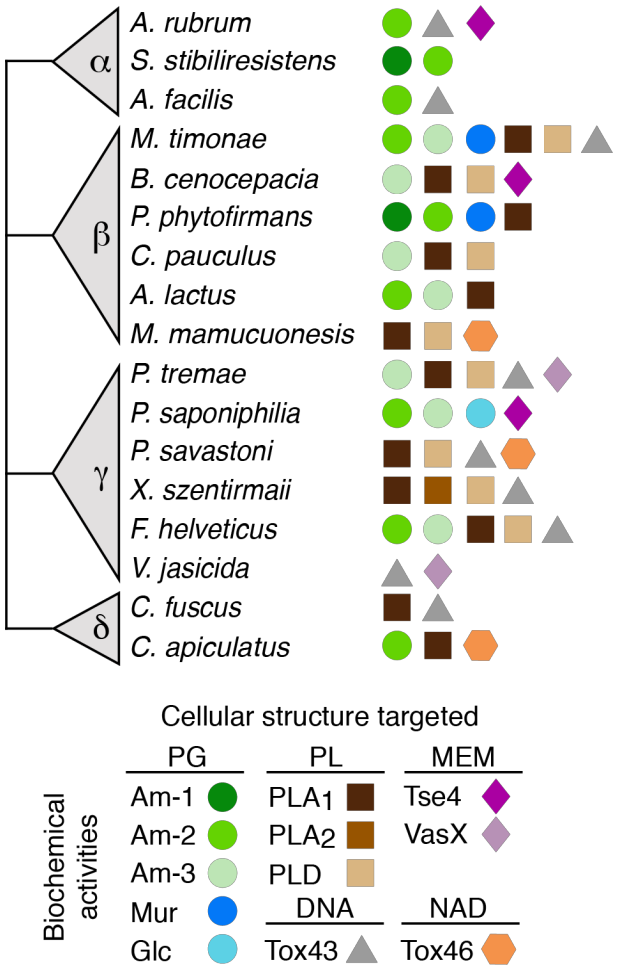

Figure 3.1: Diverse species of Gram-negative bacteria encode multiple T6SS effectors with distinct biochemical activities. Shown are select results of a custom search algorithm used to identify orthologs of biochemically characterized T6SS effectors in all sequenced Proteobacterial species (complete results provided in Supplemental Table 1). Symbols signify characterized effector activities found in the genome of the indicated species. Target molecules (shape) and distinct biochemical activities (color shade) are denoted. Abbreviations: PG, peptidoglycan; PL, phospholipids; MEM, membranes; Am, amidase; Mur, muramidase; Glc, N-acetylglucosamidase; PLA, phospholipase A; PLD, phospholipase.

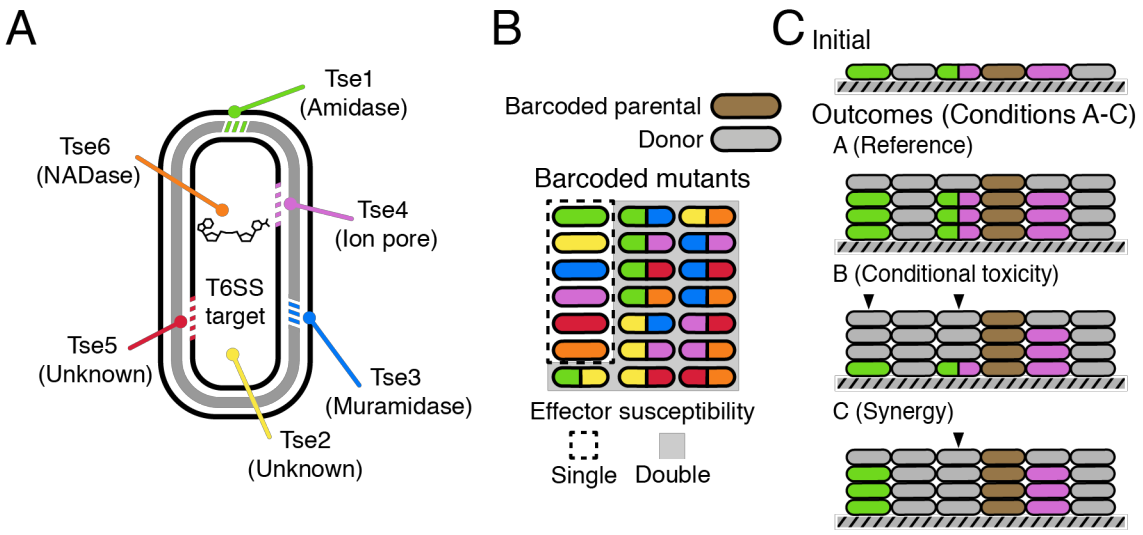

Figure 3.2: Parallel analysis of effector efficacy (PAEE).
(**A**) Diagram indicating the cellular compartment in which each H1-T6SS effector of *P. aeruginosa* acts, and their biochemical activities, when known. (**B**) Representation of the pool of strains employed in PAEE. Colors indicate effector susceptibility of each strain (Tse1-Tse6 colors correspond to Fig. 2a; barcoded parental, brown; unbarcoded donor, grey). Effector susceptibility color scheme is employed throughout subsequent figures. (**C**) Simplified depiction of potential outcomes following competition of a donor strain and recipient strains susceptible to one or both of two effectors with conditional differences in activity (A vs. B) or conditional synergy (A vs. C). Arrowheads indicate mutants with increased toxin susceptibility in comparison to the reference condition.

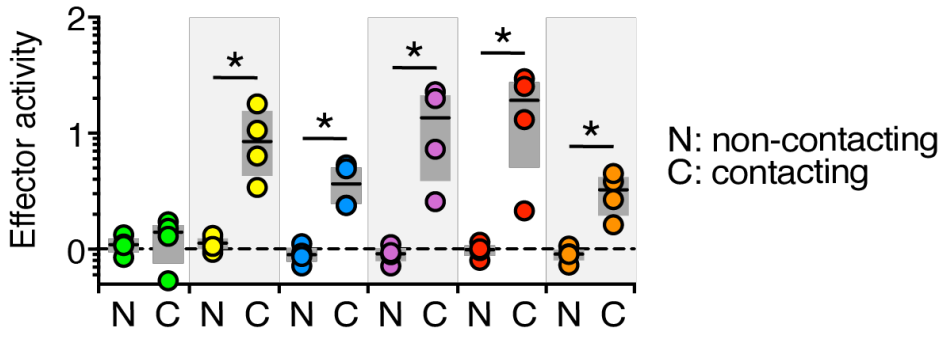

Figure 3.3: T6S effector activity is detected only under cell contact-promoting growth conditions. Relative activity of *P. aeruginosa* H1-T6SS effectors under growth conditions that promote (3% (w/v) agar, C) or limit (0.3% (w/v) agar, N) cell-cell contacts (n=4 biologically independent experiments). Effector activity calculated as in Fig. 2. growth of the pooled population. Grey boxes enclose the 25-75 percentile range and bars represent the median value.

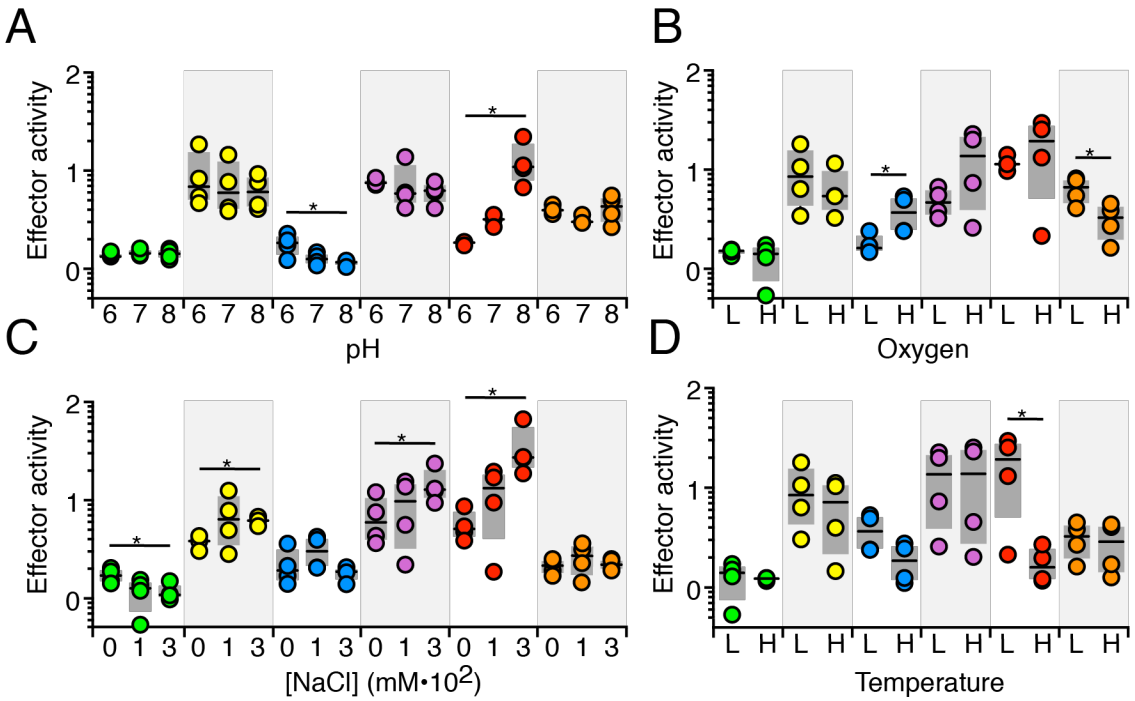

Figure 3.4: PAEE reveals that environmental conditions influence the potency of T6SS effectors. (**A-D**) Relative activity of *P. aeruginosa* H1-T6SS effectors under assorted growth conditions as determined by PAEE (n=4 biologically independent experiments). Effector activity is calculated by comparing the ratios of the barcoded parental to mutants susceptible to each effector before and after growth of the pooled population. Grey boxes enclose the 25-75 percentile range and bars represent the median value. *P<0.05 (ratio paired t-test between each condition). Conditions varied include pH (**A**), NaCl levels (**B**), oxygen availability (H vs. L oxygen) (**C**), and temperature (**D**) (42˚C, H vs. 37˚C, L).

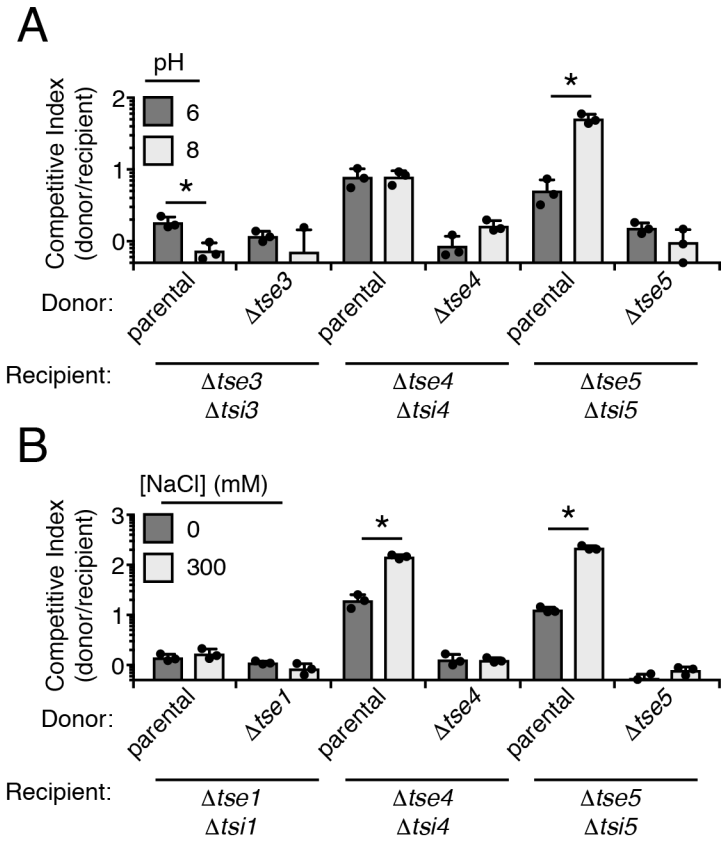

Figure 3.5: Pairwise interbacterial competition assays recapitulate conditional efficacy results. Growth competition experiments between a parental donor strain (ΔretS) and the *specified P. aeruginosa* recipient strains (n=3 biologically independent samples). Competing strains were mixed and incubated 24 hrs on M9 agar plates at pH 6 and 8 (**A**) or 8 hrs on LBNS agar plates supplemented with 0 or 300 mM NaCl (**B**). Data presented as mean values ± standard deviation. *P<0.05 (two-tailed student's t-test).

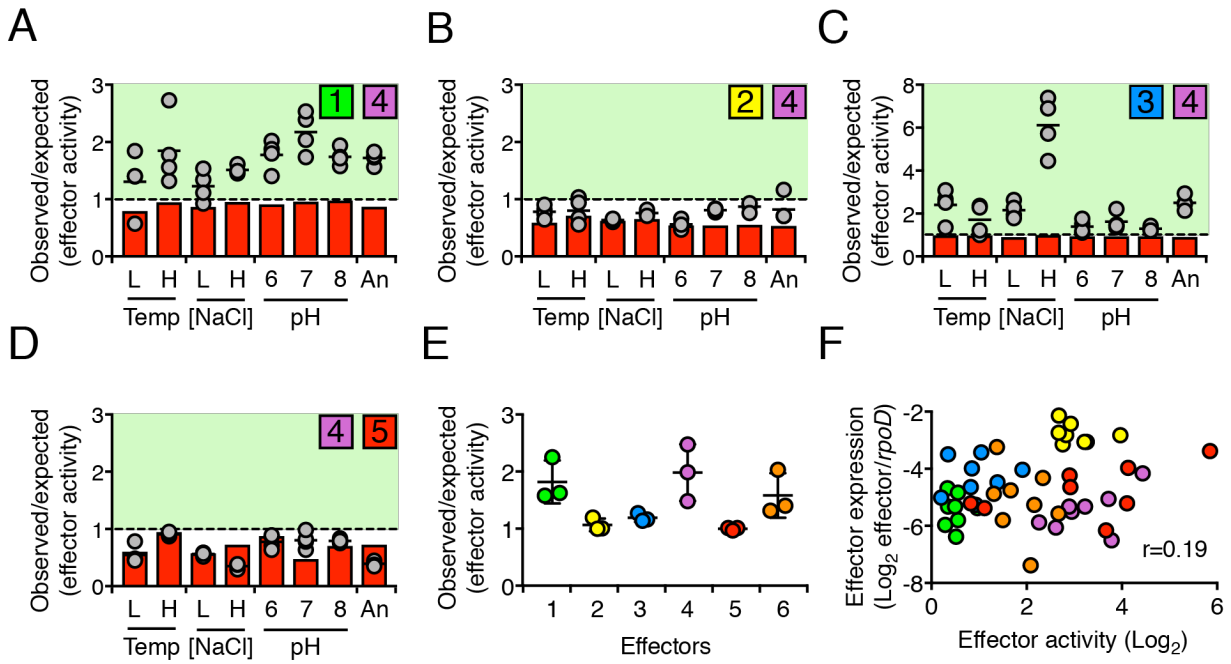

Figure 3.6: Environmental conditions and effector activities influence synergy between T6SS effectors. (**A-D**), Filled circles indicate observed (in PAEE screen):expected (sum of individual effector activities measured by PAEE) activity for the indicated effector pairs. Ratios reflecting synergistic (green) or inhibitory (red) interactions are indicated. Single and paired effector activities calculated as in Figure 2.3. Inhibitory interactions for each effector pair calculated as the portion of the additive effect that is contributed by the more active effector (red bars). Values between red bars and dashed line are additive. High temperature (H), 42°C, low (L), 37°C; high NaCl, 300 mM, low, 0 mM. (n=4 biologically independent experiments). (**E**) Average observed:expected activity for the indicated effectors paired with each other effector under a given condition. Measurements are plotted only for the conditions with the three highest average observed:expected values for a given effector. (**F**) Effector expression levels (as measured by qRT-PCR, n=3 biologically independent experiments) plotted against effector activity level (as determined by PAEE, n=4 biologically independent experiments) under the same set of conditions. Colors indicate effector identity (see Fig. 2). Pearson's correlation coefficient is indicated. (**A-E**), Data presented as mean values ± standard deviation (**E**).

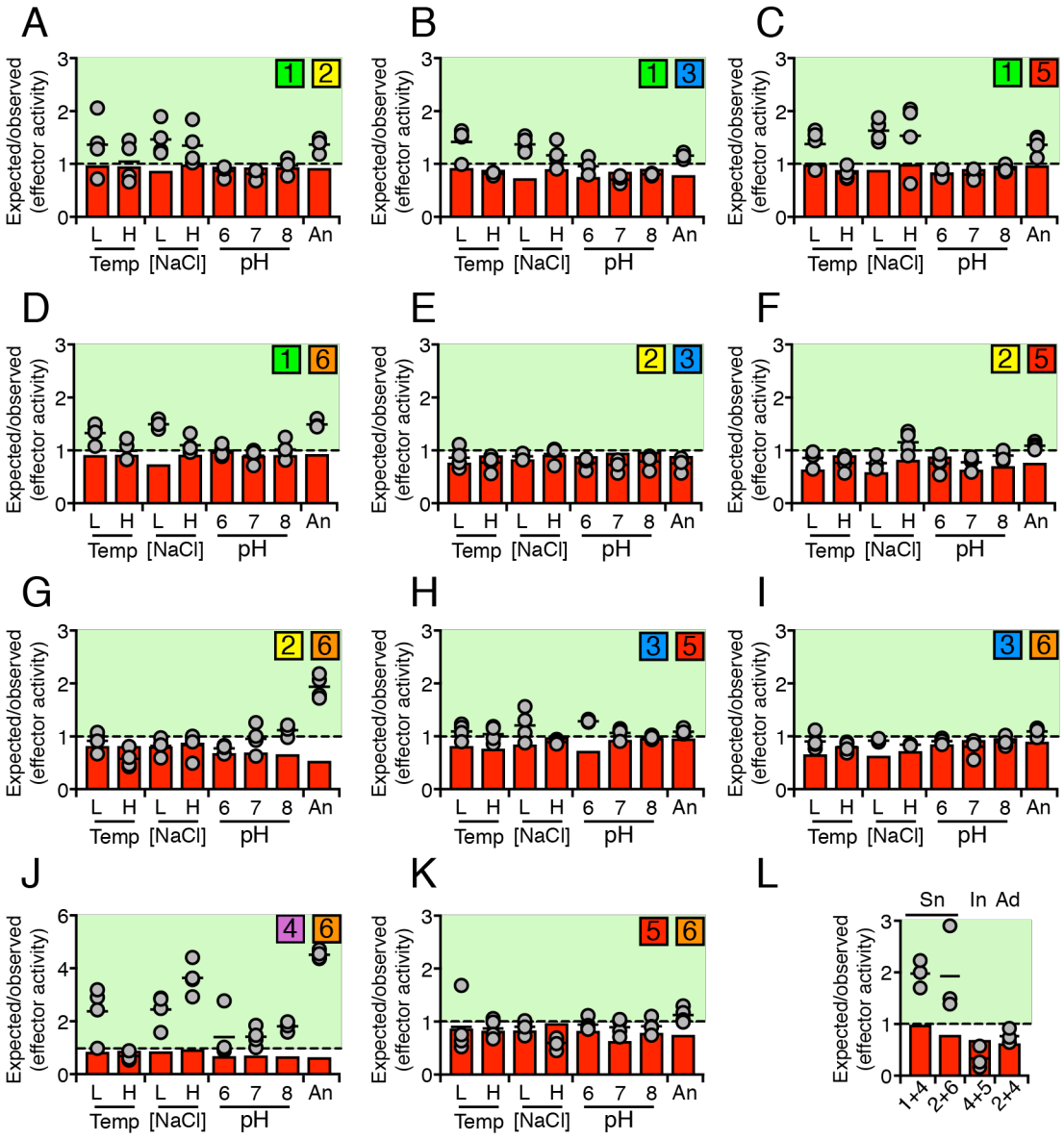

Figure 3.7: Environmental conditions and effector activities influence synergy between T6SS effectors. Ratio of observed (in PAEE screen) to expected (sum of individual effector activities measured by PAEE) activity for pairs of effectors (indicated by colored, numbered boxes), depicted as described in Figure 3.6 (n=4 biologically independent experiments). Panels (**A-K**) present all pairs of effectors not shown in Figure 3.6 (**L**), Similar to A-K, except expected and observed values were obtained from co-culture experiments between a parental donor strain and recipients susceptible to the indicated toxins (individually or in pairs). Sn, synergistic; In, inhibitory; Ad, additive. The 1+4, 4+5, and 2+4 growth competition experiments were performed on media with 300 mM NaCl, and the 2+6 growth competition experiments were performed under anaerobic conditions. (n=3 biologically independent experiments). The mean value for each data set is represented by the black bar.

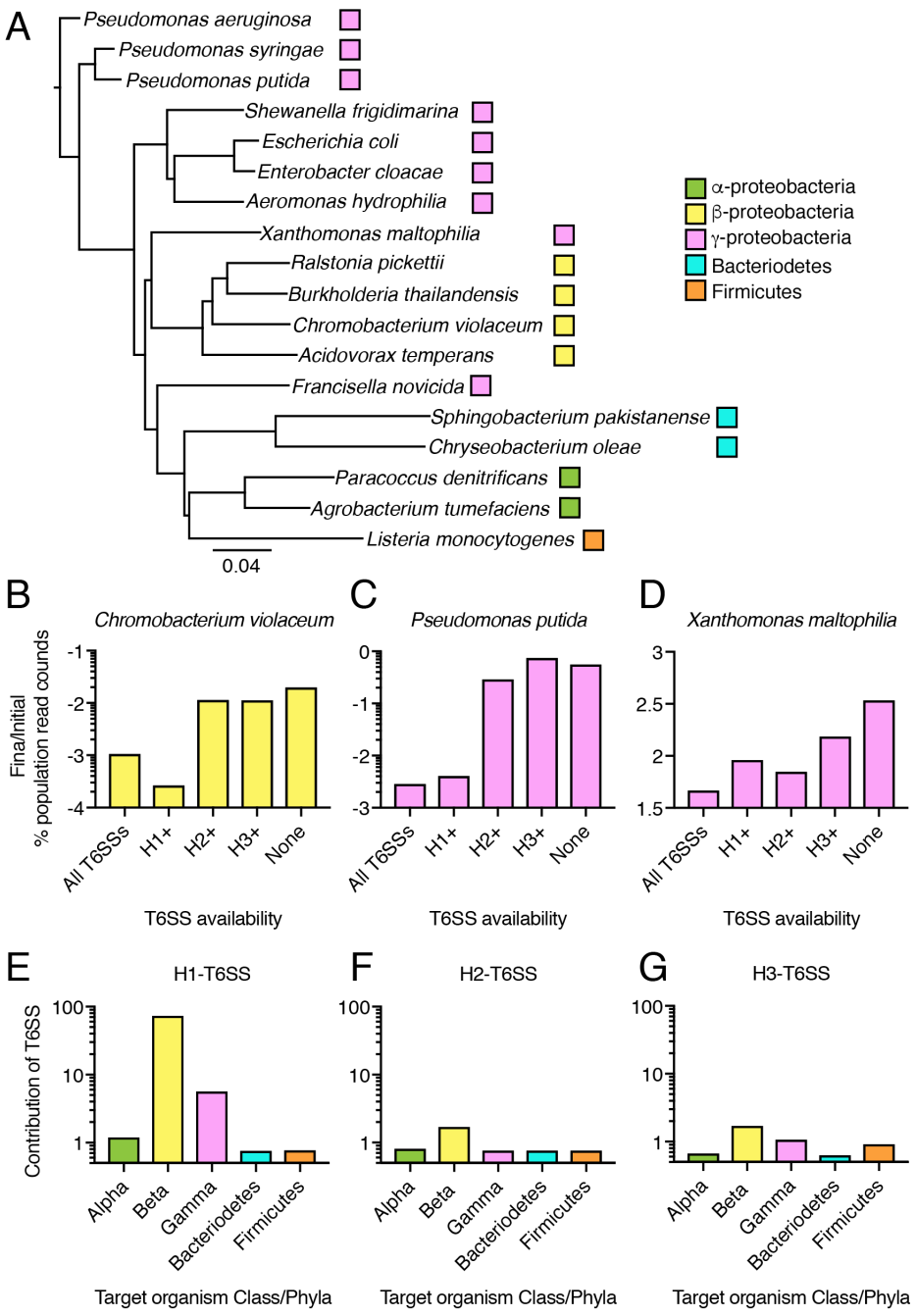

Figure 3.8: The H1-T6SS primarily targets α and β-proteobacteria.
(**A**) 16S phylogenetic tree of multi-species communities used in B-G. (**B-D**) The change in percent population (by read count) for species indicated after co-culture with *P. aeruginosa* strains with different functional T6SS capacities. (**E-F**) The contribution of a single T6SS to fitness against the indicated class or phyla compared to a Δ(H1-3)-T6SS strain. Data utilized were averages of the final/initial % population read counts for each species with evidence to be targeted by a T6SS in the experiment.

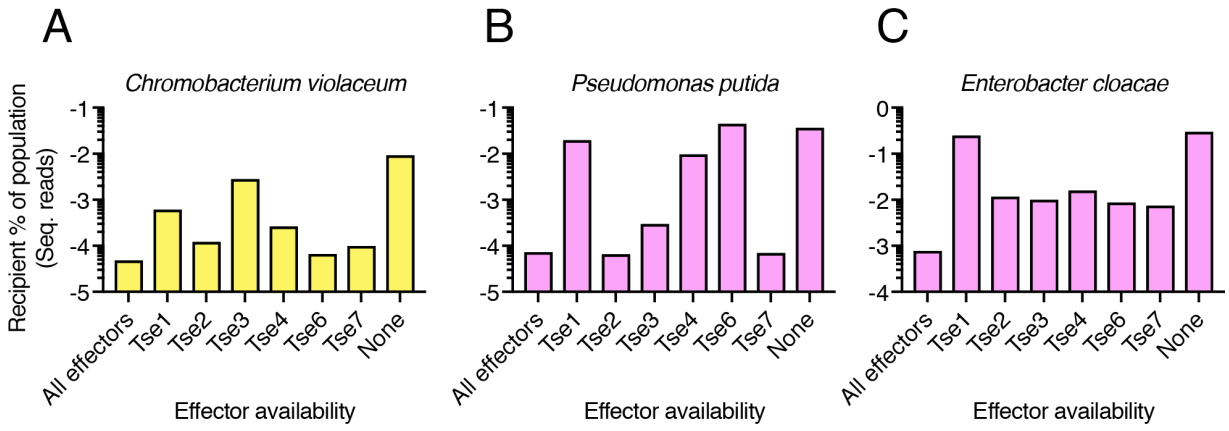

Figure 3.9: Effector activities have differential potency dependent on target species identity (**A-C**) All data is represented as the individual species percent reads of the overall reads contributed by all species in the community. The x-axis denotes which effectors were function in the *P. aeruginosa* donor.

Table 3.1: Media and conditions employed in PAEE

Condition	Medium	Incubation time	Other variables
Reference[1]	LB, 100 mM NaCl	8 hrs	
Temperature High	LB, 100 mM NaCl	8 hrs	42°C
Low salt (0)	LB, 0 NaCl	8 hrs	
High salt (300)	LB, 300 mM NaCl	8 hrs	
Anaerobic	LB, 100 mM NaCl, 40 mM KNO3	24 hours	Grown anaerobically[2]
Non-contacting	LB, 100 mM NaCl	8 hrs	0.3 % agar, no nitrocellulose
pH (6)	M9 minimal media[3], pH 6	24 hrs	
pH (7)	M9 minimal media, pH 7	24 hrs	
pH (8)	M9 minimal media, pH 8	24 hrs	

[1]Reference condition used as solid comparison to non-contacting (semi-solid), low temperature (37°C) comparison to 42°C, 100 mM NaCl comparison to high (300 mM) and low (0 mM) NaCl, and aerobic comparison to anaerobic incubation.
[2]Anaerobic conditions generated using the GasPak EZ (BD Biosciences, San Jose, CA) system
[3] Modified M9 minimal media using succinate as the carbon source and pH was established through altering the ratios of equimolar dibasic sodium phosphate and monobasic potassium phosphate

Chapter 4: Structure of the type VI secretion system TssK–TssF–TssG baseplate subcomplex revealed by cryo-electron microscopy

Published as: Park Y., **LaCourse KD**, Cambillau C., DiMaio F., Mougous JD., Veesler D. *Nature Communications* 9: 5385 (2018).

K.D.L. generated all the constructs and strains utilized in the bacterial two-hybrid assays and performed these experiments, related Western blots, and analyses. Additionally, K.D.L. wrote portions of the manuscript and edited several versions. These are presented in Figures 4.6 and 4.7.

I. Abstract

Type VI secretion systems (T6SSs) translocate effectors into target cells and are made of a contractile sheath and a tube docked onto a multi-protein transmembrane complex via a baseplate. Although some information is available about the mechanisms of tail contraction leading to effector delivery, the detailed architecture and function of the baseplate remain unknown. Here, we report the 3.7 Å resolution cryo-electron microscopy reconstruction of an enteroaggregative *Escherichia coli* baseplate subcomplex assembled from TssK, TssF and TssG. The structure reveals two TssK trimers interact with a locally pseudo-3-fold symmetrical complex comprising two copies of TssF and one copy of TssG. TssF and TssG are structurally related to each other and to components of the phage T4 baseplate and of the type IV secretion system, strengthening the evolutionary relationships among these macromolecular machines. These results, together with bacterial two-hybrid assays, provide a structural framework to understand the T6SS baseplate architecture.

II. Introduction

Bacterial secretion systems transport proteins and nucleic acids across the cell envelope. They serve essential roles in pathogenesis and in enabling communication between cells. Type VI secretion systems (T6SSs) are found in a broad range of Gram-negative bacteria and transport proteins directly into recipient cells[24,130]. They can target either bacterial cells, to provide a selective advantage enabling colonization of specific niches, or eukaryotic cells, to modulate bacteria/host interactions and pathogenesis[30,133]. As a result, the presence of one or several functional T6SSs correlates with the ability to induce host diseases or disorders for many pathogens[139].

The T6SS apparatus is assembled from at least 13 distinct types of proteins (Figure 4.1) encoded by a discrete gene cluster, so-called pathogenicity island, which generally also includes

a subset of secreted effector and cognate immunity genes[16,140,141]. The T6SS needle oligomerizes in the bacterial cytoplasm and comprises an inner tube, made of Hcp hexameric rings arranged with helical symmetry, surrounded by TssB–TssC rings forming the sheath. Localization of the needle within a donor cell is mediated by a pre-assembled cytoplasmic baseplate comprising TssK, TssF, TssG, TssE, VgrG, and a PAAR-repeat protein. The baseplate docks to the bacterial envelope via interactions with a complex assembled from the inner membrane proteins TssL and TssM and the outer membrane lipoprotein TssJ. Contraction of the TssB–TssC sheath is believed to propel the inner tube and VgrG-PAAR spike through the membrane complex of the donor cell, to puncture the envelope of a recipient cell and deliver effectors in the periplasm and/or the cytoplasm[142,143].

Crystal structures of the Hcp hexamer and of the VgrG trimeric spike revealed part of the building blocks of tailed phages, R-type pyocins, and T6SSs are structurally similar and led to the hypothesis that these nanomachines are evolutionary and functionally related[144–149]. These findings were reinforced upon determination of cryo-electron microscopy (cryoEM) and cryo-electron tomography structures of the TssB–TssC sheath in the contracted and extended states, which provided insights into the mechanism associated with effector delivery to recipient cells and subsequent recycling of the T6SS needle[150–153]. High-resolution crystal structures of isolated domains in combination with low-resolution electron microscopy studies also provided a glimpse of the TssJ–TssL–TssM membrane complex architecture that forms a fivefold symmetrical oligomer spanning the cell envelope[154,155]. This latter complex is evolutionary related to components of the type IVB secretion system (T4BSS) and demonstrates the mosaic origin of the T6SS apparatus[140].

The lack of high-resolution structural information about the three-dimensional organization of the baseplate complex has hindered our understanding of the architecture and assembly pathway of this key multi-subunit component of the T6SS. TssK was recently shown to resemble

lactoccocal phage receptor-binding proteins and to interact with the baseplate complex, via its N-terminal shoulder domain, and with the cytoplasmic domains of TssL and TssM in the membrane complex, through its head domain[156]. Bioinformatics analyses suggested TssE is a baseplate wedge component related to phage T4 gp25, P2 gpW, or Mu Mup46[144,157]. Also, TssF and TssG were proposed to respectively, resemble phage T4 gp6 and gp7, P2 gpJ and gpI, or Mu Mup47 and Mup48[156,158–160]. TssK is known to form a complex with TssF, and TssG that can be purified endogenously or upon recombinant overexpression, although the stoichiometry, architecture, and role of this complex in the T6SS apparatus remain unclear[156,159,160].

To address this knowledge gap, we report here the 3.7 Å resolution cryoEM structure of the EAEC TssK–TssF–TssG complex. Our results show TssG acts as an adaptor interacting with two TssK trimers and two TssF protomers to form part of a baseplate wedge (which also comprises TssE). We observed that TssF and TssG are structurally related to each other and to components of the phage T4 baseplate and of the T4SS, further strengthening the suggested evolutionary relationships among these macromolecular machines. Integrating our data with previous work, we propose a complete model for the needle and baseplate components and a putative assembly pathway of the T6SS apparatus.

III. Results

Structure determination of TssK–TssF–TssG

To understand the architecture of the T6SS baseplate, we overexpressed and purified an EAEC complex comprising full-lengh TssF and TssG (residues 64–366) as well as the shoulder and neck domains of TssK ($TssK_{SN}$, residues 1–315) (Figure 4.1b). We omitted from our construct the C-terminal domain of TssK (head domain), which participates to attaching the baseplate to the membrane complex, as it was previously shown to be poorly ordered and highly dynamic relative to $TssK_{SN}$[156]. Size-exclusion chromatography indicated $TssK_{SN}$–TssF–TssG eluted as a ~ 400 kDa

complex comprising multiple copies of one or several constituting proteins (Figure 4.1 c,d), as reported[156,159]. Processing of the cryoEM data set revealed TssF–TssG was mobile relative to TssK and we relied on extensive 3D classification of the data, to computationally isolate a homogeneous subset of particle images[161], as well as multi-body focused refinement with density subtraction[162](Figure 4.2a-f). The final cryoEM map has an overall resolution of 3.7 Å (3.9 Å for the TssF–TssG focused map) and is best resolved for the region corresponding to TssK, TssG, and the C-terminal domains of TssF (Figure 4.2e, Figure 4.3ab, and Table 4.1) The N-terminal and central domains of TssF feature weaker density owing to conformational heterogeneity (Figure 4.2e and Figure 4.3a,b).

We obtained a complete model of the complex by combining co-evolution-based modeling[163,164] and manual building, using Rosetta[165–169] and Coot[170], and docking the previously determined crystal structure of TssK into the density (Figure 4.3c,d, Figure 4.4a,b, and Table 4.1)[156]. The final model comprises TssK residues 1–315 (with a chain break between residues 220–230), TssF residues 45–587 (with a chain break between residues 393–404), as well as TssG residues 122–365 (with a chain break between residues 330–336,). The cryoEM map also contains a few unassigned densities that were modeled as polyalanine chains and which likely account for the N-terminal regions of TssF and TssG. The $TssK_{SN}$–TssF–TssG complex forms a nine-subunit structure, comprising six copies of TssK, two copies of TssF and one copy of TssG, with dimensions of 175 Å × 145 Å × 110 Å (Figure 4.3a-d).

Architecture of the TssF–TssG heterotrimer

TssF folds as a three-domain polypeptide comprising: (i) an α-helical N-terminus (residues 47–85); (ii) a central domain made up of three β-barrels (residues 90–457); and (iii) a C-terminal four-stranded mixed β-sheet packed against α-helices via a hydrophobic core (residues 460–587, Figure 4.5a-c). TssG adopts a fold similar to TssF although the two proteins do not share detectable sequence similarity. However, only the N-terminal α-helical region (residues 122–177)

and the C-terminal four-stranded mixed β-sheet supplemented with α-helices (residues 179–365) are present in TssG, which lacks an equivalent to the TssF central domain (Figure 4.5a,b,d). Two extended loops, designated loop 1 and loop 2, protrude from opposite ends of the TssG β-sheet but are absent in the corresponding domain of TssF (Figure 4.5c,d). The C-terminal domains of the two structures can be superimposed with an r.m.s.d of 4.5 Å over 56 aligned Cα positions (Figure 4.5e,f).

The $(TssF)_2$–$(TssG)_1$ complex assembles as a locally pseudo-symmetrical heterotrimer with a 2:1 stoichiometry (Figure 4.5a,b). The N-termini of the three modeled chains form a three-helix bundle interacting with a triangular core, which is formed upon trimerization of the C-terminal domains of TssF and TssG. The triangle is capped by the TssG loop 1 at its apex and the TssG loop 2 projects toward the periphery. The heterotrimer is highly interdigitated and buries an average surface area of 2850 $Å^2$ and 2550 $Å^2$ at the interface between TssG and each TssF protomer, whereas the two TssF protomers bury an average surface area of 1900 $Å^2$.

The TssF and TssG C-terminal domains share remote structural similarity with the *Helicobacter pylori* HP1451 protein (Figure 4.5g), which has been shown to bind to the T4SS HP0525 ATPase to regulate secretion[171], the bacteriophage T4 baseplate proteins gp6 and gp7 (Figure 4.5h) and the type II secretion system AspS pilotin (Figure 4.5i). These findings reinforce the previously proposed evolutionary connection between T6SSs, tailed phages and T4SSs, which appear to share a common set of building blocks[140,144–146,172]. Our data also suggest that an ancestral duplication event and subsequent loss or addition of the TssF central domain could have led to TssG or TssF, respectively, as previously hypothesized[173].

Attachment of TssK to the TssF–TssG heterotrimer

The architecture of the two $TssK_{SN}$ trimers in the $TssK_{SN}$−TssF−TssG complex is very similar to the one observed in the TssK structure determined in complex with nanobodies nb18 and nb27 using X-ray crystallography[156](1.1 Å r.m.s.d. over 230 aligned Cα carbons). The

$TssK_{SN}$ trimer folds as an N-terminal β-sandwich (shoulder domain) followed by a four-helix bundle (neck domain) and resembles phage receptor-binding proteins[156].

Each $TssK_{SN}$ trimer attaches to one of the two extended loops protruding from the TssG C-terminal domain. Loop 1 anchors a TssK trimer near the apex of the pseudo-threefold symmetrical $(TssF)_2$–$(TssG)_1$C-terminal triangle, whereas loop 2 binds another $TssK_{SN}$ trimer at the periphery of the triangle (Figure 4.5a-d and Figure 4.6a). The two TssK trimers are tilted ~ 60° relative to each other and interact together, burying an average surface area of 1000 $Å^2$ at their interface. These results likely explain the observation of TssK trimers and of TssK trimers and hexamers for the EAEC and *Serratia marcescens* orthologues, respectively, as the protein forms homotrimers that interact with each other within and across wedges[160,174]. TssG interacts with excellent surface complementarity with the N-termini of the TssK trimers. Specifically, three residues from loop 1 (Met228, Leu236, and Met242) or three residues from loop 2 (Leu308, Leu319, and Met325) project into the hydrophobic cavity defined by the N-terminal 15 residues of a TssK trimer, and these interactions are further strengthened via hydrogen-bonding and salt bridges at the periphery (Figure 4.6b,c). TssG loop 1 and loop 2 bury an average of 1066 $Å^2$ and 1249 $Å^2$ at the interface with a TssK trimer, respectively, whereas TssF weakly interacts with TssK within a baseplate wedge. Key hydrophobic residues in the TssK-binding loops are conserved (or conservatively substituted) across TssG orthologues found in distant Gram-negative bacterial species and TssG paralogues from different T6SSs (Figure 4.6d,e). These findings indicate that the interaction between TssG and TssK are most likely a common feature of T6SSs. Binding of TssK to TssG is reminiscent of the attachment mode observed for receptor-binding proteins to phage baseplates, such as in the cases of TP901–1[175] or p2[176] although the molecular details of the interactions are distinct.

$TssK_{SN}$–TssF–TssG interactions

To validate the interactions detected in our cryoEM reconstruction, we used a bacterial two-hybrid (BACTH) assay[177]. Our structure predicts that TssK protomers interact, as the protein forms homotrimers that contact each other. Indeed, BACTH confirmed the self-association of TssK (Figure 4.6f and Figure 4.7). We next confirmed that the C-terminal domain of TssG acts as an adaptor for the $TssK_{SN}$–TssF–TssG complex by interacting with TssK and with TssF (Figure 4.6f and Figure 4.7), as observed in the atomic model. We interpret the lack of $TssG_C$–T25 interactions with TssF and with TssK as a result of steric hindrance mediated by fusing the adenylate cyclase T25 domain at the C-terminus of the TssG C-terminal domain. This interpretation agrees with our structural data, with the detection of T25–$TssG_C$ (T25 fused at the N-terminus of the TssG C-terminal domain) interactions with TssF and with TssK, and with a previous study using a comparable experimental setup[158].

Our structure also indicates that the TssG loop 1 and loop 2 each mediate contacts with the N-terminal region of one TssK trimer. BACTH experiments support these findings since (i) removal of the TssK N-terminal 17 residues or (ii) substitution with arginine of the aforementioned three hydrophobic residues within the TssG loop 1 (Met228Arg, Leu236Arg, Met242Arg) or loop 2 (Leu308Arg, Leu319Arg, Met325Arg) abrogated binding between TssG and TssK without significantly affecting the interactions between TssG and TssF (Figure 4.6f and Figure 4.7). In summary, the outcomes of the BACTH experiments validated our atomic model and also agreed with and extend previously reported BACTH data[156,158].

Architecture of the baseplate

We generated a model of the T6SS baseplate putatively corresponding to the conformational state before sheath contraction using our structure of the EAEC $TssK_{SN}$–TssF–TssG complex and the previously determined cryoEM reconstruction of the non-contractile sheath mutant of the *Vibrio cholerae* T6SS baseplate/needle at 8 Å resolution[178].

The TssK–TssF–TssG complex, along with TssE, constitute a wedge and six such wedges are circularized in a baseplate comprising 36 copies of TssK, 12 copies of TssF, 6 copies of TssG and presumably 6 copies of TssE[159,173] (Figure 4.8a-c and Figure 4.9a-g). Rigid-body docking the $TssK_{SN}$–TssF–TssG structure into the baseplate map shows the architecture of the recombinant complex recapitulates its overall organization in the context of a fully assembled T6SS apparatus. Although the resolution of the baseplate map is limited, we could nevertheless notice local tertiary and quaternary structural differences likely corresponding to conformational switching upon assembly, as reported for the bacteriophage major tail protein[172]. As the TssK region features weak density in the baseplate reconstruction, owing to mobility relative to the rest of the baseplate and/or substoichiometric incorporation of TssK, we applied a low-pass filter at 20 Å resolution to enhance map resolvability. This procedure confirmed each wedge attaches two TssK trimers to the baseplate (Figure 4.9a-g), in agreement with the $TssK_{SN}$–TssF–TssG structure reported here. The apparent conformational heterogeneity of TssK further reinforces the similarity between phage and T6SS baseplates since receptor-binding proteins or TssK trimers are highly dynamic and this could be important for their functions[175]. The central domain of the proximal TssF protomer from each wedge contacts the VgrG oligosaccharide/oligonucleotide (OB)-fold barrel such as the latter domain is surrounded by two TssF protomers from two different wedges. VgrG thereby ensures the transition between its intrinsic threefold symmetry and the sixfold symmetry of the baseplate and needle, similarly to the phage T4 gp27 protein[148,159,179] or the Tal protein of phages TP901–1[145] and p2[176]. Lateral stabilization of the baseplate is provided by inter-wedge TssF–TssF, TssK–TssK, and TssF–TssK interactions (Figure 4.8a-d). Most of the inter-wedge TssF–TssF interactions involve contacts between a proximal TssF protomer of the wedge i (through its central and C-terminal domains) and a peripheral TssF protomer of the wedge i + 1 (through its C-terminal domain, Figure 4.8d).

Our model also suggests TssK–TssF–TssG complexes are interacting with the proximal TssB–TssC sheath ring, in agreement with previous BACTH studies[155,158]. On one hand, the

$(TssF)_2$–$(TssG)_1$ heterotrimer N-terminal stem contacts TssC. On the other hand, the N-terminal helix of TssC and the C-terminal helix of TssB protrudes in direction of the same $(TssF)_2$–$(TssG)_1$ heterotrimer to interact with the small β-barrel located within the TssF central domain. The interactions between TssB/TssC and TssF are mediated by the TssF protomers radiating at the periphery of the baseplate whereas the TssF protomers protruding toward the center of the baseplate bind to VgrG. TssE, which is absent in the model presented here, is expected to interact with the $(TssF)_2$–$(TssG)_1$ heterotrimer N-terminal stem and with the TssB/TssC sheath, based on similarity with the phage T4 baseplate structure[144,159,179].

IV. Discussion

The results presented here further our knowledge about the T6SS baseplate architecture and assembly pathway. Hexamerization of the $(TssK)_6$–$(TssF)_2$–$(TssG)_1$–$(TssE)_1$ wedge leads to formation of the baseplate complex around a VgrG trimer bound to a PAAR-repeat protein at its distal extremity[178]. As we could not detect baseplate-like complexes upon overexpression and purification of $TssK_{SN}$–TssF–TssG (even at high concentration), we propose VgrG nucleates the assembly of individual baseplate wedges, as previously suggested[156]. We expect that docking of the six proximal TssF protomers, through their central domain, near one of the three VgrG OB-fold domains initiates circularization. Once adjacent baseplate wedges are hexamerized and surround the central VgrG trimer, the wedges are sealed via proximal/distal TssF interactions. In the case of EAEC, TssA, TssM, and TssL participate to docking of the baseplate to the cytoplasmic side of the inner membrane through interactions formed by (i) the TssK head domain with the cytoplasmic domains of TssL and of TssM, (ii) the N-terminal domain of TssA with TssE and TssK, (iii) the C-terminal domain of TssA with VgrG, and (iv) TssG with the cytoplasmic domain of TssM[155,156,158,180].

Once assembly of the baseplate is completed, the tail tube and sheath polymerize, either sequentially or simultaneously, via addition of hexameric Hcp rings and of TssB–TssC rings or

rows at the growing extremity[181]. Stabilization of the TssB–TssC ring directly contacting the baseplate occurs (i) through binding of TssC to the $(TssF)_2$–$(TssG)_1$ N-terminal helical stem, (ii) attachment of the peripheral TssF central domain to the C- and N-termini of TssB and TssC, respectively, and (iii) putatively via interactions of TssE with TssB–TssC. Additional interactions between a hexameric Hcp ring and the pseudo-six-fold symmetrical VgrG trimer participate to initiation of tube formation[155].

The $(TssF)_2$–$(TssG)_1$ heterotrimer assembles with the same stoichiometry as the T4 $(gp6)_2$–$(gp7)_1$heterotrimer and the four proteins appear to share a distant ancestor. Specifically, the $(TssF)_2$–$(TssG)_1$ C-terminal domains form a pseudo-3-fold symmetrical triangle, which resembles the T4 $(gp6)_2$–$(gp7)_1$trifurcation domain recently described[159,179] and the domains involved all adopt a similar fold. Moreover, both $(TssF)_2$–$(TssG)_1$ and $(gp6)_2$–$(gp7)_1$ form a three-helix bundle arranged roughly perpendicularly with respect to the triangle motif. This similarity is strengthened by the observation that the $(TssF)_2$–$(TssG)_1$heterotrimer participate to circularizing the baseplate, recruiting TssK (which is structurally and to some degree functionally related to phage receptor-binding proteins) and interacting with the central spike and the tail sheath, similarly to T4 $(gp6)_2$–$(gp7)_1$[159,173]. Circularization of the T6SS and the T4 baseplates, however, is mediated by distinct types of interactions, as inter-wedge contacts occur between C-terminal triangular-shaped cores through proximal and peripheral TssF protomers or between proximal and peripheral gp6 C-terminal domains (which are distinct from the trifurcation domains), respectively. Overall, the T6SS baseplate appears to be related to the baseplate of contractile bacteriophages as $(TssF)_2$–$(TssG)_1$ shares structural, topological, and functional traits with T4 gp6/gp7 and orthologous proteins found in other contractile phages[159,173,182]The baseplate of some non-contractile phages, however, rely on a single unrelated protein forming quasi-equivalent trimers, such as TP901–1 BppU[175], to perform the same function.

V. Methods

Plasmid design and protein expression and purification

The plasmid for expression of the $TssK_{SN}$–TssF–TssG complex (pCDF–$TssK_{SN}$6His–TssF–TssG) comprises three open-reading frames encoding $TssK_{SN}$ (residues 1–315) with a C-terminal His_6-tag, full-length TssF, and TssG (residues 64–366) under the control of a single T7 promoter[156]. *Escherichia coli*BL21DE3 (Novagen) cells bearing pCDF-$TssK_{SN}$6His–TssF–TssG were grown at 37 °C in Luria-Bertani (LB) supplemented with 50 µg/ml streptomycin. Protein expression was induced with 0.5 mM isopropyl β-D-1-thiogalactopyranoside (IPTG) for 16 h at 18 °C. Cells were harvested, resuspended in Tris-HCl 20 mM pH 8.0, NaCl 150 mM with lysozyme and lysed using a French press. Soluble proteins were separated from insoluble material by centrifugation 30 min at 20,000 g. The $TssK_{SN}$–TssF–TssG complex was purified using Ni-NTA affinity chromatography and eluted with 300 mM imidazole. Subsequently, it was further purified by gel-filtration chromatography using a Superose 6 10/300 GL column (GE Life Sciences) equilibrated in 20 mM Tris-HCl (pH 7.8), 150 mM NaCl, 5% Glycerol, and 0.5 mM TCEP. The purity of the sample was assessed by Coomassie-stained sodium dodecyl sulfate–polyacrylamide gel electrophoresis.

CryoEM data acquisition and processing

Three microliters of the purified $TssK_{SN}$–TssF–TssG complex (0.12 mg/ml) in 20 mM Tris-HCl pH 7.8 and 150 mM NaCl was applied to glow discharged C-flat holey carbon grids covered with a thin layer of carbon. Grids were then plunge-frozen in liquid ethane with a FEI MK4 Vitrobot with a 3 s blot time. The chamber was maintained at 20 °C and 100% humidity during the blotting process. Data were collected with the Leginon data collection software[183] on an FEI Titan Krios electron microscope operated at 300 kV and equipped with an energy filter (slit width of 20 eV), and a direct electron detector Gatan K2 Summit. The dose rate was adjusted to eight counts per pixel per second, and each movie was acquired in super-resolution counting mode fractionated in 50 frames of 200 ms. A total of 2601 micrographs were collected with a defocus range between 0.2 and 4.0 µm. Particles were automatically selected using Dog Picker[184] within the Appion pipeline[185]. Movie frame alignment was carried out with dose weighting using MotionCorr2[186].

Defocus parameters were estimated with GCTF[187]. An initial model was obtained using cryoSPARC[188] and all 2D and 3D classifications and refinements were performed using RELION 2.1. Subsequently, Relion3.0beta was used to refine per-particle defocus values before reclassification of the data focusing on the TssF–TssG C-terminal domain. Finally, multi-body refinement[162] was used with signal subtraction to produce a map focused on the two TssK trimers and a map focused on the $(TssF)_2$–$(TssG)_1$heterotrimer. The reported resolution is based on the gold-standard FSC = 0.143 criterion[189,190] and Fourier shell correlation curves were corrected for the effects of soft masking by high-resolution noise substitution[191]. Local resolution estimation was performed using blocres[192].

Model building and refinement

TssK was modeled based on the available X-ray crystal structures[156], whereas TssF and TssG were modeled de novo by initially building a backbone trace of their C-terminal domains into a preliminary 4.2 Å resolution reconstruction. Modeling of TssF and TssG relied on both the global map and the focused map obtained using multi-body refinement. Co-evolution derived constraints provide a way of inferring structural information given large families of evolutionarily related sequences of a protein. By identifying residues that frequently mutate together, structural information may be inferred. The strength of this “co-evolution” is strongly predictive of residue–residue contacts in the 3D structure of the protein[163,164,168,193]. For both TssF and TssG, there was sufficient sequence data to perform co-evolution analysis, and models were built using Rosetta guided by this co-evolution data[164]. These models were built by domain (three domains for TssF and two domains for TssG), and the C-terminal domain models were converged and placed into density with the help of the aforementioned backbone trace (a long insertion corresponding to TssG loop 1 allowed discrimination of TssF from TssG density). Several long insertions that poorly converged using the co-evolution information alone were rebuilt into density using RosettaES[169.] Subsequent modeling of the TssG coordinates was carried out using a combination of Coot[170],and

Rosetta[166,167] refinement, with the final model refined with Rosetta. The rest of the TssF structure (residues 20–459) was derived from the Rosetta co-evolution model and fit into density before rebuilding and refinement using a combination of Coot[170] and Rosetta[166,167]. Building and refinement was carried out using the TssK and TssF–TssG focused maps before performing a final refinement round in the TssK–TssF–TssG map. The TssF and TssG atomic models agree with 247 out of 250 and 105 out of 106 co-evolution constraints, respectively. Interaction surface area was calculated using PISA[194]. All figures were generated with UCSF Chimera[195] and UCSF ChimeraX[196].

Bacterial two-hybrid and western blotting

E. coli BTH101 cells were co-transformed with plasmids encoding the T18 and T25 fragments of *Bordetella pertussis* adenylate cyclase fused to the proteins of interest. Stationary phase cells were normalized to OD_{600} 0.5 and plated on LB agar containing 80 mg/mL X-gal, 0.5 mM IPTG, 50 mg/mL kanamycin and 150 mg/mL carbenicillin and grown for 24 h at 30 °C. pKT25 and pKNT25 constructs added T25 to the N or C-terminus, respectively, and the transformed cells were grown in the presence of 50 mg/mL kanamycin. pUC18 and pUC18C constructs added T18 to the C or N-terminus, respectively, and the transformed cells were grown in the presence of 150 mg/mL carbenicillin. Cloning was performed using Gibson assembly. Western blotting was performed using a mouse anti-CyaA (1:5000, Santa Cruz Biotechnologies #: SC-13582, Lot: C2715) and detected with an anti-mouse horseradish peroxidase-conjugated antibodies (1:5000, Sigma). Western blots were developed using chemiluminescent substrate (SuperSignal West Pico Substrate, Thermo Scientific) and imaged with an Azure c500 (Azure Biosystems). The leucine zipper interactions of the yeast protein GCN4 served as a positive control.

VI. Figures

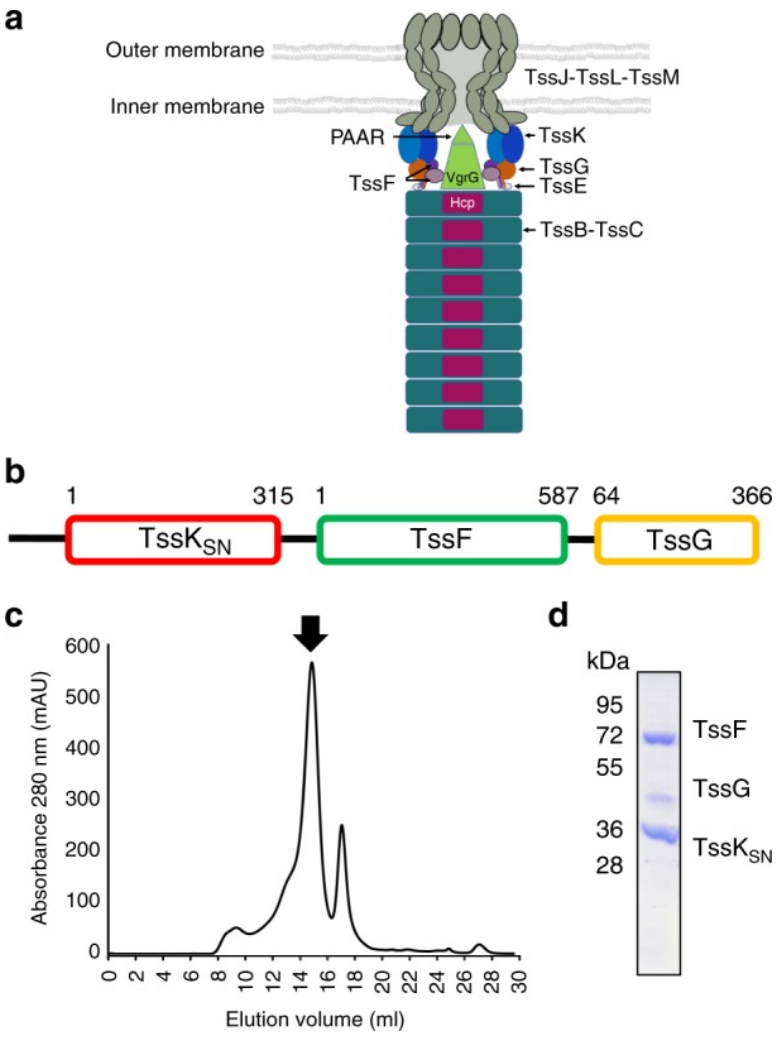

\

Figure 4.1: Schematic of the T6SS apparatus, construct design, expression, and purification of the EAEC TssK$_{SN}$-TssF–TssG complex. (**A**) Schematic of the T6SS apparatus. TssE is rendered semi-transparently owing to uncertainty in its position. TssA is not shown. (**B**) Schematic representation of the construct used for recombinant expression. (**C**) Size-exclusion chromatogram after affinity purification. (**D**) SDS-PAGE of the fraction indicated with an arrow in **C**. Molecular weights from the ladder are indicated on the left.

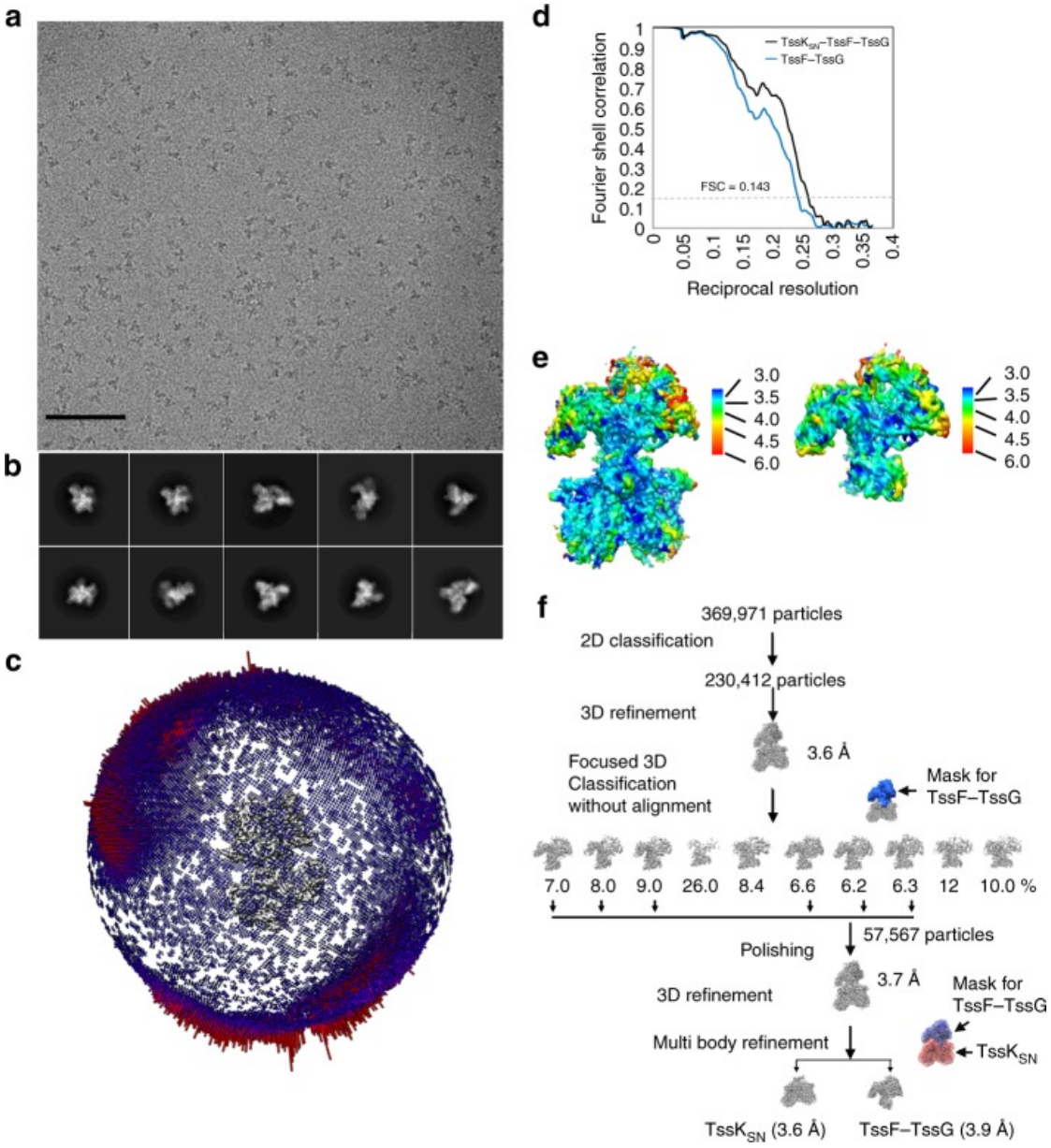

Figure 4.2: CryoEM characterization of the EAEC TssK$_{SN}$–TssF–TssG complex.
(**A**) Micrograph of frozen-hydrated particles adsorbed on a thin layer of carbon. Scale bar: 100 nm. (**B**) Reference-free 2D class averages. (**C**) Distribution of orientations of particle images used for the final reconstruction. (**D**) Gold-standard Fourier shell correlation curves for the global reconstruction (black) and the reconstruction focused on $(TssF)_2$-$(TssG)_1$ (blue). The 0.143 cutoff is indicated in gray. (**E**) Local resolution estimates of the global and TssF-TssG focused maps. (**F**) Flow-chart summarizing the data processing strategy employed.

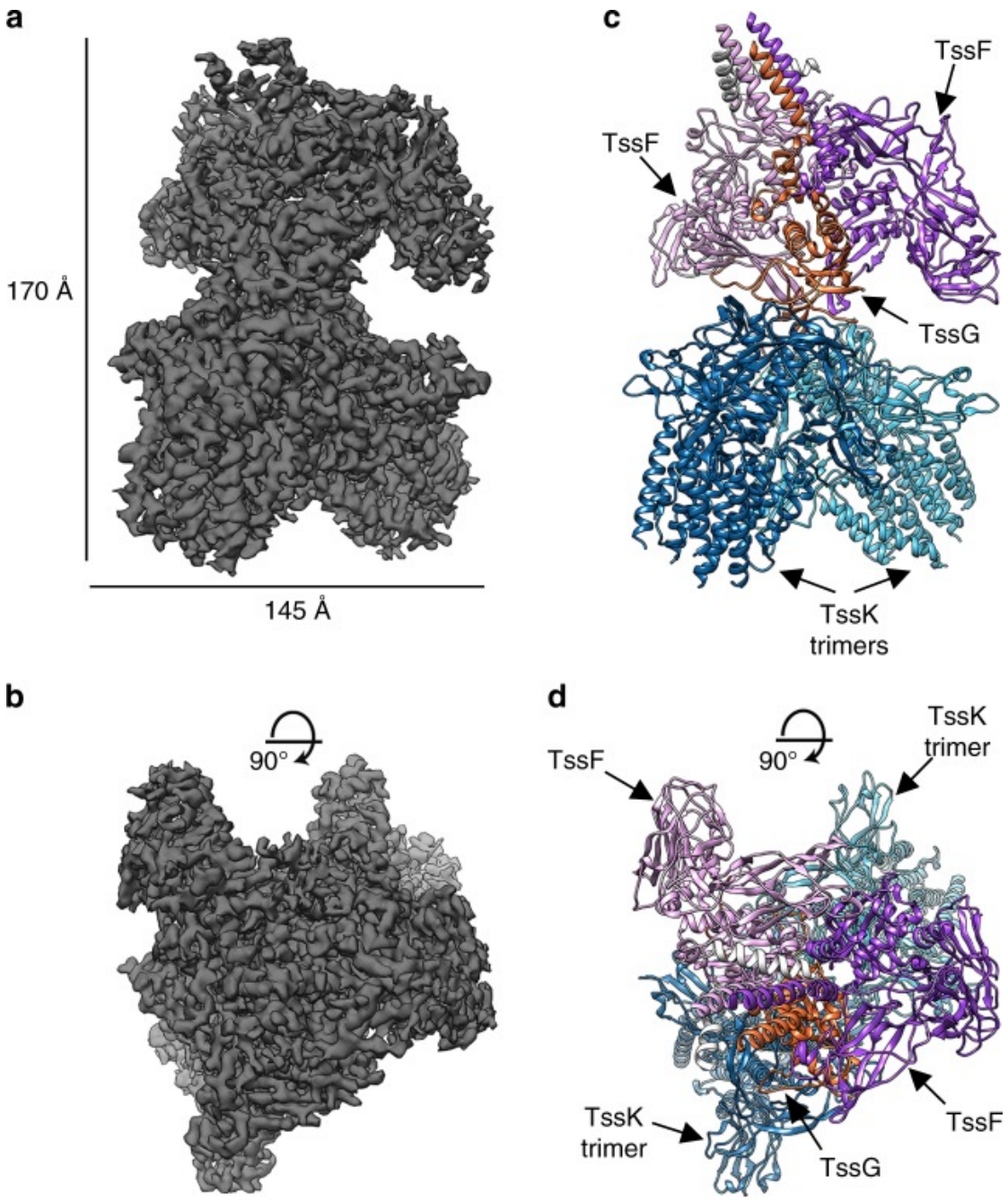

Figure 4.3 CryoEM structure of the EAEC $TssK_{SN}$–TssF–TssG complex.
(**A,B**) Two orthogonal views of the reconstruction. (**C,D**) Ribbon diagrams of the atomic model in orientations corresponding to **A,B**. Each subunit is colored differently. TssK: dark and light blue, TssF: purple and pink, TssG: orange, and two short unassigned segments are colored light gray.

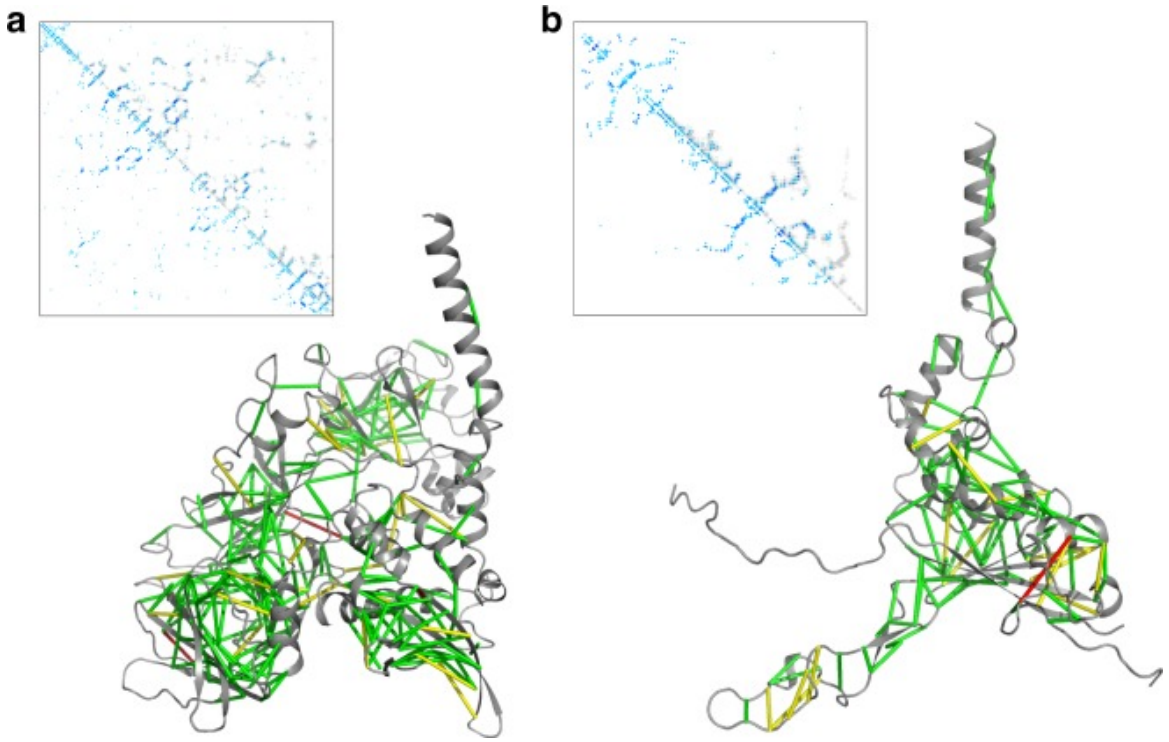

Figure 4.4: Co-evolution-predicted distance constraints for TssF and for TssG.
(**A,B**) Ribbon diagrams of TssF a and TssG b showing coevolving pairs of residues with lines colored according to the distance between coevolving residues: green, Cα < 6 Å; yellow, Cα < 10 Å; red, Cα > 10 Å. The insets show contact maps from the models (light gray dots) and those predicted from co-evolution data (blue dots). The gray dots are residue contacts from 5 A (dark gray) to 10 A (light gray). The blue dots are predicted contacts, with the darker and larger dots indicating higher confidence.

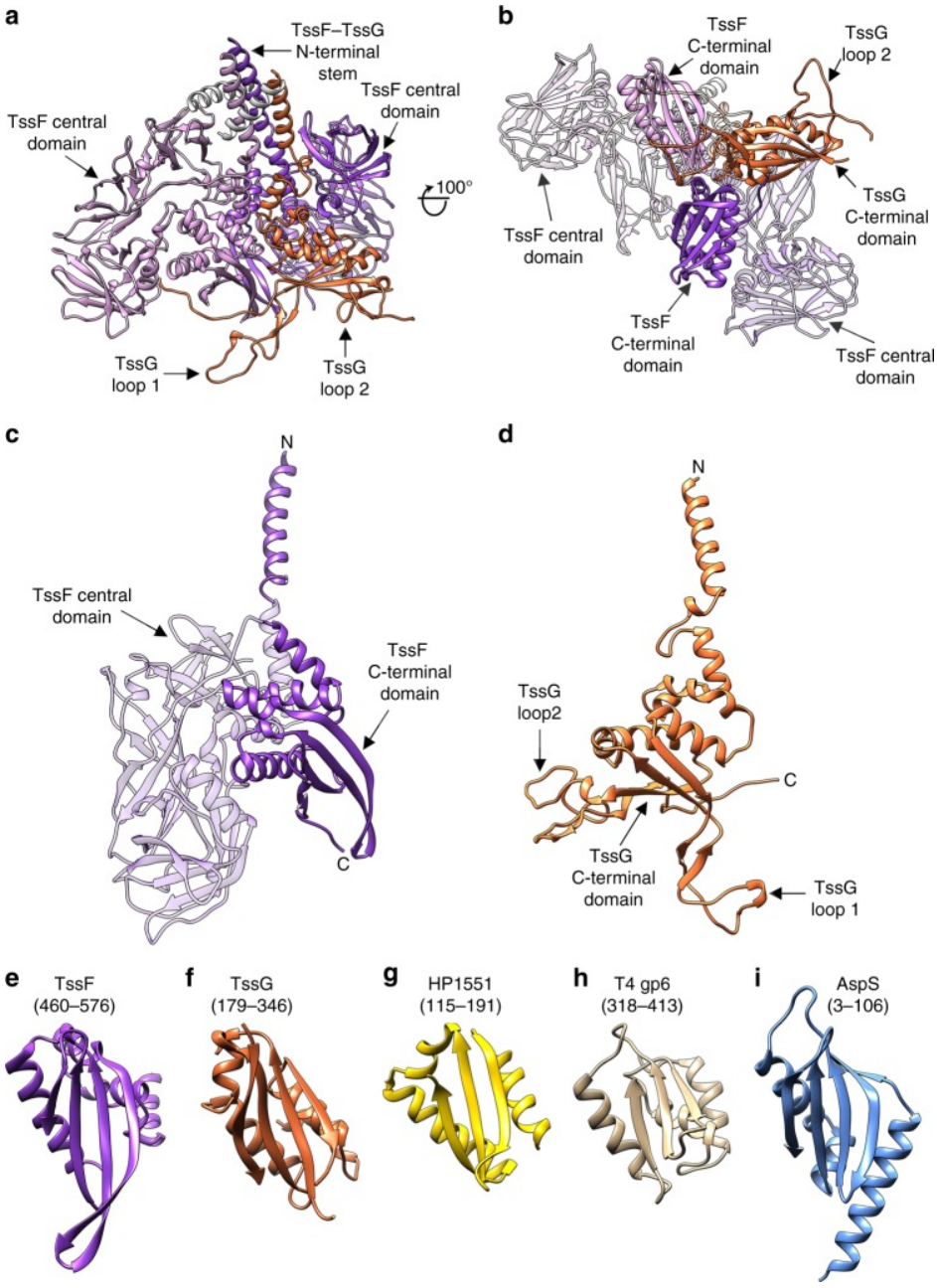

Figure 4.5: Architecture of the TssF–TssG heterotrimer.
(**A,B**) Ribbon diagrams of the TssF–TssG atomic model in two quasi-orthogonal orientations. (**C,D**) A TssF protomer c and a TssG protomer d oriented similarly to each other to emphasize their structural similarity. The TssF and TssG N- and C-termini are labeled. (**E,F**) The TssF e and TssG f C-terminal domains. (**G**) H. pylori T4SS HP1451 (gold, PDB ID 2PT7, 3.9 Å r.m.s.d. over 76 Cα carbons aligned with TssF). (**H**) Phage T4 gp7 (tan, PDB ID 5IV5, 4.2 Å r.m.s.d. over 43 Cα carbons aligned with TssF). (**I**) *V. cholerae* T2SS AspS pilotin (blue, PDB ID 4FTF, 2.7 Å r.m.s.d. over 62 Cα carbons aligned with TssF). TssF and TssG are colored identically to Figure 4.1 except for the TssF central domains, which are rendered semi-transparently in b, c for clarity. For **E-I**, the residue boundaries of the domains are shown in parentheses

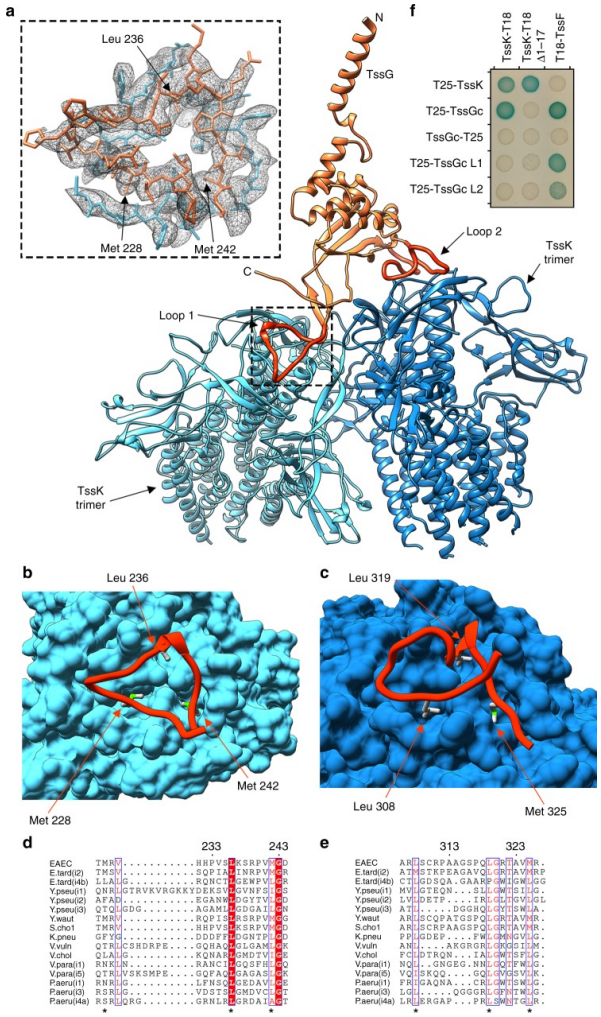

Figure 4.6 Attachment of TssK to the TssF–TssG heterotrimer. (**A**) Ribbon diagram showing that TssG loop 1 and loop 2 each anchor one TssK trimer to a baseplate wedge. The TssG N- and C-termini are labeled. The inset shows the atomic model built into the cryoEM density (gray mesh). (**B,C**) Zoomed-in view of the TssG loop 1-TssK **B**) and TssG loop 2-TssK **C** interactions. (**D,E**) Sequence alignment of TssG loop 1 **D** and loop 2 **E** from different bacterial species. In panels **A**, **C**, TssG is colored identically to Figure 4.1 except for loop 1 and loop 2 that are rendered in orange/red and TssF is omitted for clarity. In **B**, **C**, TssK is rendered in surface representation. Hydrophobic residues that were mutated for the BACTH assay are labeled in **A**–**C** and indicated with * in **D–E**. (**F**) Bacterial two-hybrid analysis of protein–protein interactions within the EAEC TssK–TssF–TssG complex. BTH101 reporter cells producing the indicated proteins or domains (TssGc: C-terminal domain of TssG, TssGc L1: C-terminal domain of TssG with the Met228Arg, Leu236Arg and Met242Arg substitutions, TssGc L2: C-terminal domain of TssG with Leu308Arg, Leu319Arg and Met325Arg substitutions, and TssK Δ1–17: TssK with deletion of the 17 N-terminal residues) fused to the T18 or T25 domain of the Bordetella adenylate cyclase were spotted on plates supplemented with IPTG and the chromogenic substrate X-Gal. Interaction between the two fusion proteins is attested by the dark blue color of the colony.

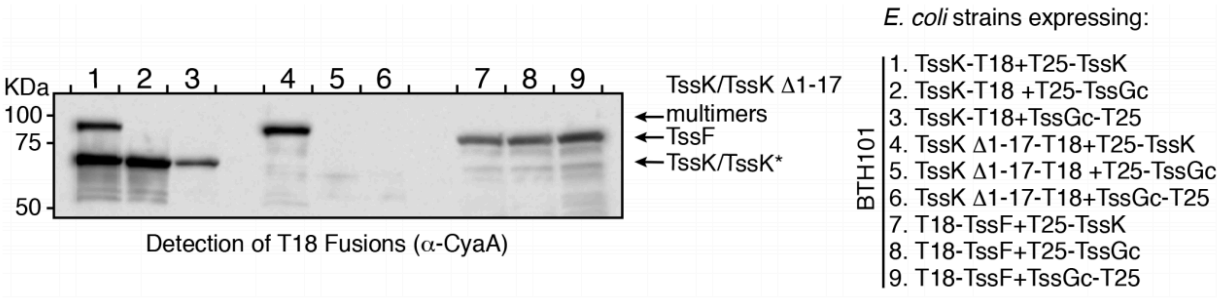

Figure 4.7: Western blot of T18-fused expression constructs utilized in BACTH.
a-CyaA Western blot to detect expression of BACTH fusion proteins. Lane assignments are depicted on the right.

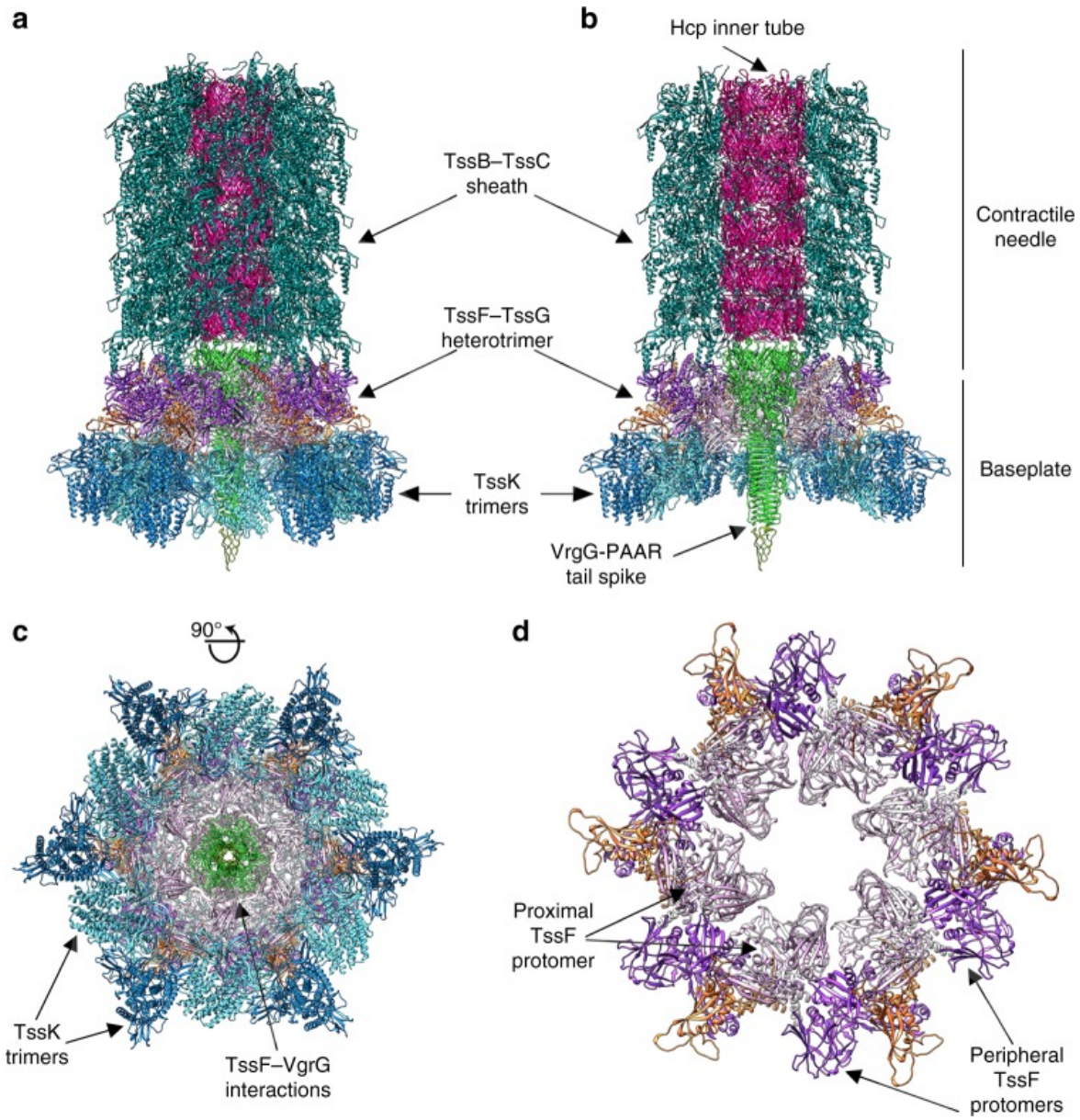

Figure 4.8: Model of the T6SS baseplate and needle complex architecture before sheath contraction. (**A**) A model was obtained by rigid-body docking subcomplex structures into the single particle cryoEM reconstruction of the non-contractile sheath mutant of the Vibrio Cholerae T6SS baseplate/needle at 8 Å resolution (EMD 3879). (**B**) Cut-away view of the model shown in **A**. (**C**) Orthogonal view of the model shown in **A**. (**D**) Circularization of the (TssF)2-(TssG)1 complex in the context of the T6SS baseplate. TssK, TssF, TssG are colored identically to Figure 4.1; TssB–TssC: teal (PDB ID 3j9g); Hcp: magenta (PDB 5OJQ); VgrG-PAAR: green-olive (PDB ID 4MTK and 4JIV)

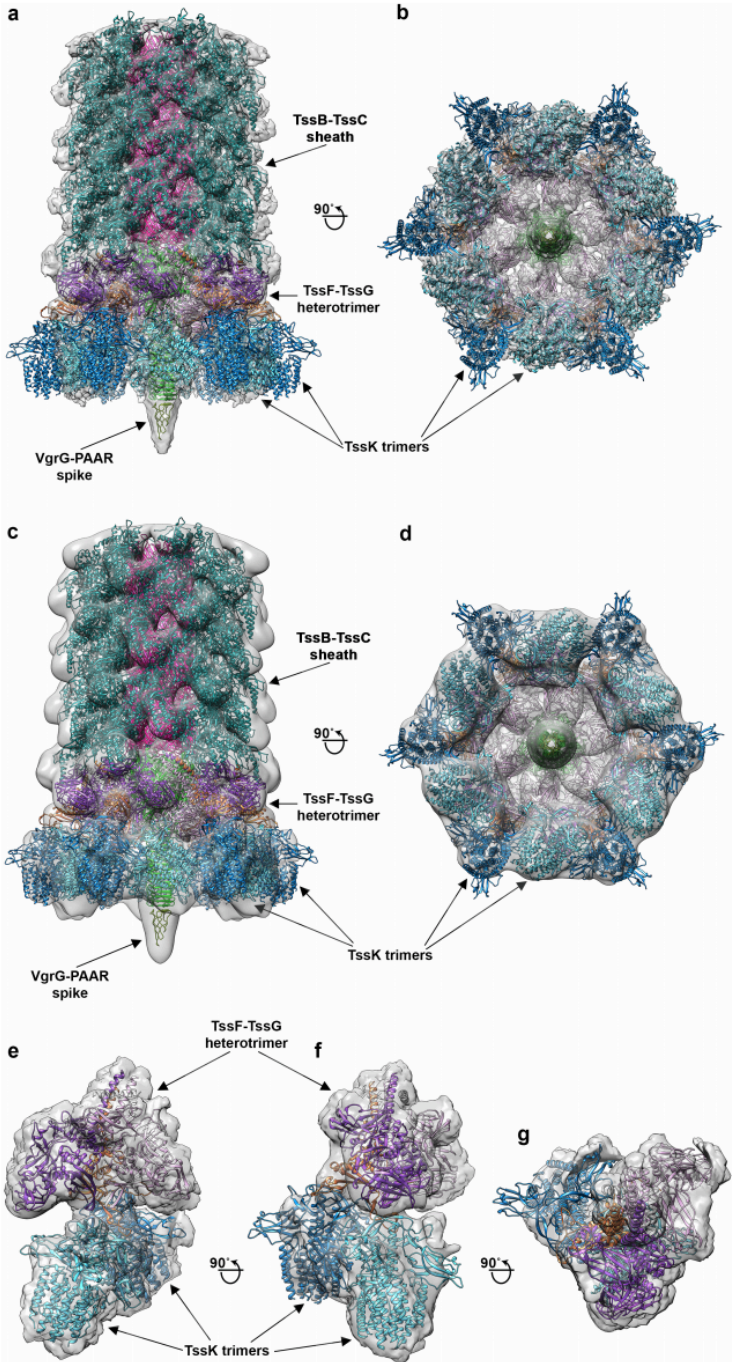

Figure 4.9: Supramolecular architecture of the T6SS baseplate and needle complex before sheath contraction. (**A**) A model was obtained by rigid-body docking subcomplex structures into the single particle cryoEM reconstruction of the non-contractile sheath mutant of the *Vibrio cholerae* T6SS baseplate/needle at 8 Å resolution (EMD 3879). (**B**) Cut-away view of the model shown in **A**. (**C**) Orthogonal view of the model shown in **A**. (**D**) Circularization of the $(TssF)_2$-$(TssG)_1$ complex in the context of the T6SS baseplate. TssK, TssF, TssG are colored identically to Figure 4.1; TssB–TssC: teal (PDB ID 3j9g); Hcp: magenta (PDB 5OJQ); VgrG-PAAR: green-olive (PDB ID 4MTK and 4JIV).

Table 4.1: CryoEM data collection, refinement, and validation statistics

	$TssK_{SN}FG$ (EMDB-9341) (PDB 6N38)	**$TssK_{SN}$ (EMDB-9342)**	**TssFG (EMDB-9343)**
Data collection and processing			
Magnification	36,496	36,496	36,496
Voltage (kV)	300	300	300
Electron exposure (e–/Å^2)	40	40	40
Defocus range (μm)	0.2–4.0	0.2-4.0	0.2-4.0
Pixel size (Å)	1.37	1.37	1.37
Symmetry imposed			
Initial particle images (no.)	369,971	369,971	369,971
Final particle images (no.)	57,567	57,567	57,567
Map resolution (Å)	3.7	3.6	3.9
FSC threshold	0.143	0.143	0.143
Map resolution range (Å)			
Refinement			
Model resolution (Å)	3.7		
FSC threshold	0.5		
Model resolution range (Å)			
Map sharpening *B* factor (Å^2)	−69		
Model composition			
Non-hydrogen atoms	24,934		
Protein residues	3145		
Ligands			
R.m.s. deviations			
Bond lengths (Å)	0.013		
Bond angles (°)	1.286		
Validation			
MolProbity score	0.95		
Clashscore	1.02		
Poor rotamers (%)	0.07		
Ramachandran plot			
Favored (%)	97.2		
Allowed (%)	2.67		
Disallowed (%)	0.13		

Chapter 5: Conclusions and Future Directions

I. Significance

Throughout my graduate career, our understanding of type VI secretion system function has expanded dramatically. We are starting to get a glimpse of the elegant mechanisms T6SS toxins use to target vital structures in target cells[17,72,76]. Additionally, a greater number of studies have begun focusing on the contribution of T6SSs in bacterial survival and niche colonization in their natural ecosystems[70,197–199]. Literature from the last decade has recognized the primary function of T6SSs as antibacterial antagonism, and it is increasingly apparent that these systems have tremendous implications for human health. Bacterial T6SSs directly influence microbial community composition through selection for compatibility in free-living environments and environments such as the human gastrointestinal tract[197]. While T6SSs are important for microbiota community organization, they can also help invading pathogens create a niche within pre-existing polymicrobial communities[199]. Deeper insight into how these systems are regulated, and how bacteria utilize them effectively, is needed to further our understanding of the roles T6SSs play in bacterial fitness.

My thesis work was motivated by the desire to understand the forces that drive the diversity present in T6SS effectors, and how bacteria in natural environments coordinate multiple systems to engage in competitive interactions. For these studies, I utilized *Pseudomonas aeruginosa* as a model organism to study T6SS. Antibacterial T6-effectors were first discovered in *P. aeruginosa* which encodes the T6SS with the most well-defined toxin repertoire, and contains three functionally independent T6SSs[30].

During my thesis project, I developed multiple sequencing-based strategies to assess effector potency under a variety of environmental conditions. Additionally, I generated a series of *P. aeruginosa* strains to examine its three T6SS independently of one another as well as to toggle which effectors were available to the cell to evaluate species-specific toxicity and synergistic toxin activities. This work is the first example of a systems-level approach to identify when toxins are efficacious. Ultimately these experiments uncovered a role for T6SS effector diversity in

promoting toxin synergy and overcoming the unpredictability of environmental parameters. This project became the first published study investigating the cellular benefits of multiple effector secretion. In this chapter, I will detail how my work has contributed to the collective knowledge of the T6SS field, the immediate future directions for this work, and what outstanding questions remain to be answered.

II. Uncovering the function of an enigmatic T6-effector, Tse4

The enzymatic activities of most T6SS effectors have been determined by bioinformatic identification of common motifs present in effector homologs, followed by experimental validation[42,50,64,68]. During my thesis work, I sought to characterize an effector,Tse4, with unknown activity from the H1-T6SS in *P. aeruginosa*. Tse4 had no homology to characterized proteins, and iterative Hidden Markov Modeling did not identify any motifs or conserved residues that might inform its biochemical activity. To determine the activity of Tse4, I investigated the cellular outcome to Tse4 intoxication. I found Tse4 is toxic in the periplasm of bacterial cells and causes cellular depolarization, disruption of specific-ion gradients, and bacteriostasis. All of these phenotypes are consistent with Tse4 being a small, ion-selective pore-forming toxin that acts in the inner membrane of cells. This study is the first description of a T6-secreted pore-forming toxin that generates ion-specific channels. Before Tse4, VasX from *Vibrio cholerae* was the only known pore-forming T6-effector to be characterized[65]. VasX forms large pores in the inner membrane leading to cell lysis. Tse4 and VasX do not resemble each other via sequence homology or secondary structure prediction, signifying they each comprise their own evolutionarily distinct family of proteins. My work uncovered a novel family of antimicrobial toxins and increased our understanding of the complexity of H1-T6SS substrates.

Purification of Tse4 for in vitro and structural studies

One future direction for research would be to characterize Tse4 *in vitro*. The initial purification of Tse4 was challenging due to insolubility and low yield. While I have developed a protocol for purification of Tse4, the total yield is still modest. An extensive panel of various detergents and lipid mixtures needs to be tested for their capacity to extract Tse4 from the lipid membrane while also maintaining the structural stability required for *in vitro* work and structural determination. The main techniques for structural determination of small proteins (Tse4 is 19 KDa) are X-ray crystallography or MicroED[200,201]. However, since both of these methods require protein crystallization, an alternative approach could be to use cryo-EM. Once a structure of Tse4 is obtained, it could then be compared to other publicly-available pore-forming toxin domains to ascertain structural similarity, potentially lending substantial mechanistic insight into the activity of this unique protein.

Defining the mechanism of ion-selectivity

Ion-selective toxins function by oligomerizing to form a pore in a membrane, with part of the resulting channel constricting to form a 'selectivity filter'[124,202]. This filter consists of a narrow passage lined with charged residues that interact with or repulse cations or anions, which dictate transport through the pore. There are currently no published data describing ion selectivity in T6 pore-forming toxins. One method to define ion selectivity is *in vitro* lipid bilayer reconstitution of the pore followed by electrophysiology[203,204]. If the protein is forming a channel in the lipid bilayer that allows an ion through, you can measure differential conductance across a trans-well setup. Changing the salts, buffer pH, and lipid species informs ion-selectivity, pH gating, and the lipid preferences of the protein. In combination with secondary structure prediction, or preferably the 3D protein structure, residues of interest can be mutated to assess their role in ion-selective gating. Ion-selectivity is poorly understood for many pore-forming proteins, and an in-depth characterization of Tse4 may inform the mechanism of ion-selectivity for other bacterial pore-forming toxins.

III. Identifying conditional and synergistic toxin activities

A major gap in our knowledge of T6SS effectors is how (or if) the secreted effectors of a single T6SSs act in concert to disable a cell. Additionally, little work has been done to understand if there are external factors that could compromise T6 effector efficacy. I developed an assay called parallel analysis of effector efficacy (PAEE), which allows us to study the efficacy of multiple T6SS effectors simultaneously under a variety of environmental conditions. One advantage of this technique is that it can be adapted to any bacterial T6SS substrate, or any set of bacterial T6SS substrates, as long as the conditions are known to promote T6 secretion. This method enabled the investigation of conditional effector toxicity as the identification of effector activities with synergistic outcomes.

This study is the first example of a method to measure effector synergy for an antimicrobial contact inhibition system, although it has long been hypothesized the deployment of multiple effectors could promote synergistic interactions[205,206]. My work also demonstrated that external environmental conditions can alter the potency of these effectors. Therefore, under a given condition, it is plausible that not all secreted T6 effectors are contributing to fitness at maximal capacity.

An alternative theory for why bacteria maintain multiple effectors, is that this increases the fitness advantage of the cell during competitive interactions with a wide phylogenetic range of bacterial species. While T6-effectors exclusively target essential structures within the cell, cells could modify these molecules or encode different repair or response pathways to deal with the damage. To test this theory, I utilized a 16S sequencing approach to determine the competitive advantage of utilizing functionally distinct T6SSs against multispecies communities. I then measured the contribution of individual effectors to fitness against this community. From this study, I found that only one T6SS in *P. aeruginosa*, the H1-T6SS, consistently targets α and β-proteobacterial species.

Additionally, by utilizing strains with only one functional effector, I found that several effectors exhibit species-specific activity. This method could be applied to other bacterial T6SSs to identify natural targets of T6 activity and which effectors are most toxic toward a particular species. This is the first study to reveal a differential role for effectors against an assortment of species.

Do bacterial T6SS repertoires reflect their environmental lifestyle?

My thesis work demonstrates changes in external pH, salinity, oxygen availability, and temperature can significantly alter the toxicity of T6-delivered effectors. These experimental conditions were chosen to reflect changes *P. aeruginosa* commonly experiences in the environment. A natural question that arises from this study is whether a given bacterium's T6SS effector repertoire reflects the environment that organism inhabits. Do ubiquitous bacteria have a larger, more diverse subset of effectors to compensate for the unpredictability of their surroundings? In contrast, would an organism that lives in a specific niche, such as the human gastrointestinal tract or marine habitat, have fewer effectors, and would these smaller subsets of effectors be optimal for maximal activity in that environment? For example, membrane targeting toxins are more potent in higher salinities, whereas peptidoglycan degrading effectors are less toxic. Therefore, we could hypothesize a T6SS+ marine bacterium would enrich for membrane-associated toxins. In this vein, I believe it would be informative to look bioinformatically at a large number of T6SS+ organisms to identify their potential effector subsets. Each organism can then be grouped by their environmental niches to analyze whether their effects are fine-tuned to their habitat. This type of study could inform whether conditional effector efficacy applies sufficient evolutionary pressure for bacteria to maintain horizontally acquired effectors optimal for competition within specific niches.

How do T6SS effectors act synergistically?

Work presented in this thesis demonstrates that T6SS-effectors can interact with each other synergistically. For example, I found PG-targeting effectors synergize with Tse4, a pore-forming effector that dissipates membrane potential. Loss of membrane potential in *P. aeruginosa* triggers the production of native autolysins that digest PG, which could positively affect the potency of effectors that cleave PG. Tse4 activity also increases the toxicity of an $NAD(P)^+$ glycohydrolase effector, Tse6, particularly in anaerobic conditions. During anaerobiosis, cells rely exclusively on NAD^+ and ion gradients to maintain the proton motive force. Since Tse4 depolarizes cells by disruption of essential ion gradients and Tse6 limits NAD+ availability, co-intoxication by Tse4 and Tse6 likely exacerbates their toxicity toward the recipeint cell. While we have many hypotheses for why effector synergy occurs, none have been formally tested, and there is a possibility synergy might be obtained through alternative mechanisms. The next step to understanding T6-effector synergy within recipient cells is to monitor how each toxin affects cellular processes independently and in tandem, to dissect how the activity one a toxin could influence another toxins efficacy.

Why do effectors have species-specificity?

In this thesis, for the first time I provide evidence for effectors with species-specific toxicity. These findings are interesting but will require rigorous follow-up studies in order to discern the mechanisms behind these differences in potency. One hypothesis is a particular toxin cannot target certain species due to intrinsic differences in its target substrate. In this scenario, it is critical to compare and contrast the targeted structure found in susceptible cells versus those resistant to the toxin, to identify modifications or pathways that contribute to protection.

IV. Dissecting T6SS baseplate component interactions

In Chapter 4, we worked in collaboration with the laboratory of Dr. David Veesler (University of Washington Biochemistry) to dissect the architecture of the T6SS baseplate- a

structure composed of proteins that are evolutionarily related to contractile phage components. The Veesler laboratory has recently determined a high-resolution structure of the enteroaggregative *E. coli* baseplate subcomplex via cryo-electron microscopy[207]. This structure revealed the stoichiometry of the TssK, TssF, and TssG complex, and suggested multiple protein domains and regions potentially critical for mediating protein-protein contacts. In order to validate these interactions, I designed constructs for various putative interaction partners and performed bacterial two-hybrid analysis. I generated a series of full-length, truncated, and point mutant versions of TssK, TssF, and TssG fused to portions of broken adenylate cyclase to assay for protein interactions. This analysis corroborated the atomic structure on several accounts including the self-association of TssK protomers and the N-terminal region of TssK binding to two loop regions in TssG. TssG has two loop regions that appear by the structure to mediate contact to TssK through hydrophobic interactions. Substitution of these hydrophobic residues to asparagine arginine abrogated binding of TssK without affecting TssG interaction with TssF. Analysis of protein expression and stability by Western blotting demonstrated the fusions in the experiment were correctly expressed. This analysis also revealed that TssK protomers form SDS-resistant multimers, suggesting tight intramolecular binding. Data from the Cascales and Camillau laboratories on the enteroaggregative *E. coli* baseplate complex also agree with the main conclusions of our study and the BACTH analysis[208]. Future work will be needed to determine the order of baseplate assembly and to understand how these proteins evolved to interact.

References

1. Stubbendieck, R. M. & Straight, P. D. Multifaceted Interfaces of Bacterial Competition. *J. Bacteriol.* (2016). doi:10.1128/jb.00275-16
2. Foster, K. R. & Bell, T. Competition, not cooperation, dominates interactions among culturable microbial species. *Curr. Biol.* (2012). doi:10.1016/j.cub.2012.08.005
3. Yang, N. J. & Hinner, M. J. Getting across the cell membrane: an overview for small molecules, peptides, and proteins. *Methods in molecular biology (Clifton, N.J.)* (2015). doi:10.1007/978-1-4939-2272-7_3
4. Masi, M., Réfregiers, M., Pos, K. M. & Pagès, J. M. Mechanisms of envelope permeability and antibiotic influx and efflux in Gram-negative bacteria. *Nat. Microbiol.* (2017). doi:10.1038/nmicrobiol.2017.1
5. Cascales, E. *et al.* Colicin Biology. *Microbiol. Mol. Biol. Rev.* (2007). doi:10.1128/MMBR.00036-06
6. Kleanthous, C. Swimming against the tide: Progress and challenges in our understanding of colicin translocation. *Nature Reviews Microbiology* (2010). doi:10.1038/nrmicro2454
7. Lopez, J. & Feldman, M. F. Expanding the molecular weaponry of bacterial species. *Journal of Biological Chemistry* (2018). doi:10.1074/jbc.H118.001463
8. Hayes, C. S., Aoki, S. K. & Low, D. A. Bacterial Contact-Dependent Delivery Systems. *Annu. Rev. Genet.* (2010). doi:10.1146/annurev.genet.42.110807.091449
9. Whitney, J. C. *et al.* A broadly distributed toxin family mediates contact-dependent antagonism between gram-positive bacteria. *Elife* (2017). doi:10.7554/eLife.26938
10. Granato, E. T., Foster, K. R., Meiller-Legrand, T. A. & Foster, K. R. The evolution and ecology of bacterial warfare. *Curr. Biol.* **29**, 1–39 (2019).
11. Coulthurst, S. The Type VI secretion system: a versatile bacterial weapon. *Microbiology* (2019). doi:10.1099/mic.0.000789
12. Russell, A. B., Peterson, S. B. & Mougous, J. D. Type VI secretion system effectors: Poisons with a purpose. *Nat. Rev. Microbiol.* **12**, 137–148 (2014).
13. Whitney, J. C. *et al.* Genetically distinct pathways guide effector export through the type VI secretion system. *Mol. Microbiol.* (2014). doi:10.1111/mmi.12571
14. Unterweger, D., Kostiuk, B. & Pukatzki, S. Adaptor Proteins of Type VI Secretion System Effectors. *Trends in Microbiology* (2017). doi:10.1016/j.tim.2016.10.003
15. Russell, A. B. *et al.* A type VI secretion-related pathway in bacteroidetes mediates interbacterial antagonism. *Cell Host Microbe* (2014). doi:10.1016/j.chom.2014.07.007
16. Eshraghi, A. *et al.* Secreted Effectors Encoded within and outside of the Francisella Pathogenicity Island Promote Intramacrophage Growth. *Cell Host Microbe* (2016). doi:10.1016/j.chom.2016.10.008
17. Ledvina, H. E. *et al.* A Phosphatidylinositol 3-Kinase Effector Alters Phagosomal Maturation to Promote Intracellular Growth of Francisella. *Cell Host Microbe* (2018). doi:10.1016/j.chom.2018.07.003
18. Hachani, A., Wood, T. E. & Filloux, A. Type VI secretion and anti-host effectors. *Current Opinion in Microbiology* (2016). doi:10.1016/j.mib.2015.11.006
19. Wang, T. *et al.* Type VI Secretion System Transports Zn^{2+} to Combat Multiple Stresses and Host Immunity. *PLoS Pathog.* (2015). doi:10.1371/journal.ppat.1005020
20. Si, M. *et al.* Manganese scavenging and oxidative stress response mediated by type VI secretion system in Burkholderia thailandensis . *Proc. Natl. Acad. Sci.* (2017). doi:10.1073/pnas.1614902114
21. Bladergroen, M. R., Badelt, K. & Spaink, H. P. Infection-Blocking Genes of a Symbiotic Rhizobium leguminosarum Strain That Are Involved in Temperature-Dependent Protein Secretion . *Mol. Plant-Microbe Interact.* (2007). doi:10.1094/mpmi.2003.16.1.53
22. Srinivasa Rao, P. S., Yamada, Y., Yuen, P. T. & Ka, Y. L. Use of proteomics to identify

novel virulence determinants that are required for Edwardsiella tarda pathogenesis. *Mol. Microbiol.* (2004). doi:10.1111/j.1365-2958.2004.04123.x
23. Boyer, F., Fichant, G., Berthod, J., Vandenbrouck, Y. & Attree, I. Dissecting the bacterial type VI secretion system by a genome wide in silico analysis: What can be learned from available microbial genomic resources? *BMC Genomics* (2009). doi:10.1186/1471-2164-10-104
24. Pukatzki, S. *et al.* Identification of a conserved bacterial protein secretion system in Vibrio cholerae using the Dictyostelium host model system. *Proc. Natl. Acad. Sci. U. S. A.* (2006). doi:10.1073/pnas.0510322103
25. Schwarz, S. *et al.* Burkholderia type vi secretion systems have distinct roles in eukaryotic and bacterial cell interactions. *PLoS Pathog.* (2010). doi:10.1371/journal.ppat.1001068
26. Schwarz, S., Hood, R. D. & Mougous, J. D. What is type VI secretion doing in all those bugs? *Trends in Microbiology* (2010). doi:10.1016/j.tim.2010.09.001
27. Ma, A. T. & Mekalanos, J. J. In vivo actin cross-linking induced by Vibrio cholerae type VI secretion system is associated with intestinal inflammation. *Proc. Natl. Acad. Sci.* (2010). doi:10.1073/pnas.0915156107
28. Suarez, G. *et al.* Molecular characterization of a functional type VI secretion system from a clinical isolate of Aeromonas hydrophila. *Microb. Pathog.* (2008). doi:10.1016/j.micpath.2007.10.005
29. Schell, M. A. *et al.* Type VI secretion is a major virulence determinant in Burkholderia mallei. *Mol. Microbiol.* (2007). doi:10.1111/j.1365-2958.2007.05734.x
30. Hood, R. D. *et al.* A Type VI Secretion System of Pseudomonas aeruginosa Targets a Toxin to Bacteria. *Cell Host Microbe* (2010). doi:10.1016/j.chom.2009.12.007
31. Russell, A. B. *et al.* Type VI secretion delivers bacteriolytic effectors to target cells. *Nature* (2011). doi:10.1038/nature10244
32. Alcoforado Diniz, J., Liu, Y. C. & Coulthurst, S. J. Molecular weaponry: Diverse effectors delivered by the Type VI secretion system. *Cellular Microbiology* (2015). doi:10.1111/cmi.12532
33. Russell, A. B. *et al.* Diverse type VI secretion phospholipases are functionally plastic antibacterial effectors. *Nature* **496**, 508–512 (2013).
34. Sana, T. G., Lugo, K. A. & Monack, D. M. T6SS: The bacterial 'fight club' in the host gut. *PLoS Pathogens* (2017). doi:10.1371/journal.ppat.1006325
35. Jiang, F., Waterfield, N. R., Yang, J., Yang, G. & Jin, Q. A Pseudomonas aeruginosa type VI secretion phospholipase D effector targets both prokaryotic and eukaryotic cells. *Cell Host Microbe* (2014). doi:10.1016/j.chom.2014.04.010
36. Dar, Y., Salomon, D. & Bosis, E. The Antibacterial and Anti-Eukaryotic Type VI Secretion System MIX-Effector Repertoire in Vibrionaceae. *Mar. Drugs* (2018). doi:10.3390/md16110433
37. Coulthurst, S. J. The Type VI secretion system - a widespread and versatile cell targeting system. *Res. Microbiol.* (2013). doi:10.1016/j.resmic.2013.03.017
38. Schwarz, S. *et al.* Burkholderia type VI secretion systems have distinct roles in eukaryotic and bacterial cell interactions. *PLoS Pathog.* (2010). doi:10.1371/journal.ppat.1001068
39. Spiewak, H. L. *et al.* Burkholderia cenocepacia utilizes a type VI secretion system for bacterial competition. *Microbiologyopen* (2019). doi:10.1002/mbo3.774
40. Alcoforado Diniz, J. & Coulthurst, S. J. Intraspecies Competition in Serratia marcescens Is Mediated by Type VI-Secreted Rhs Effectors and a Conserved Effector-Associated Accessory Protein. *J. Bacteriol.* (2015). doi:10.1128/jb.00199-15
41. Lien, Y.-W. & Lai, E.-M. Type VI Secretion Effectors: Methodologies and Biology. *Front. Cell. Infect. Microbiol.* (2017). doi:10.3389/fcimb.2017.00254
42. Russell, A. B. *et al.* A Widespread Bacterial Type VI Secretion Effector Superfamily Identified Using a Heuristic Approach. *Cell Host Microbe* (2012).

doi:10.1016/j.chom.2012.04.007
43. Salomon, D. *et al.* Marker for type VI secretion system effectors. *Proc. Natl. Acad. Sci.* (2014). doi:10.1073/pnas.1406110111
44. Ma, J. *et al.* PAAR-Rhs proteins harbor various C-terminal toxins to diversify the antibacterial pathways of type VI secretion systems. *Environ. Microbiol.* (2017). doi:10.1111/1462-2920.13621
45. Hachani, A., Allsopp, L. P., Oduko, Y. & Filloux, A. The VgrG proteins are 'à la carte' delivery systems for bacterial type VI effectors. *J. Biol. Chem.* (2014). doi:10.1074/jbc.M114.563429
46. Koskiniemi, S. *et al.* Rhs proteins from diverse bacteria mediate intercellular competition. *Proc. Natl. Acad. Sci.* (2013). doi:10.1073/pnas.1300627110
47. Zhang, D., de Souza, R. F., Anantharaman, V., Iyer, L. M. & Aravind, L. Polymorphic toxin systems: Comprehensive characterization of trafficking modes, processing, mechanisms of action, immunity and ecology using comparative genomics. *Biol. Direct* (2012). doi:10.1186/1745-6150-7-18
48. Liang, X. *et al.* Identification of divergent type VI secretion effectors using a conserved chaperone domain. *Proc. Natl. Acad. Sci.* (2015). doi:10.1073/pnas.1505317112
49. Bondage, D. D., Lin, J.-S., Ma, L.-S., Kuo, C.-H. & Lai, E.-M. VgrG C terminus confers the type VI effector transport specificity and is required for binding with PAAR and adaptor–effector complex. *Proc. Natl. Acad. Sci.* (2016). doi:10.1073/pnas.1600428113
50. Ma, L. S., Hachani, A., Lin, J. S., Filloux, A. & Lai, E. M. Agrobacterium tumefaciens deploys a superfamily of type VI secretion DNase effectors as weapons for interbacterial competition in planta. *Cell Host Microbe* (2014). doi:10.1016/j.chom.2014.06.002
51. De Maayer, P. *et al.* Comparative genomics of the type VI secretion systems of Pantoea and Erwinia species reveals the presence of putative effector islands that may be translocated by the VgrG and Hcp proteins. *BMC Genomics* (2011). doi:10.1186/1471-2164-12-576
52. Altindis, E., Dong, T., Catalano, C. & Mekalanos, J. Secretome analysis of Vibrio cholerae type VI secretion system reveals a new effector-immunity pair. *MBio* (2015). doi:10.1128/mBio.00075-15
53. Miyata, S. T., Kitaoka, M., Brooks, T. M., McAuley, S. B. & Pukatzki, S. Vibrio cholerae requires the type VI secretion system virulence factor vasx to kill dictyostelium discoideum. *Infect. Immun.* (2011). doi:10.1128/IAI.01266-10
54. Russell, A. B. *et al.* A widespread bacterial type VI secretion effector superfamily identified using a heuristic approach. *Cell Host Microbe* (2012). doi:10.1016/j.chom.2012.04.007
55. Fritsch, M. J. *et al.* Proteomic Identification of Novel Secreted Antibacterial Toxins of the Serratia marcescens Type VI Secretion System . *Mol. Cell. Proteomics* (2013). doi:10.1074/mcp.m113.030502
56. Wan, B. *et al.* Type VI secretion system contributes to Enterohemorrhagic Escherichia coli virulence by secreting catalase against host reactive oxygen species (ROS). *PLoS Pathog.* (2017). doi:10.1371/journal.ppat.1006246
57. Silverman, J. M. *et al.* Haemolysin Coregulated Protein Is an Exported Receptor and Chaperone of Type VI Secretion Substrates. *Mol. Cell* (2013). doi:10.1016/j.molcel.2013.07.025
58. Bugg, T. D. H., Braddick, D., Dowson, C. G. & Roper, D. I. Bacterial cell wall assembly: Still an attractive antibacterial target. *Trends in Biotechnology* (2011). doi:10.1016/j.tibtech.2010.12.006
59. Yount, N. Y. & Yeaman, M. R. Peptide antimicrobials: Cell wall as a bacterial target. *Ann. N. Y. Acad. Sci.* (2013). doi:10.1111/nyas.12005
60. Typas, A., Banzhaf, M., Gross, C. A. & Vollmer, W. From the regulation of peptidoglycan synthesis to bacterial growth and morphology. *Nature Reviews Microbiology* (2012).

doi:10.1038/nrmicro2677
61. Weber, B. S. *et al.* Genetic Dissection of the Type VI Secretion System in Acinetobacter and Identification of a Novel Peptidoglycan Hydrolase, TagX, Required for Its Biogenesis . *MBio* (2016). doi:10.1128/mbio.01253-16
62. Rojas, E., Theriot, J. A. & Huang, K. C. Response of Escherichia coli growth rate to osmotic shock. *Proc. Natl. Acad. Sci.* (2014). doi:10.1073/pnas.1402591111
63. Zhang, Y. M. & Rock, C. O. Membrane lipid homeostasis in bacteria. *Nature Reviews Microbiology* (2008). doi:10.1038/nrmicro1839
64. Russell, A. B. *et al.* Diverse type VI secretion phospholipases are functionally plastic antibacterial effectors. *Nature* (2013). doi:10.1038/nature12074
65. Miyata, S. T., Unterweger, D., Rudko, S. P. & Pukatzki, S. Dual Expression Profile of Type VI Secretion System Immunity Genes Protects Pandemic Vibrio cholerae. *PLoS Pathog.* (2013). doi:10.1371/journal.ppat.1003752
66. LaCourse, K. D. *et al.* Conditional toxicity and synergy drive diversity among antibacterial effectors. *Nat. Microbiol.* (2018). doi:10.1038/s41564-018-0113-y
67. Mariano, G. *et al.* A new family of Type VI secretion system-delivered effector proteins displays ion-selective pore-forming activity. *bioRxiv* 676247 (2019). doi:10.1101/676247
68. Pissaridou, P. *et al.* The Pseudomonas aeruginosa T6SS-VgrG1b spike is topped by a PAAR protein eliciting DNA damage to bacterial competitors . *Proc. Natl. Acad. Sci.* (2018). doi:10.1073/pnas.1814181115
69. Ma, J. *et al.* The Hcp proteins fused with diverse extended-toxin domains represent a novel pattern of antibacterial effectors in type VI secretion systems. *Virulence* (2017). doi:10.1080/21505594.2017.1279374
70. Bernal, P., Allsopp, L. P., Filloux, A. & Llamas, M. A. The Pseudomonas putida T6SS is a plant warden against phytopathogens. *ISME J.* (2017). doi:10.1038/ismej.2016.169
71. Wallace, S. S. Base excision repair: A critical player in many games. *DNA Repair (Amst).* (2014). doi:10.1016/j.dnarep.2014.03.030
72. Whitney, J. C. *et al.* An Interbacterial NAD(P)+ Glycohydrolase Toxin Requires Elongation Factor Tu for Delivery to Target Cells. *Cell* (2015). doi:10.1016/j.cell.2015.09.027
73. Tang, J. Y., Bullen, N. P., Ahmad, S. & Whitney, J. C. Diverse NADase effector families mediate interbacterial antagonism via the type VI secretion system. *J. Biol. Chem.* (2018).
74. Bi, E. & Lutkenhaus, J. FtsZ ring structure associated with division in Escherichia coli. *Nature* (1991). doi:10.1038/354161a0
75. Bisson-Filho, A. W. *et al.* Treadmilling by FtsZ filaments drives peptidoglycan synthesis and bacterial cell division. *Science (80-.).* (2017). doi:10.1126/science.aak9973
76. Ting, S.-Y. *et al.* Bifunctional Immunity Proteins Protect Bacteria against FtsZ-Targeting ADP-Ribosylating Toxins. *Cell* 1–13 (2018). doi:10.1016/j.cell.2018.09.037
77. Durand, E., Cambillau, C., Cascales, E. & Journet, L. VgrG, Tae, Tle, and beyond: The versatile arsenal of Type VI secretion effectors. *Trends in Microbiology* (2014). doi:10.1016/j.tim.2014.06.004
78. Fischbach, M. A. Combination therapies for combating antimicrobial resistance. *Current Opinion in Microbiology* (2011). doi:10.1016/j.mib.2011.08.003
79. Vollmer, W. Structural variation in the glycan strands of bacterial peptidoglycan. *FEMS Microbiology Reviews* (2008). doi:10.1111/j.1574-6976.2007.00088.x
80. Mahapatra, S., Crick, D. C., McNeil, M. R. & Brennan, P. J. Unique structural features of the peptidoglycan of Mycobacterium leprae. *J. Bacteriol.* **190**, 655–661 (2008).
81. Folkening, W. J., Nogami, W., Martin, S. A. & Rosenthal, R. S. Structure of Bordetella pertussis peptidoglycan. *J. Bacteriol.* (1987). doi:10.1128/jb.169.9.4223-4227.1987
82. Billini, M., Biboy, J., Kühn, J., Vollmer, W. & Thanbichler, M. A specialized MreB-dependent cell wall biosynthetic complex mediates the formation of stalk-specific peptidoglycan in Caulobacter crescentus. *PLoS Genet.* (2019). doi:10.1371/journal.pgen.1007897

83. Fiser, A., Filipe, S. R. & Tomasz, A. Cell wall branches, penicillin resistance and the secrets of the MurM protein. *Trends Microbiol.* (2003).
84. Sohlenkamp, C. & Geiger, O. Bacterial membrane lipids: Diversity in structures and pathways. *FEMS Microbiol. Rev.* **40**, 133–159 (2015).
85. Nguyen, N. A. T., Sallans, L. & Kaneshiro, E. S. The major glycerophospholipids of the predatory and parasitic bacterium Bdellovibrio bacteriovorus HID5. *Lipids* (2008). doi:10.1007/s11745-008-3235-9
86. Lata, P., Lal, D. & Lal, R. Flavobacterium ummariense sp. nov., isolated from hexachlorocyclohexane-contaminated soil, and emended description of Flavobacterium ceti Vela et al. 2007. *Int. J. Syst. Evol. Microbiol.* (2012). doi:10.1099/ijs.0.030916-0
87. Vollmer, W., Blanot, D. & De Pedro, M. A. Peptidoglycan structure and architecture. *FEMS Microbiology Reviews* (2008). doi:10.1111/j.1574-6976.2007.00094.x
88. Hurst, A. Bacterial injury: a review. *Can. J. Microbiol.* (2010). doi:10.1139/m77-139
89. Bollenbach, T. Antimicrobial interactions: Mechanisms and implications for drug discovery and resistance evolution. *Current Opinion in Microbiology* (2015). doi:10.1016/j.mib.2015.05.008
90. Yan, H. & Hancock, R. E. W. Synergistic interactions between mammalian antimicrobial defense peptides. *Antimicrob. Agents Chemother.* (2001). doi:10.1128/AAC.45.5.1558-1560.2001
91. Roemer, T. & Boone, C. Systems-level antimicrobial drug and drug synergy discovery. *Nat. Chem. Biol.* **9**, 222–231 (2013).
92. Brochado, A. R. *et al.* Species-specific activity of antibacterial drug combinations. *Nature* **559**, 259–263 (2018).
93. Driscoll, J. A., Brody, S. L. & Kollef, M. H. The epidemiology, pathogenesis and treatment of Pseudomonas aeruginosa infections. *Drugs* (2007). doi:10.2165/00003495-200767030-00003
94. Gjødsbøl, K. *et al.* Multiple bacterial species reside in chronic wounds: A longitudinal study. *Int. Wound J.* (2006). doi:10.1111/j.1742-481X.2006.00159.x
95. Rudkjøbing, V. B. *et al.* The microorganisms in chronically infected end-stage and non-end-stage cystic fibrosis patients. *FEMS Immunol. Med. Microbiol.* (2012). doi:10.1111/j.1574-695X.2011.00925.x
96. Chen, L., Zou, Y., She, P. & Wu, Y. Composition, function, and regulation of T6SS in Pseudomonas aeruginosa. *Microbiological Research* (2015). doi:10.1016/j.micres.2015.01.004
97. Mougous, J. D., Gifford, C. A., Ramsdell, T. L. & Mekalanos, J. J. Threonine phosphorylation post-translationally regulates protein secretion in Pseudomonas aeruginosa. *Nat. Cell Biol.* (2007). doi:10.1038/ncb1605
98. Lesic, B., Starkey, M., He, J., Hazan, R. & Rahme, L. G. Quorum sensing differentially regulates Pseudomonas aeruginosa type VI secretion locus I and homologous loci II and III, which are required for pathogenesis. *Microbiology* (2009). doi:10.1099/mic.0.029082-0
99. Le Roux, M. *et al.* Kin cell lysis is a danger signal that activates antibacterial pathways of pseudomonas aeruginosa. *Elife* **2015**, 1–65 (2015).
100. Silverman, J. M. *et al.* Separate inputs modulate phosphorylation-dependent and -independent type VI secretion activation. *Mol. Microbiol.* (2011). doi:10.1111/j.1365-2958.2011.07889.x
101. Sana, T. G., Berni, B. & Bleves, S. The T6SSs of Pseudomonas aeruginosa Strain PAO1 and Their Effectors: Beyond Bacterial-Cell Targeting. *Front. Cell. Infect. Microbiol.* **6**, (2016).
102. Allsopp, L. P. *et al.* RsmA and AmrZ orchestrate the assembly of all three type VI secretion systems in Pseudomonas aeruginosa . *Proc. Natl. Acad. Sci.* (2017). doi:10.1073/pnas.1700286114

103. Sana, T. G. *et al.* The second type VI secretion system of Pseudomonas aeruginosa strain PAO1 is regulated by quorum sensing and fur and modulates internalization in epithelial cells. *J. Biol. Chem.* (2012). doi:10.1074/jbc.M112.376368
104. Sana, T. G., Soscia, C., Tonglet, C. M., Garvis, S. & Bleves, S. Divergent Control of Two Type VI Secretion Systems by RpoN in Pseudomonas aeruginosa. *PLoS One* (2013). doi:10.1371/journal.pone.0076030
105. Ting, S. Y. *et al.* Bifunctional Immunity Proteins Protect Bacteria against FtsZ-Targeting ADP-Ribosylating Toxins. *Cell* (2018). doi:10.1016/j.cell.2018.09.037
106. Eddy, S. R. *HMMER User's Guide: Biological sequence analysis using profile hidden Markov models*. *Dictionary of Bioinformatics and Computational Biology* (2018). doi:10.1002/9780471650126.dob0323.pub2
107. Ho, B. T., Basler, M. & Mekalanos, J. J. Type 6 secretion system-mediated immunity to type 4 secretion system-mediated gene transfer. *Science (80-.).* (2013). doi:10.1126/science.1243745
108. Stylianidou, S., Brennan, C., Nissen, S. B., Kuwada, N. J. & Wiggins, P. A. SuperSegger: robust image segmentation, analysis and lineage tracking of bacterial cells. *Mol. Microbiol.* (2016). doi:10.1111/mmi.13486
109. Li, M. *et al.* Structural basis for type VI secretion effector recognition by a cognate immunity protein. *PLoS Pathog.* (2012). doi:10.1371/journal.ppat.1002613
110. Krogh, A., Larsson, B., Von Heijne, G. & Sonnhammer, E. L. L. Predicting transmembrane protein topology with a hidden Markov model: Application to complete genomes. *J. Mol. Biol.* (2001). doi:10.1006/jmbi.2000.4315
111. Casabona, M. G., Vandenbrouck, Y., Attree, I. & Couté, Y. Proteomic characterization of Pseudomonas aeruginosa PAO1 inner membrane. *Proteomics* (2013). doi:10.1002/pmic.201200565
112. Kim, S. *et al.* Transmembrane glycine zippers: Physiological and pathological roles in membrane proteins. *Proc. Natl. Acad. Sci.* (2005). doi:10.1073/pnas.0501234102
113. Hunte, C. *et al.* Structure of a Na+/H+ antiporter and insights into mechanism of action and regulation by pH. *Nature* (2005). doi:10.1038/nature03692
114. Wu, X., Altman, R., Eiteman, M. A. & Altman, E. Effect of overexpressing nhaA and nhaR on sodium tolerance and lactate production in Escherichia coli. *J. Biol. Eng.* (2013). doi:10.1186/1754-1611-7-3
115. Rimon, A., Tzubery, T. & Padan, E. Monomers of the NhaA Na+/H+ antiporter of Escherichia coli are fully functional yet dimers are beneficial under extreme stress conditions at alkaline pH in the presence of Na+ or Li+. *J. Biol. Chem.* (2007). doi:10.1074/jbc.M704469200
116. Oren, A. Microbial life at high salt concentrations: Phylogenetic and metabolic diversity. *Saline Systems* (2008). doi:10.1186/1746-1448-4-2
117. Rietz, D. N. & Haynes, R. J. Effects of irrigation-induced salinity and sodicity on soil microbial activity. *Soil Biol. Biochem.* (2003). doi:10.1016/S0038-0717(03)00125-1
118. Bénédetti, H., Lloubès, R., Lazdunski, C. & Letellier, L. Colicin A unfolds during its translocation in Escherichia coli cells and spans the whole cell envelope when its pore has formed. *EMBO J.* (1992). doi:10.1002/j.1460-2075.1992.tb05073.x
119. Brogden, K. A. Antimicrobial peptides: Pore formers or metabolic inhibitors in bacteria? *Nature Reviews Microbiology* (2005). doi:10.1038/nrmicro1098
120. Maloney, P. C., Kashket, E. R. & Wilson, T. H. A Protonmotive Force Drives ATP Synthesis in Bacteria. *Proc. Natl. Acad. Sci.* (1974). doi:10.1073/pnas.71.10.3896
121. Hoffman, J. F. & Laris, P. C. Determination of membrane potentials in human and Amphiuma red blood cells by means of a fluorescent probe. *J. Physiol.* (1974). doi:10.1113/jphysiol.1974.sp010581
122. Mahon, M. J. pHluorin2: an enhanced, ratiometric, pH-sensitive green florescent protein.

Adv. Biosci. Biotechnol. (2011). doi:10.4236/abb.2011.23021
123. Greenfield, N. J. Using circular dichroism spectra to estimate protein secondary structure. *Nat. Protoc.* (2007). doi:10.1038/nprot.2006.202
124. Peraro, M. D. & Van Der Goot, F. G. Pore-forming toxins: Ancient, but never really out of fashion. *Nature Reviews Microbiology* (2016). doi:10.1038/nrmicro.2015.3
125. Shen, H. *et al.* Structural basis for the modulation of voltage-gated sodium channels by animal toxins. *Science (80-.).* (2018). doi:10.1126/science.aau2596
126. Favre, I., Moczydlowski, E. & Schild, L. On the structural basis for ionic selectivity among Na+, K+, and Ca2+ in the voltage-gated sodium channel. *Biophys. J.* (1996). doi:10.1016/S0006-3495(96)79505-X
127. Stover, C. K. *et al.* Complete genome sequence of Pseudomonas aeruginosa PAO1, an opportunistic pathogen. *Nature* (2000). doi:10.1038/35023079
128. Hoang, T. T., Kutchma, A. J., Becher, A. & Schweizer, H. P. Integration-proficient plasmids for Pseudomonas aeruginosa: Site- specific integration and use for engineering of reporter and expression strains. *Plasmid* (2000). doi:10.1006/plas.1999.1441
129. Kulasekara, B. R. *et al.* c-di-GMP heterogeneity is generated by the chemotaxis machinery to regulate flagellar motility. *Elife* (2013). doi:10.7554/elife.01402
130. Mougous, J. D. *et al.* A virulence locus of Pseudomonas aeruginosa encodes a protein secretion apparatus. *Science (80-.).* (2006). doi:10.1126/science.1128393
131. Hibbing, M. E., Fuqua, C., Parsek, M. R. & Peterson, S. B. Bacterial competition: surviving and thriving in the microbial jungle. *Nat. Rev. Microbiol.* (2010). doi:10.1038/nrmicro2259
132. Hood, R. D., Peterson, S. B. & Mougous, J. D. From Striking Out to Striking Gold: Discovering that Type VI Secretion Targets Bacteria. *Cell Host and Microbe* (2017). doi:10.1016/j.chom.2017.02.001
133. Pukatzki, S., Ma, A. T., Revel, A. T., Sturtevant, D. & Mekalanos, J. J. Type VI secretion system translocates a phage tail spike-like protein into target cells where it cross-links actin. *Proc. Natl. Acad. Sci.* (2007). doi:10.1073/pnas.0706532104
134. Goodman, A. L. *et al.* A signaling network reciprocally regulates genes associated with acute infection and chronic persistence in Pseudomonas aeruginosa. *Dev. Cell* (2004). doi:10.1016/j.devcel.2004.08.020
135. LeRoux, M. *et al.* Quantitative single-cell characterization of bacterial interactions reveals type VI secretion is a double-edged sword. *Proc. Natl. Acad. Sci.* (2012). doi:10.1073/pnas.1213963109
136. Robb, C. S., Robb, M., Nano, F. E. & Boraston, A. B. The Structure of the Toxin and Type Six Secretion System Substrate Tse2 in Complex with Its Immunity Protein. *Structure* (2016). doi:10.1016/j.str.2015.11.012
137. Baym, M., Stone, L. K. & Kishony, R. Multidrug evolutionary strategies to reverse antibiotic resistance. *Science* (2016). doi:10.1126/science.aad3292
138. Albanese, D., Fontana, P., De Filippo, C., Cavalieri, D. & Donati, C. MICCA: A complete and accurate software for taxonomic profiling of metagenomic data. *Sci. Rep.* **5**, 1–7 (2015).
139. Cascales, E. The type VI secretion toolkit. *EMBO Reports* (2008). doi:10.1038/embor.2008.131
140. Cascales, E. & Cambillau, C. Structural biology of type VI secretion systems. *Philosophical Transactions of the Royal Society B: Biological Sciences* (2012). doi:10.1098/rstb.2011.0209
141. Nguyen, V. S. *et al.* Towards a complete structural deciphering of Type VI secretion system. *Current Opinion in Structural Biology* (2018). doi:10.1016/j.sbi.2018.01.007
142. Shneider, M. M. *et al.* PAAR-repeat proteins sharpen and diversify the type VI secretion system spike. *Nature* (2013). doi:10.1038/nature12453
143. Basler, M., Pilhofer, M., Henderson, G. P., Jensen, G. J. & Mekalanos, J. J. Type VI

secretion requires a dynamic contractile phage tail-like structure. *Nature* (2012). doi:10.1038/nature10846
144. Leiman, P. G. *et al.* Type VI secretion apparatus and phage tail-associated protein complexes share a common evolutionary origin. *Proc. Natl. Acad. Sci. U. S. A.* (2009). doi:10.1073/pnas.0813360106
145. Veesler, D. & Cambillau, C. A Common Evolutionary Origin for Tailed-Bacteriophage Functional Modules and Bacterial Machineries. *Microbiol. Mol. Biol. Rev.* (2011). doi:10.1128/MMBR.00014-11
146. Cardarelli, L. *et al.* Phages have adapted the same protein fold to fulfill multiple functions in virion assembly. *Proc. Natl. Acad. Sci.* (2010). doi:10.1073/pnas.1005822107
147. Ge, P. *et al.* Atomic structures of a bactericidal contractile nanotube in its pre- and postcontraction states. *Nat. Struct. Mol. Biol.* (2015). doi:10.1038/nsmb.2995
148. Kanamaru, S. *et al.* Structure of the cell-puncturing device of bacteriophage T4. *Nature* (2002). doi:10.1038/415553a
149. Leiman, P. G., Chipman, P. R., Kostyuchenko, V. A., Mesyanzhinov, V. V. & Rossmann, M. G. Three-dimensional rearrangement of proteins in the tail of bacteriophage T4 on infection of its host. *Cell* (2004). doi:10.1016/j.cell.2004.07.022
150. Wang, J. *et al.* Cryo-EM structure of the extended type VI secretion system sheath-tube complex. *Nat. Microbiol.* (2017). doi:10.1038/s41564-017-0020-7
151. Kudryashev, M. *et al.* Structure of the Type VI secretion system contractile sheath. *Cell* (2015). doi:10.1016/j.cell.2015.01.037
152. Clemens, D. L., Ge, P., Lee, B. Y., Horwitz, M. A. & Zhou, Z. H. Atomic structure of T6SS reveals interlaced array essential to function. *Cell* (2015). doi:10.1016/j.cell.2015.02.005
153. Chang, Y., Rettberg, L. A., Ortega, D. R. & Jensen, G. J. In vivo structures of an intact type VI secretion system revealed by electron cryotomography . *EMBO Rep.* (2017). doi:10.15252/embr.201744072
154. Durand, E. *et al.* Biogenesis and structure of a type VI secretion membrane core complex. *Nature* (2015). doi:10.1038/nature14667
155. Zoued, A. *et al.* Priming and polymerization of a bacterial contractile tail structure. *Nature* (2016). doi:10.1038/nature17182
156. Nguyen, V. S. *et al.* Type VI secretion TssK baseplate protein exhibits structural similarity with phage receptor-binding proteins and evolved to bind the membrane complex. *Nat. Microbiol.* (2017). doi:10.1038/nmicrobiol.2017.103
157. Zoued, A. *et al.* TssA: The cap protein of the Type VI secretion system tail. *BioEssays* (2017). doi:10.1002/bies.201600262
158. Brunet, Y. R., Zoued, A., Boyer, F., Douzi, B. & Cascales, E. The Type VI Secretion TssEFGK-VgrG Phage-Like Baseplate Is Recruited to the TssJLM Membrane Complex via Multiple Contacts and Serves As Assembly Platform for Tail Tube/Sheath Polymerization. *PLoS Genet.* (2015). doi:10.1371/journal.pgen.1005545
159. Taylor, N. M. I. *et al.* Structure of the T4 baseplate and its function in triggering sheath contraction. *Nature* (2016). doi:10.1038/nature17971
160. English, G., Byron, O., Cianfanelli, F. R., Prescott, A. R. & Coulthurst, S. J. Biochemical analysis of TssK, a core component of the bacterial Type VI secretion system, reveals distinct oligomeric states of TssK and identifies a TssK–TssFG subcomplex. *Biochem. J.* (2014). doi:10.1042/BJ20131426
161. Walls, A. *et al.* Crucial steps in the structure determination of a coronavirus spike glycoprotein using cryo-electron microscopy. *Protein Sci.* (2017). doi:10.1002/pro.3048
162. Nakane, T., Kimanius, D., Lindahl, E. & Scheres, S. H. Characterisation of molecular motions in cryo-EM single-particle data by multi-body refinement in RELION. *Elife* (2018). doi:10.7554/elife.36861
163. Ovchinnikov, S. *et al.* Large-scale determination of previously unsolved protein structures

using evolutionary information. *Elife* (2015). doi:10.7554/elife.09248
164. Ovchinnikov, S. *et al.* Protein structure determination using metagenome sequence data. *Science (80-.).* (2017). doi:10.1126/science.aah4043
165. Song, Y. *et al.* High-resolution comparative modeling with RosettaCM. *Structure* (2013). doi:10.1016/j.str.2013.08.005
166. Wang, R. Y.-R. *et al.* Automated structure refinement of macromolecular assemblies from cryo-EM maps using Rosetta. *Elife* (2016). doi:10.7554/elife.17219
167. Dimaio, F. *et al.* Atomic-accuracy models from 4.5-Å cryo-electron microscopy data with density-guided iterative local refinement. *Nat. Methods* (2015). doi:10.1038/nmeth.3286
168. Ovchinnikov, S. *et al.* Improved de novo structure prediction in CASP11 by incorporating coevolution information into Rosetta. *Proteins Struct. Funct. Bioinforma.* (2016). doi:10.1002/prot.24974
169. Frenz, B., Walls, A. C., Egelman, E. H., Veesler, D. & Di Maio, F. RosettaES: A sampling strategy enabling automated interpretation of difficult cryo-EMmaps. *Nat. Methods* (2017). doi:10.1038/nmeth.4340
170. Emsley, P., Lohkamp, B., Scott, W. G. & Cowtan, K. Features and development of Coot . *Acta Crystallogr. Sect. D Biol. Crystallogr.* (2010). doi:10.1107/s0907444910007493
171. Hare, S. *et al.* Identification, structure and mode of action of a new regulator of the Helicobacter pylori HP0525 ATPase. *EMBO J.* (2007). doi:10.1038/sj.emboj.7601904
172. Pell, L. G., Kanelis, V., Donaldson, L. W., Lynne Howell, P. & Davidson, A. R. The phage major tail protein structure reveals a common evolution for long-tailed phages and the type VI bacterial secretion system. *Proc. Natl. Acad. Sci.* (2009). doi:10.1073/pnas.0900044106
173. Taylor, N. M. I., van Raaij, M. J. & Leiman, P. G. Contractile injection systems of bacteriophages and related systems. *Molecular Microbiology* (2018). doi:10.1111/mmi.13921
174. Zoued, A. *et al.* TssK is a trimeric cytoplasmic protein interacting with components of both phage-like and membrane anchoring complexes of the type VI secretion system. *J. Biol. Chem.* (2013). doi:10.1074/jbc.M113.499772
175. Veesler, D. *et al.* Structure of the phage TP901-1 1.8 MDa baseplate suggests an alternative host adhesion mechanism. *Proc. Natl. Acad. Sci.* (2012). doi:10.1073/pnas.1200966109
176. Sciara, G. *et al.* Structure of lactococcal phage p2 baseplate and its mechanism of activation. *Proc. Natl. Acad. Sci.* (2010). doi:10.1073/pnas.1000232107
177. Karimova, G., Pidoux, J., Ullmann, A. & Ladant, D. A bacterial two-hybrid system based on a reconstituted signal transduction pathway. *Proc. Natl. Acad. Sci. U. S. A.* (1998).
178. Nazarov, S. *et al.* Cryo-EM reconstruction of Type VI secretion system baseplate and sheath distal end. *EMBO J.* (2018). doi:10.15252/embj.201797103
179. Yap, M. L. *et al.* Role of bacteriophage T4 baseplate in regulating assembly and infection. *Proc. Natl. Acad. Sci.* (2016). doi:10.1073/pnas.1601654113
180. Logger, L., Aschtgen, M. S., Guérin, M., Cascales, E. & Durand, E. Molecular Dissection of the Interface between the Type VI Secretion TssM Cytoplasmic Domain and the TssG Baseplate Component. *J. Mol. Biol.* (2016). doi:10.1016/j.jmb.2016.08.032
181. Vettiger, A., Winter, J., Lin, L. & Basler, M. The type VI secretion system sheath assembles at the end distal from the membrane anchor. *Nat. Commun.* (2017). doi:10.1038/ncomms16088
182. Böck, D. *et al.* In situ architecture, function, and evolution of a contractile injection system. *Science (80-.).* (2017). doi:10.1126/science.aan7904
183. Suloway, C. *et al.* Automated molecular microscopy: The new Leginon system. *J. Struct. Biol.* (2005). doi:10.1016/j.jsb.2005.03.010
184. Voss, N. R., Yoshioka, C. K., Radermacher, M., Potter, C. S. & Carragher, B. DoG Picker

and TiltPicker: software tools to facilitate particle selection in single particle electron microscopy. *J. Struct. Biol.* (2009).
185. Lander, G. C. *et al.* Appion: an integrated, database-driven pipeline to facilitate EM image processing. *J. Struct. Biol.* (2009).
186. Zheng, S. Q. *et al.* MotionCor2: anisotropic correction of beam-induced motion for improved cryo-electron microscopy. *Nat. Methods* (2017). doi:10.1038/nmeth.4193
187. Zhang, K. Gctf: Real-time CTF determination and correction. *J. Struct. Biol.* (2016). doi:10.1016/j.jsb.2015.11.003
188. Punjani, A., Rubinstein, J. L., Fleet, D. J. & Brubaker, M. A. CryoSPARC: Algorithms for rapid unsupervised cryo-EM structure determination. *Nat. Methods* (2017). doi:10.1038/nmeth.4169
189. Scheres, S. H. W. & Chen, S. Prevention of overfitting in cryo-EM structure determination. *Nat. Methods* (2012). doi:10.1038/nmeth.2115
190. Rosenthal, P. B. & Henderson, R. Optimal determination of particle orientation, absolute hand, and contrast loss in single-particle electron cryomicroscopy. *J. Mol. Biol.* (2003). doi:10.1016/j.jmb.2003.07.013
191. Chen, S. *et al.* High-resolution noise substitution to measure overfitting and validate resolution in 3D structure determination by single particle electron cryomicroscopy. *Ultramicroscopy* (2013). doi:10.1016/j.ultramic.2013.06.004
192. Cardone, G., Heymann, J. B. & Steven, A. C. One number does not fit all: Mapping local variations in resolution in cryo-EM reconstructions. *J. Struct. Biol.* (2013). doi:10.1016/j.jsb.2013.08.002
193. Marks, D. S., Hopf, T. A. & Sander, C. Protein structure prediction from sequence variation. *Nature Biotechnology* (2012). doi:10.1038/nbt.2419
194. Krissinel, E. & Henrick, K. Inference of Macromolecular Assemblies from Crystalline State. *J. Mol. Biol.* (2007). doi:10.1016/j.jmb.2007.05.022
195. Goddard, T. D., Huang, C. C. & Ferrin, T. E. Visualizing density maps with UCSF Chimera. *J. Struct. Biol.* (2007). doi:10.1016/j.jsb.2006.06.010
196. Goddard Thomas, D. *et al.* UCSF ChimeraX: Meeting modern challenges in visualization and analysis. *Protein Sci.* (2017). doi:10.1002/pro.3235
197. Verster, A. J. *et al.* The Landscape of Type VI Secretion across Human Gut Microbiomes Reveals Its Role in Community Composition. *Cell Host Microbe* (2017). doi:10.1016/j.chom.2017.08.010
198. Ross, B. D., Verster, A. J., Radey, M. C. & Schmidtke, D. T. Acquired interbacterial defense systems provide fitness in the human gut microbiome. 1–13 (2018).
199. Sana, T. G. *et al.* Salmonella Typhimurium utilizes a T6SS-mediated antibacterial weapon to establish in the host gut . *Proc. Natl. Acad. Sci.* (2016). doi:10.1073/pnas.1608858113
200. Nannenga, B. L. & Gonen, T. The cryo-EM method microcrystal electron diffraction (MicroED). *Nature Methods* (2019). doi:10.1038/s41592-019-0395-x
201. Gonen, T. MicroED: Three Dimensional Electron Crystallography of Protein Micro-Crystals. *Acta Crystallogr. Sect. A Found. Adv.* (2014). doi:10.1107/s2053273314089360
202. Roux, B. Ion channels and ion selectivity. *Essays Biochem.* (2017). doi:10.1042/ebc20160074
203. Siontorou, C. G., Nikoleli, G. P., Nikolelis, D. P. & Karapetis, S. K. Artificial lipid membranes: Past, present, and future. *Membranes* (2017). doi:10.3390/membranes7030038
204. Zakharian, E. Recording of ion channel activity in planar lipid bilayer experiments. *Methods Mol. Biol.* (2013). doi:10.1007/978-1-62703-351-0_8
205. Whitney, J. C. *et al.* Identification, structure, and function of a novel type VI secretion peptidoglycan glycoside hydrolase effector-immunity pair. *J. Biol. Chem.* (2013). doi:10.1074/jbc.M113.488320

206. Benz, J. & Meinhart, A. Antibacterial effector/immunity systems: It's just the tip of the iceberg. *Current Opinion in Microbiology* (2014). doi:10.1016/j.mib.2013.11.002
207. Park, Y. J. *et al.* Structure of the type VI secretion system TssK–TssF–TssG baseplate subcomplex revealed by cryo-electron microscopy. *Nat. Commun.* (2018). doi:10.1038/s41467-018-07796-5
208. Allain, F. *et al.* Biogenesis and structure of a type VI secretion baseplate. *Nat. Microbiol.* (2018). doi:10.1038/s41564-018-0260-1